# Highly Excited Ro-vibrational States of Small Molecules using Discrete Variable Representations

by

**James R. Henderson**

A thesis submitted to
THE UNIVERSITY OF LONDON
for the degree of
DOCTOR OF PHILOSOPHY

University College London September 1990

*To my son, Zac.*

## Abstract

Calculated ro-vibrational levels ($J \leq 4$) and transition intensities are presented for $^7Li_3^+$ and $^7Li_2\,^6Li^+$ . These studies are made using conventional Finite Basis Representation (FBR) methods.

A formulation of the nuclear motion problem for small molecules is then presented in the Discrete Variable Representation (DVR). The theory is developed in a highly generalised set of internal co-ordinates using an exact Hamiltonian operator. Having used the DVR for vibrational ($J = 0$) calculations, it is rather simply extended to ro-vibrational ($J > 0$) case.

It is demonstrated that the DVR is extremely powerful in dealing with molecules that can undergo very large amplitude (coupled) motions on what may be a particularly complicated potential energy surface.

Calculations on the isomerising LiCN/LiNC system are presented using a 2D (CN frozen) potential energy surface. Some 900 vibrational levels are stabilised using a DVR in the angular co-ordinate of scattering (or Jacobi) co-ordinates. Contour plots of the wavefunctions are made and analysed; this yields information about the very highly excited dynamics of the system, well above the isomerisation barrier, for the very first time.

Full three-mode calculations on the $H_3^+$ molecular ion are presented, using a very accurate *ab initio* potential energy surface. Ro-vibrational studies are made using a DVR in the angular co-ordinate of scattering co-ordinates. A multidimensional DVR in scattering co-ordinates is then employed and three $H_3^+$ surfaces are used. These calculations converge *all* the $J = 0$ bound states of the system to within $10cm^{-1}$, giving at least 881 states for each potential. The wavefunctions are analysed in an attempt to find assignablel or spatially localised states. The significance of these calculations to the unassigned near-dissociation spectra is discussed.

# Contents

# List of Tables

# List of Figures

## Acknowledgements

The guidance, expertise and enthusiasm of Jonathan Tennyson have made this study possible and a great pleasure. He has introduced me to a most interesting and exciting area of science. He is most gratefully acknowledged. Steven Miller is thanked similarly, as is Brian Sutcliffe. All three are thanked also for their very careful reading of this thesis, and their suggestions for improvements.

I am extremely grateful to my mother and father for their endless encouragement and their determination to assist and advise me. I also thank them both tremendously for the financial support they have provided during my studentship. Financial help was also kindly given by John and Gloria Mead; I thank them for this.

All calculations presented in this thesis were performed on the Cray XMP/28 computer at The University of London Computer Centre. I would like to thank the staff there for their help in various aspects of computing. In particular I thank Elizabeth Woodman, Alison Taylor, David Winstanley and Malcolm Keach.

I am grateful to the SERC for providing my Studentship.

# Chapter 1

# Theoretical Background

## 1.1 Introduction

The study and knowledge of small molecular systems has excelled considerably in recent years. In particular, the study of molecular spectroscopy and dynamics has developed into a very active research area. Investigation of molecular rotation-vibration states leads to understanding of potential energy and dipole surfaces, unimolecular reactions, the assignment of complicated spectra, and phenomena such as 'forbidden' transitions.

Quantum theoretical studies involve the solution of the Schrödinger equation. One popular approach is to use the secular equation method. This involves the diagonalisation of a Hamiltonian matrix to yield, from first principles, the nuclear motion rotation-vibration eigenenergies and wavefunctions for the system. Information concerning the nuclear motion dynamics is extracted from the wavefunctions. More spectroscopic information must be obtained from calculations using the dipole surface.

Somewhat unfortunately, accurate theoretical data can only be obtained for molecules with two or three atoms. This is due primarily to the way in which the

size of the matrices scales as a function of the number of modes of the system. Furthermore, the derivation of an appropriate Hamiltonian operator in a particular (internal) co-ordinate system becomes non-trivial if the number of modes in a system is more than 2. For accurate calculations one is essentially confined to triatomic molecules, although the position is improving and tetratomics are beginning to be studied successfully. The job of solving accurately an N-atomic problem fully quantum mechanically is by no means trivial (and is usually impossible for large N); there certainly exists no general method of solution. The work presented in this thesis is confined to triatomic systems, with the aim being the study of very highly excited states of these systems.

The theoretical and experimental work on triatomics go very much hand in hand, assisting each other - although in certain areas the theoretical techniques certainly lack the power to compete with the experimentally produced data. In particular the experimentalist, thanks to advances in laser and molecular beam techniques, is now able to probe the very highly ro-vibrationally excited states of small molecules - even up to and above dissociation. The theoretical equivalent can pose major problems, usually associated with basis set sizes.

A relatively novel technique using discrete variables is employed in this work to attempt to circumvent the conventional problems when dealing with very highly excited states. A major incentive is the challenge presented by the largely unexplained infrared predissociation spectrum of $H_3^+$ recorded by Carrington and Kennedy[1,2]. These workers observed some 27,000 lines in a 222 $cm^{-1}$ window in the predissociation region, thought to be in the moderately highly excited rotational states of the system (total angular momentum $J \leq 25$). One of the major puzzles is the coarse-grained regularity of the spectrum under low resolution. The $H_3^+$ studies presented here in chapters 5 and 6 represent, for the first time, a full quantum mechanical attempt at studying this system at

such high energies. A considerable contribution is made to our understanding of the highly excited dynamics of this electronically simple, but physically very complex, system.

The following subsections discuss the notion of the potential energy surface, the Born-Oppenheimer approximation, and the use of perturbation theory. Then the variational principle is proved and the early variational-type calculations are reviewed. The use over the last decade of internal co-ordinate calculations is discussed. The pioneering work in this area is highlighted, along with a discussion of why it is sometimes necessary to find an alternative to this Finite Basis Representation (FBR) expansion approach. This then leads to the Discrete Variable Representation (DVR) and other pointwise representaions, which are introduced in the final part of this chapter.

Chapter 2 gives an account of the theory of one implementation of the FBR and examines the lithium trimer cation as a case study. The full theory of the DVR is given in chapter 3. The LiNC/LiCN system has been studied in a DVR and is reported in chapter 4. Extensive studies are made on the $H_3^+$ molecular ion; the work which employs a 1-dimensional DVR is described in chapter 5, and a multi-dimensional DVR study, to very high vibrational energy, is reported in chapter 6.

## 1.2 The Potential Energy Surface

An approximation which is of major use in molecular calculations is the so-called Born-Oppenheimer approximation, proposed in 1927[3]. Indeed, it is also important to say that this approximation is of paramount importance in appreciating the the notions of molecular shape and structure[4]. The full Hamiltonian operator for any molecule is a function of both the nuclear and electronic co-

ordinates. In the Born-Oppenheimer approximation it is said that, due to the relative masses of the electrons and nuclei, the nuclei move very slowly compared to the electrons. Consequently this enables the separation of the nuclear and electronic wavefunctions of the molecule; the electrons will adjust instantaneously to any motion of the nuclei.

As a result of this approximation, the theorist is then able to solve the bound state Schrödinger equation for the system by solving the rotation-vibration nuclear motion dynamics on a particular (ground state) potential energy surface, which is parametrically a function of the nuclear co-ordinates only. Hence one needs only to derive a nuclear motion Hamiltonian operator – not the full one.

So, within the Born-Oppenheimer approximation, the theorist wanting to solve the ro-vibrational problem must obtain an electronic potential surface. This may be computed *ab initio* at a grid of points and fitted to a functional form. Alternatively the surface may be (semi-)empirical, obtained by inverting spectroscopic data obtained in the laboratory. A surface may be refined by modifying it until differences between the computed and experimental data are minimised. This, of course, depends on the existence (and understanding) of the experimental data. Fitting data to a perturbational Hamiltonian operator, for example, has also been widely used.

For a typical triatomic molecule the Born-Oppenheimer approximation leads to an error of approximately 500 $cm^{-1}$ in the absolute energy of the surface[5]. For most spectroscopic transitions this creates a negligible error as the whole surface is shifted. There are systems for which the Born-Oppenheimer approximation breaks down: when two electronic states are very close (or even overlap) in energy, for example, and ro-vibronic effects are important.

For polyatomic molecules most surfaces are not of spectroscopic accuracy. One impressive exception to this however is the *ab initio* $H_3^+$ surface used for

several of the calculations presented in this thesis. This extremely accurate surface, due to Meyer, Botchswina and Burton (MBB)[6], is a direct fit to functional form of the potential energy evaluated *ab initio* on a three-dimensional grid of points. The accuracy of the surface is exemplified by the crucial role it played in the first ever extraterrestial detection of $H_3^+$ recently[7].

## 1.3 The use of Perturbation Theory

Given a potential energy surface the next step is to develop suitable methodologies to compute wavefunctions and energies on the potential surface. It is precisely this problem that the thesis deals with.

For many years the method of choice for solving the nuclear motion on a potential energy hypersurface was perturbation theory. In perturbation theory a system is considered to be a slight modification to one with known solutions. For molecular spectroscopy the potential energy function is often assumed to be perturbed from a standard model of uncoupled harmonic oscillators and a rigid rotor. These two models have Hermite polynomials and Wigner rotation matrices respectively as their eigenfunctions.

One perturbational approach is to find the rotation-vibration energies (within the Born-Oppenheimer approximation) as eigenvalues of matrices whose elements are functions of spectroscopic quantities called rotation-vibration constants. These constants are functions of the nuclear masses, the equilibrium structure and the shape of the potential surface. The rotation-vibration constants can be found by fitting to observed energies. The equilibrium structure and potential parameters can then be obtained by interpreting these constants. Experimentalists use perturbation theory to invert their data, obtaining fits to perturbational Hamiltonian operators containing molecular constants. This in

turn leads to details of the potential energy surface.

The most popular theoretical approach has been the use of the classical rotation-vibration Hamiltonian operator of Eckart[8]. The Hamiltonian is expressed in terms of small displacements from equilibrium in the normal coordinates of the system. Various quantum mechanical forms of this operator have appeared, but without doubt the simplest and most elegant is that derived by Watson[9]. The potential is then expressed as a Taylor series about equilibrium. The Hamiltonian is thus seen as a zero-order operator plus contributions from the harmonic, cubic, quartic etc. terms. Substitution of this, and similar expansions for the wavefunctions and energies, into the Schrödinger equation leads to standard perturbation equations[10].

The solutions are given in terms of truncated sums, as shown by Krohn *et al* [11]. An extension to the usual perturbative approach is that proposed by Van Vleck in 1929[12] to help manage the bookkeeping of perturbation theory. It is based on a contact transformation of the Schrödinger equation and leads to the direct evaluation of definite operator integrals, as opposed to the traditional evaluation of off-diagonal matrix elements.

The fundamental problem with all perturbational treatments is the limitation that the vibration displacements in the molecule be small. Large amplitude displacements simply cause non-convergence, or very slow convergence, of the perturbation theory. A further complication is that in the standard approach linear and nonlinear molecules have different Hamiltonian operators, thus causing problems, for example, when a nonlinear system reaches linearity[9].

When small amplitude motions are of interest and/or great accuracy is not required then the perturbational approach is usually sufficient. This is certainly not the case if moderately to highly excited states are required, or if the potential energy well is particularly shallow and if high accuracy is required. To calculate

high–lying vibration–rotation states with significant displacements from equilibrium, however, new methodologies have to be employed. Certainly if one is interested in the region of molecular dissociation (as with the $H_3^+$ system in this thesis) then the use of perturbation theory would be totally inadequate.

Note that an interesting hybrid approach has been employed by Bunker and co-workers[13]. Perturbation theory is used in small-displacement modes, whilst others are treated more accurately. This so-called 'non-rigid bender' approach has been applied to many systems including $H_2O$[14,15] and $CH_2$[16,17].

## 1.4 The Variational Principle

The use of the variational principle within the Born-Oppenheimer approximation circumvents some of the problems associated with perturbational techniques. It has proved very much a success story over the last two decades. The variational principle was first presented by Rayleigh and Ritz[18], and has been used extensively by electronic structure theorists[19].

The variational principle essentially allows one to construct and diagonalise a Hamiltonian matrix which is defined in terms of matrix elements linking some set of basis functions. It can then be shown that the better the representation offered by the set of basis functions, the lower the calculated energies will be. Hence, in a series of calculations, as one continues to make the basis set better/bigger, it will be seen that the energies approach monotonically from above the 'exact' values.

In order to prove this for the ground state of a system one investigates the properties of the energy expectation value,

$$\mathcal{E} = \int \phi^* \hat{H} \phi dv, \tag{1.1}$$

where $\phi$ is an arbitrary, normalised wavefunction which is single-valued, finite

and continuous in the accessible space, and $\hat{H}$ is the full Hamiltonian operator for the system. If $\phi$ is set equal to the true ground state of the system, $\psi_0$, then

$$\int \psi_0^* \hat{H} \psi_0 dv = E_0. \tag{1.2}$$

$\phi$ can be written as an expansion in the true wavefunctions, $\psi_n$, of the system,

$$\phi = \sum_{n=0}^{\infty} a_n \psi_n. \tag{1.3}$$

The true wavefunctions form an orthonormal set and so we have the additional condition

$$\sum_{n,m=0}^{\infty} a_n^* a_m = \delta_{mn}. \tag{1.4}$$

Substituting this into eqn. (1.1) gives

$$\mathcal{E} = \sum_{n,m=0}^{\infty} a_n^* a_m \int \psi_n^* \hat{H} \psi_m dv. \tag{1.5}$$

Since the $\psi_n$ are the true wavefunctions of the system we have

$$\hat{H} \psi_n = E_n \psi_n \tag{1.6}$$

and

$$\mathcal{E} = \sum_n a_n^* a_n E_n. \tag{1.7}$$

Subtracting $\sum_n a_n^* a_n E_0$ from each side of eqn. (1.7), and using

$$\sum_n a_n^* a_n E_0 = E_0 \sum_n a_n^* a_n = E_0 \tag{1.8}$$

leads to

$$\mathcal{E} - E_0 = \sum_{n=0}^{\infty} a_n^* a_n (E_n - E_0). \tag{1.9}$$

The product $a_n^* a_n$ is either zero or positive. Since $E_0$ is the energy corresponding to the lowest state of the system, then $E_n$ must be greater than or equal to $E_0$. Therefore it is true that

$$\mathcal{E} \geq E_0. \tag{1.10}$$

It is therefore shown that the calculated ground state energy is always greater than or equal to the true value of the ground state energy. Furthermore, it can be shown that the above mathematical treatment can be extended to the general case for the $i$th level. This variational principle for the excited states has been given by MacDonald[20];

$$E_i \leq \mathcal{E}_{n+1}^i \leq \mathcal{E}_n^i \leq \mathcal{E}_n^{i+1}, \tag{1.11}$$

where $\mathcal{E}_{n+1}^i$ is the energy of the $i$th level calculated using one more basis set expansion function than that using $n$ functions, and $E_i$ is the exact value. The variational principle then says that minimising the calculated energies allows the best possible values of the energies and coefficients to be obtained.

## 1.5 Early Variational Calculations

The earliest variational studies, performed in the 1970's, have been reviewed by Carney, Sprandel and Kern[10]. Of particular note, mentioned therein, are the variational calculations of Suzuki[21,22,23] on diatomic systems – in particular CO and HCl. These studies yielded information about force constants and also provided some insight into the usefulness of different types of stretching function.

Some of the earliest fully variational triatomic calculations were performed by Carney and co-workers[10]. A system of much interest in early studies was the water molecule. In particular, variational studies were able to take the experimentally obtained potential functions of $H_2O$ and help to refine them. Water was also the subject of studies by Whitehead and Handy[24]. These workers used the two forms of the Eckart-Watson Hamiltonian (for linear and non-linear systems), with products of Hermite polynomials (harmonic oscillator eigenfunctions) as basis functions in the normal co-ordinates of the system. They also introduced Gaussian quadrature schemes for the numerical integration to com-

pute the matrix elements. This was shown to be highly efficient and is widely used in this area. $SO_2$ and the linear OCS were studied at the same time. It was generally accepted that this was the method of choice for calculating the low-lying levels of fairly rigid molecules. The results obtained have thus been used as a benchmark against which other methods are tested.

Also during this period Carney and Porter produced pioneering work on the $H_3^+$ molecular ion[25,26,27,28]. They calculated and fitted a potential surface *ab initio* in order to calculate the low-lying ro-vibrational levels. These calculations led to the first assigned spectra of $H_3^+$[29] and $D_3^+$[30] in 1980.

Van der Waals complexes form a class of large amplitude loosely bound systems and hence can lend themselves as good methodological tests. The early variational studies have been reviewed by Le Roy and Carley[31]. These workers discuss the various aspects of the close coupling approach in both space-fixed and body-fixed co-ordinates. The secular equation method and its link to close coupling is presented.

## 1.6 Variational Calculations in Internal Co-ordinates

The variational normal co-ordinate/Watson Hamiltonian approach, as typified by Whitehead and Handy[24], was shown to be problematic in the early eighties when these so-called 'floppy' systems were studied. In particular, studies on KCN[32,33,34] and $CH_2^+$[35,36,37,38,39,40,41] highlighted major weaknesses and practical problems with the Watson Hamiltonian for this type of molecule.

The major reason for the problems with the Eckart-Watson method was the method's inherent assumption of some equilibrium geometry for the molecule,

with the motions of the nuclei being just small displacements from this. For moderately excited systems with more than one potential minimum and/or shallow well(s) this assumption is simply not valid. Clearly new methodologies were necessary.

One of the earliest variational studies which did not use normal co-ordinates was that of Lai on the water molecule[42]. These calculations were performed in the so-called bondlength–bondangle co-ordinates. Following this several workers developed formally exact Hamiltonian operators[34,38,42,43,44,45] in a variety of internal co-ordinates for different types of molecule. One drawback is that it can be shown that in body-fixed internal co-ordinates the Hamiltonian operator will always have singular points[46], although one may have the power to avoid them or possibly move them. The major advantage though is that the Eckart assumption has been dropped and very large amplitude internal motions can be catered for without any bias.

Sutcliffe[46] has been a pioneer of such internal co-ordinate techniques. He and Tennyson[47] produced an exact triatomic Hamiltonian operator in the most general set of internal co-ordinates. A large subset of those co-ordinates (shown in Figure 2.1 of chapter 2) is used in the theory sections later in this thesis.

A further important advance has been the treatment of rotational excitation. Tennyson and Sutcliffe[48] introduced a very powerful two-step rotational method in 1986, and it is now generally accepted that the problem of rotational excitation is solved. The calculations of Miller and Tennyson[49] at the rotational dissociation of $H_3^+$ exemplify this. A similar, but less flexible, method was proposed at about the same time by Chen and co-workers in their rotational studies of the water molecule[50].

These theoretical advances have made it possible now to perform calculations on certain triatomic systems to near-spectroscopic accuracy[7]. Consequently

there is now a reasonable amount of theoretical data available, and indeed public-domain computer packages exist to enable 'routine' (albeit sometimes restricted) calculations to be made on small systems[51,52]. As well as the conventional benefits to experimental spectroscopy, of being able to assign, predict and interpret spectra, astrophysics is now gaining much assistance from this field of research also.

The variational bound state methods mentioned above typically employs a Finite Basis Representation (FBR) in the internal co-ordinates of the molecule. This means essentially that the Hamiltonian operator for the system is represented, on the ground state potential energy surface, in terms of matrix elements linking some set of (usually orthogonal) polynomial basis functions – the internal co-ordinates being their argument. In this type of calculation bending motions are usually carried by (associated) Legendre polynomials or Jacobi functions. The radial co-ordinates are usually represented in either harmonic or Morse-type functions that are 'adapted' to the potential, or sometimes spherical oscillator functions. There is however a very wide range of radial functions that various people have used for various systems/motions. Le Roy and co-workers[31], for example, used numerically generated basis functions rather than polynomial functions. The use of Gaussian basis functions has also proved favourable. Bačić and Light[53], for example, found the use of multi-centred Gaussians on the strongly coupled potential surface of HCN/HNC to be useful.

Having chosen the basis in which to represent the wavefunctions, matrix elements are computed to construct the secular matrix. Diagonalisation of this Hamiltonian secular matrix then yields the energies (eigenvalues) and wavefunctions (eigenfunctions) of the molecular bound states. The FBR is explained and discussed in detail in the following chapter. A case study of the $Li_3^+$ metal cluster is also presented.

For a given potential energy surface the FBR method can in principle obtain 'variationally exact' solutions to the nuclear motion problem. In practice what tends to happen, of course, is that fairly accurate wavefunctions can be obtained up to a certain energy, and then one begins to struggle if higher energies are to be calculated. The size of the basis sets becomes the limiting factor in producing manageable matrices. The FBR method is, however, still useful and widely applicable.

## 1.7 Pointwise Representations

The employment of the Discrete Variable Representation (DVR) by Light and co-workers[53,54] about five years ago, was an attempt to alleviate some of the problems encountered in an FBR (see section 2.7). The method has proved to be exceptionally powerful in dealing with very 'floppy' systems which can undergo very large amplitude and strongly coupled motions – accessing highly anharmonic regions of a complicated potential energy surface which might contain several minima and/or critical points.

As implied by the name, the DVR is used to solve the nuclear motion problem in a discretised co-ordinate (or point) space – rather than in the continuous function space of the FBR. The DVR is achieved by taking the Hamiltonian operator in the FBR and transforming to point space using a unitary similarity transformation matrix. Such methods were originally proposed by Harris *et al* [55]. It was subsequently shown by Dickinson and Certain[56], that formal equivalences exist between an FBR and a DVR; the orthogonal transformation to the appropriate quadrature points yields an isomorphism. The major advantage of the DVR is that one can successively construct and diagonalise reduced dimension Hamiltonian matrices, and use a *contracted* set of these intermediate solutions

as a basis to solve the next higher dimension Hamiltonian. This results in a final Hamiltonian matrix of much reduced size (compared to an equivalent FBR calculation) and of very high information content. Another important (computational) advantage is that, to a very good approximation, the DVR theory makes the potential energy function totally diagonal in the DVR grid points.

The idea of diagonalisation and truncation has been used for several years by Carter and Handy[57]. They do not define a grid but rather define reduced dimension Hamiltonian operators with the other co-ordinate(s) frozen at equlibrium. This method is similar to the DVR but certainly not as powerful for strongly coupled or very anisotropic surfaces. The method has been used recently on the HCN/HNC system[58]. Impressive results have also very recently been obtained for $H_3^+$ and $Na_3^+$[59].

An approach similar to the DVR, called the Fourier Grid Hamiltonian method (FGH), has been developed by Marston and Balint-Kurti[60]. It relies on the Fourier transform as the transformation between a momentum and a co-ordinate representation, and utilises heavily (as in the DVR) the idea of the potential being diagonal on some grid of points.

The collocation method for the determination of bound states has been proposed by Yang and Peet[61,62,63]. One attraction of this method is its apparent simplicity compared to conventional variational procedures, and indeed its claim to be the simplest of pointwise methods[61]. The applications of this method appear to have been very limited so far however.

# Chapter 2

# The Finite Basis Representation

## 2.1 The Hamiltonian Operator

This section presents a Hamiltonian operator for the nuclear motion (i.e. assuming the Born-Oppenheimer approximation) of a triatomic molecule in a generalised set of *internal* or *body-fixed* co-ordinates. These co-ordinates describe the relative motions of the nuclei – each internal co-ordinate can be thought of as representing one of the degrees of freedom of the system. Internal co-ordinates are generally considered to be advantageous as they lend themselves naturally to the distinction between rotations and vibrations. Certain computational advantages are also apparent.

For an $N$-body system, the number of internal co-ordinates is $3N-6$. These are arrived at by taking the $3N$ absolute co-ordinates, subtracting away 3 of these which describe the translational motion of the system, and then subtracting another 3 which are associated with the complete rotational motion of the system. Note that for a linear molecule, where one of the rotations is trivial, there are $3N-5$ internal co-ordinates.

A highly generalised set of internal co-ordinates for a triatomic molecule is

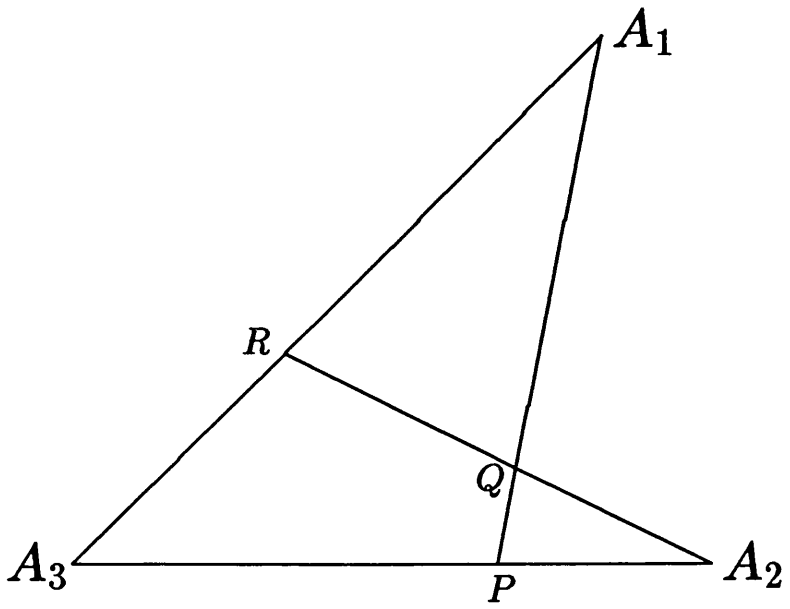


Figure 2.1: Triatomic co-ordinate system. $A_i$ represents atom $i$. The co-ordinates in this work are given by $r_1 = A_2 - R$, $r_2 = A_1 - P$ and $\theta = A_1\hat{Q}A_2$.

shown in Figure 2.1. These co-ordinates are used in the studies presented in this thesis. The system is defined in terms of two lengths and an included angle.

The most general use of these coordinates is given by Sutcliffe and Tennyson[47]. For our use it is sufficient to use the parameters $g_1$ and $g_2$ given by

$$g_1 = \frac{A_3 - P}{A_3 - A_2} \qquad g_2 = \frac{A_3 - R}{A_3 - A_1} \qquad (0 \leq g_1, g_2 \leq 1) \tag{2.1}$$

Subsets of this set include the common Jacobi (or scattering) co-ordinates where $g_1 = \frac{m_2}{m_2+m_3}, g_2 = 0$, bondlength–bondangle co-ordinates with $g_1 = g_2 = 0$, and the so-called Radau co-ordinates[64] with $g_1 = 1 - \frac{\alpha}{\alpha+\beta-\alpha\beta}, g_2 = 1 - \frac{\alpha}{1-\beta+\alpha\beta}$,

where $\alpha = (\frac{m_3}{m_1+m_2+m_3})^{\frac{1}{2}}$ and $\beta = \frac{m_2}{m_1+m_2}$. Choices of co-ordinate systems and their efficiency for different molecules will be discussed in later chapters.

For a three-body system the Hamiltonian is given by

$$\hat{H} = \frac{-\hbar^2}{2}\sum_{i=1}^{3}\frac{1}{m_i}\nabla_i^2(x_i) + V, \tag{2.2}$$

where $\nabla_i^2(x_i)$ is the Laplacian operating on the *ith* particle of mass $m_i$ and $V$ represents the potential energy of the system. The axis frame in this form for the Hamiltonian can be regarded as arbitrary since the potential energy is invariant to translation or rotation.

It is necessary to remove the translational motion from the kinetic energy operators in the Hamiltonian. This is achieved by using a co-ordinate transformation of the form[34,47]

$$t_i = \sum_{j=1}^{N} x_j V_{ji} \qquad\qquad i = 1, 2, ..., N-1$$

or

$$\mathbf{t} = \mathbf{x}\,\mathbf{V} \tag{2.3}$$

where N is the total number of particles and the elements of $\mathbf{V}$ are chosen such that

$$\sum_{j=1}^{N} V_{ji} = 0, \qquad\qquad i = 1, 2, ..., N-1 \tag{2.4}$$

to ensure the invariance of the $t_i$ under uniform translation. The $t_i$ are often said to be a set of space-fixed coordinates. In terms of the new coordinates the translation-free part of the kinetic energy operator can be written as

$$\hat{K} = \frac{-\hbar^2}{2}\sum_{i,j=1}^{N-1}\mu_{ij}^{-1}\vec{\nabla}(t_i).\vec{\nabla}(t_j) \tag{2.5}$$

where $\vec{\nabla}(t_i)$ is the usual grad operator expressed in the variable $t_i$ and where $\mu_{ij}^{-1}$ is

$$\mu_{ij}^{-1} = \sum_{k=1}^{N} m_k^{-1} V_{ki} V_{kj} \tag{2.6}$$

in which the $m_k$ are the particle masses. For ease of writing, the diagonal reduced masses, $\mu_{ii}$, will be written simply as $\mu_i$.

For the co-ordinates of interest here, in terms of $g_1$ and $g_2$, **V** may be written as

$$\mathbf{V} = \begin{pmatrix} -g_2 & 1 \\ 1 & -g_1 \\ g_2 - 1 & g_1 - 1 \end{pmatrix}. \tag{2.7}$$

To enable a unique description of proper rotational motion of the system it is now necessary to fix the molecular system to the axis frame, by a process known as axis embedding. The body-fixed frame is related to the old frame via an orthogonal transformation. The matter of choosing the best embedding can be very important when rotational calculations are performed. Sutcliffe and Tennyson[47] have recently discussed the Hamiltonian operator in a most general set of co-ordinates and embeddings.

The required transformation can be expressed in terms of the conventional Euler angles $(\alpha, \beta, \gamma)$ associated with the rotation of the molecule. This is most conveniently done using a Wigner rotation matrix $D^J_{kM}(\alpha, \beta, \gamma)$, where $J$ is the total angular momentum, $k$ is it's projection onto the body-fixed $z$-axis, and $M$ the projection onto the space-fixed $z$-axis.

If the space-fixed frame is denoted by Cartesian unit vectors $\hat{e}_\alpha$ and the new, embedded frame by $\hat{\epsilon}_\alpha$, then

$$\hat{\epsilon} = \hat{\mathbf{e}}\mathbf{C}, \tag{2.8}$$

where **C** is the orthogonal transformation matrix for the particular embedding.

The next step is to transform Equation (2.5) to the new co-ordinate system. The algebra involved is extremely lengthy and intricate, and omitted here. It has been fully presented by Sutcliffe[46] and also by Tennyson and Sutcliffe[34].

The result is an exact Hamiltonian operator for body-fixed co-ordinates which

has operators in $r_1, r_2$ and $\theta$. The method of choice is then to employ the close-coupling technique of Arthurs and Dalgarno[65].

Effectively this entails defining angular basis functions of the form

$$\mid j,k >= \Theta_{j,k}(\theta) D^J_{Mk}(\alpha,\beta,\gamma) \tag{2.9}$$

where $\Theta_{j,k}(\theta)$ is an associated Legendre polynomial (assumed normalised) in the phase convention of Condon and Shortley[66] and $D^J_{Mk}(\alpha,\beta,\gamma)$ is the Wigner rotation matrix in the Euler angles mentioned above.

One then lets the Hamiltonian operator act on $\mid j,k >$, multiplies from the left by $< j',k' \mid$ and integrates over all the angular variables. This results in an effective radial Hamiltonian of the form

$$\hat{H}(r_1,r_2) = \hat{K}^{(1)}_V + \hat{K}^{(2)}_V + \hat{K}^{(1)}_{VR} + \hat{K}^{(2)}_{VR} + \delta_{k'k} < j'k \mid V(r_1,r_2,\theta) \mid jk >_\theta \tag{2.10}$$

where $V(r_1,r_2,\theta)$ is the potential energy function. The kinetic energy operators are given by

$$\hat{K}^{(1)}_V = \delta_{j'j}\delta_{k'k}\left[-\frac{\hbar^2}{2\mu_1}\frac{\partial^2}{\partial r_1^2} - \frac{\hbar^2}{2\mu_2}\frac{\partial^2}{\partial r_2^2} + \frac{\hbar^2}{2}j(j+1)\left(\frac{1}{\mu_1 r_1^2} + \frac{1}{\mu_2 r_2^2}\right)\right], \tag{2.11}$$

$$\hat{K}^{(1)}_{VR} = -\delta_{j'j}\delta_{k'k}\frac{\hbar^2}{2\mu_1 r_1^2}[J(J+1) - 2k^2] - \delta_{j'j}\delta_{k'k\pm1}\frac{\hbar^2}{2\mu_1 r_1^2}C^{\pm}_{Jk}C^{\pm}_{jk}, \tag{2.12}$$

$$\begin{aligned}\hat{K}^{(2)}_V &= -\delta_{j'j+1}\delta_{k'k}d_{jk}\frac{\hbar^2}{2\mu_{12}}\left(\frac{\partial}{\partial r_1} - \frac{j+1}{r_1}\right)\left(\frac{\partial}{\partial r_2} - \frac{j+1}{r_2}\right) \\ &\quad -\delta_{j'j-1}\delta_{k'k}d_{j-1,k}\frac{\hbar^2}{2\mu_{12}}\left(\frac{\partial}{\partial r_1} + \frac{j}{r_1}\right)\left(\frac{\partial}{\partial r_2} + \frac{j}{r_2}\right),\end{aligned} \tag{2.13}$$

$$\begin{aligned}\hat{K}^{(2)}_{VR} &= \delta_{j'j+1}\delta_{k'k\pm1}\frac{\hbar^2}{2\mu_{12}}C^{\pm}_{Jk}\frac{a_{j,\pm k}}{r_1}\left(\frac{j+1}{r_2} - \frac{\partial}{\partial r_2}\right) \\ &\quad +\delta_{j'j-1}\delta_{k'k\pm1}\frac{\hbar^2}{2\mu_{12}}C^{\pm}_{Jk}\frac{b_{j,\pm k}}{r_1}\left(\frac{j}{r_2} - \frac{\partial}{\partial r_1}\right).\end{aligned} \tag{2.14}$$

The angular factors used above are defined as

$$C^{\pm}_{Jk} = [J(J+1) - k(k\pm1)]^{1/2}, \tag{2.15}$$

$$d_{jk} = \left[\frac{(j-k+1)(j+k+1)}{(2j+1)(2j+3)}\right]^{1/2}, \tag{2.16}$$

$$a_{jk} = \left[\frac{(j+k+1)(j+k+2)}{(2j+1)(2j+3)}\right]^{1/2}, \tag{2.17}$$

$$b_{jk} = \left[\frac{(j-k)(j-k-1)}{(4j^2-1)}\right]^{1/2}. \tag{2.18}$$

The above operators are for the body-fixed $z$-axis embedded along the $r_1$ direction. Embedding the $z$-axis along the $r_2$ direction necessitates the changes $r_1 \leftrightarrow r_2$ and $\mu_1 \leftrightarrow \mu_2$ in the terms involving the rotational quantum numbers J and $k$.

The reduced masses, in terms of the parameters $g_1$ and $g_2$, are given by.

$$\mu_1^{-1} = g_2^2 m_1^{-1} + m_2^{-1} + (1-g_2)^2 m_3^{-1}, \tag{2.19}$$

$$\mu_{12}^{-1} = (1-g_1)(1-g_2)m_3^{-1} - g_2 m_1^{-1} - g_1 m_2^{-1}, \tag{2.20}$$

$$\mu_2^{-1} = g_1^2 m_2^{-1} + m_1^{-1} + (1-g_1)^2 m_3^{-1}. \tag{2.21}$$

It should be noted that coordinate systems for which $\mu_{12}^{-1} = 0$ give $\hat{K}_V^{(2)} = \hat{K}_{VR}^{(2)} = 0$. Such systems include scattering and Radau coordinates, and any other $(g_1, g_2)$ solutions of $\mu_{12}^{-1} = 0$. In this context, such co-ordinate systems are often referred to as orthogonal[51]. This simplification of the Hamiltonian operator can offer computational savings, although in some cases the physics demands the use of non-orthogonal co-ordinates.

## 2.2 Basis Functions

One wishes to express the wavefunction in terms of products of polynomial functions within a finite expansion. The degree of success of a particular calculation can be very highly dependent on the choice of basis functions. Suitable functions must be chosen that offer a good representation for the wavefunction and,

of course, these functions must not misbehave for any energetically accessible geometries of the system. Clearly also, one wishes to choose functions representative enough to allow the size of the basis to be kept as small as possible.

The angular basis functions used in all the calculations presented in this thesis have already been presented in the previous subsection when the kinetic energy operator was integrated over the angular variables. (Note that the potential energy function still requires angular integration – this will be discussed in the following subsection).

The use of the associated Legendre polynomials for angular co-ordinates is fairly common and generally accepted to be a good choice for systems such as those studied in this thesis. The somewhat more general Jacobi functions (of which Legendre functions are a special case) have also been used successfully by Johnson and Reinhardt[64] for calculations on the water molecule.

The situation for the radial co-ordinates is not usually so straightforward. As mentioned in the introduction, Le Roy and co-workers[31,67] have used numerically defined radial basis functions for their work on Van der Waals dimers. For certain simple systems, in particular complexes involving molecular hydrogen, these functions can be very efficient[68]. However in applications to more strongly bound and more strongly coupled systems, such as KCN[33] or LiCN[69], it is more difficult to find a suitable model potential with which to define these numerical functions. Furthermore, even with current supercomputer technology, working with numerically defined functions in more than one dimension is difficult.

For the calculations presented in this thesis the radial stretching co-ordinates appear to be very well represented in terms of the Morse oscillator-like functions presented by Tennyson and Sutcliffe[34]. A Morse function represents the solution to a pseudo-diatomic stretching potential in a reasonably flexible way, and

so would appear to be a good choice of radial basis function. One immediate problem is that the Morse potential only has a finite number of bound states and so for the Morse oscillator functions to form a complete set the inclusion of some continuum functions is required. Tennyson and Sutcliffe neatly got around this problem by defining their Morse oscillator-like functions

$$| n >= H_n(r) = \beta^{\frac{1}{2}} N_{n\alpha} \exp\left(-\frac{x}{2}\right) x^{\frac{\alpha+1}{2}} L_n^{\alpha}(x), \tag{2.22}$$

with

$$x = A \exp\left[-\beta(r - r_e)\right] \tag{2.23}$$

where

$$A = \frac{4D_e}{\beta}, \qquad \beta = \omega_e \left(\frac{\mu}{2D_e}\right)^{\frac{1}{2}}. \tag{2.24}$$

In the above $N_{n\alpha}L_n^{\alpha}$ is a normalised associated Laguerre polynomial[70] and $\mu$ is the reduced mass of the relevant coordinate. This corresponds to solutions of the Morse potential

$$V(r) = D_e \left(1 - \exp[-\beta(r - r_e)^2]\right) \tag{2.25}$$

if $\alpha = A-(2n+1)$ . Instead Tennyson and Sutcliffe decided to work with functions defined by fixing $\alpha$ equal to the integer part of $A$. These functions, the lowest of which corresponds closely to the ground state of the Morse potential, form an orthonormal set and belong to a single set of polynomials.

In principle the parameters which define the Morse potential, $r_e$, $\omega_e$ and $D_e$, can be associated respectively with the equilibrium separation, fundamental frequency and dissociation energy of the relevant coordinate. In practice ($r_e$, $\omega_e$, $D_e$) are treated as variational parameters and optimized accordingly. These optimizable functions have proved very successful for a whole variety of problems. Unless otherwise stated, all the applications discussed in subsequent chapters use Morse oscillator-like functions for the radial coordinates.

Morse oscillators (and the Morse oscillator-like functions) do not behave satisfactorily at $r = 0$. This is not a problem for coordinates which represent explicitly the distance between two nuclear centres as the vibrational wavefunction is vanishingly small at this limit. However, for other coordinates, such as $r_2$ in scattering coordinates, this may be physically accessible for some systems. In atom-diatom scattering coordinates the $r_2 = 0$ geometry corresponds to a linear geometry with the atom inserted at the center-of-mass of the diatom. For systems where such behaviour is significant alternative basis functions have to be found.

Tennyson and Sutcliffe[37,71] suggested the use of spherical oscillators for situations where the $r = 0$ limit is important. These may be defined by

$$| n >= H_n(r) = 2^{\frac{1}{2}}\beta^{\frac{3}{4}}N_{n\alpha}\exp(-\frac{x}{2})x^{\frac{\alpha}{2}}L_n^{\alpha+\frac{1}{2}}(x) \qquad (2.26)$$

$$x = \beta r^2$$

where

$$\beta = (\mu\omega_e)^{\frac{1}{2}} \qquad (2.27)$$

and $(\alpha, \omega_e)$ are treated as variational parameters.

Spherical oscillators have been used successfully for a number of calculations, but have generally been found to be less efficient than the Morse oscillator-like functions when these are also viable. Spherical oscillators have an additional disadvantage. For (quasi-)linear systems the value of $\alpha$ depends on the state being considered[72]. Thus when the system has amplitude at $r = 0$, for instance in its rotational ground state, then $\alpha$ must be chosen equal to zero. But when the same system is then rotationally excited, removing the amplitude from the region, the optimum value of $\alpha$ increases. This is not only inconvenient; it leads to a severe problems in calculating rotational constants for heavy systems by performing calculations for several rotational states. This is because the

usual cancelation of convergence errors which occurs when each calculation is performed with the same basis functions no longer occurs.

For a Finite Basis Representation (FBR) we are now in a position to write down the (unsymmetrized) expression for the wavefunction of the system. In terms of the basis functions described above, the approximation to the $s^{th}$ energy level, $E_s^J$, has a wavefunction

$$\Psi_s^J = \sum_k \sum_{jmn} d_{kjmn}^{Js} \mid j,k > \mid m > \mid n > \tag{2.28}$$

where $\mid m >$ and $\mid n >$ are the radial basis functions associated with the $r_1$ and $r_2$ coordinates respectively, and $\mid j,k >$ are the angular functions defined earlier.

In this approach the variational coefficients, $d_{kjmn}^{Js}$, are determined by diagonalising the secular matrix, with generalised element

$$< j'k'm'n' \mid \hat{H} \mid jkmn > . \tag{2.29}$$

## 2.3 Basis set selection

Performing a calculation within a finite basis representation gives some flexibility about how the basis set is actually chosen. As described above the internal coordinate basis is simply a product of one-dimensional basis functions for each coordinate. If all terms up to some $N_i$ ($i = 1,2,\theta$ for $r_1, r_2, \theta$ respectively), are taken for each expansion then one obtains a basis set of dimension $N_1 N_2 N_\theta$. This basis contains the function $(N_1, N_2, N_\theta)$ but not $(N_1+1,0,0), (0, N_2+1, 0)$ or $(0,0,N_\theta+1)$. It is therefore likely that this is not the best method of choosing a product function.

Two methods of preselecting basis functions have been tried for the FBR calculations on $Li_3^+$ presented in §2.8. One method calculates the diagonal matrix element for a large number of candidate basis functions. The final basis is then

chosen as the functions that have the $L$ lowest diagonal elements, where $L$ is the size of secular matrix desired. This approach can be regarded as loosely founded on perturbation theory. The logical next step has been taken by Hutson[73] and Hutson and Le Roy[74] who developed a method which used perturbation theory to give the contribution from functions omitted from the basis set expansions.

An alternative method is based on quantum numbers. All functions are selected which satisfy the relationship

$$Q \geq \frac{n_1}{d_1} + \frac{n_2}{d_2} + \frac{n_\theta}{d_\theta}, \tag{2.30}$$

where $n_i$ are the number of quanta in mode $i$. The $d_i$ serve to weight this selection as one mode, for example a low frequency bend, may require more functions than some other mode. This method has also been used by other workers, see for example refs. [50,75].

These methods, which can also be used in hybrid form, are both found to give greatly enhanced convergence compared to taking the full product. Further discussion, including comparison of convergence with the different selection criteria, can be found in ref. [76].

## 2.4 Matrix Elements

The integration for the matrix elements of the potential energy function and the radial basis functions is now discussed. Note that, providing the integrals can be evaluated 'exactly', then the FBR method is strictly variational and so converged answers should be exact for a given potential energy surface.

If the potential is expressed as an expansion in Legendre polynomials in $\cos\theta$,

$$V(r_1, r_2, \theta) = \sum_\lambda V_\lambda(r_1, r_2) P_\lambda(\cos\theta), \tag{2.31}$$

then the matrix elements over the potential for the angular basis functions can be evaluated analytically as

$$< j'k' \mid P_\lambda(\cos\theta) \mid j,k >= \delta_{k'k}(-1)^k[(2j'+1)(2j+1)]^{\frac{1}{2}} \begin{pmatrix} j' & \lambda & j \\ 0 & 0 & 0 \end{pmatrix} \begin{pmatrix} j' & \lambda & j \\ -k & 0 & k \end{pmatrix}. \tag{2.32}$$

The angular integration is over all angular variables and the $3j$ symbols making up the Gaunt coefficient are conventional. If the potential energy function in question is not expressed in the Legendre expansion shown above then this can be very efficiently arranged by employing a Gauss-Legendre quadrature scheme[77]. The appropriate quadrature yields the coefficients $V_\lambda$ for each $(r_1, r_2)$ of interest.

Expressions are now sought for matrix elements over the radial operators in the kinetic energy terms given by Equations (2.11) to (2.14). It should be noted that for orthogonal co-ordinate systems the only radial operators in question are $r^{-2}$ and $\partial^2/\partial r^2$. For non-orthogonal co-ordinates, when $\mu_{12} \neq 0$, there are also contributions from $r^{-1}$ and $\partial/\partial r$. Using the technique given by Tennyson and Sutcliffe[34] it is possible to find analytic closed forms for the matrix elements of the differential operators (for the Morse oscillator-like functions):

$$\begin{aligned} < n' \mid \frac{\partial^2}{\partial r^2} \mid n > \; = \; & \frac{\beta^{\frac{1}{2}}}{4}(\delta_{n'n}[2n(\alpha+n+1)+\alpha+1]^{\frac{1}{2}} \\ & -\delta_{n'n-2}[(\alpha+n)(\alpha+n-1)n(n-1)]^{\frac{1}{2}} \\ & -\delta_{n'n+2}[(\alpha+n+2)(\alpha+n+1)(n+2)(n+1)]^{\frac{1}{2}}) \end{aligned} \tag{2.33}$$

$$\begin{aligned} < n' \mid \frac{\partial}{\partial r} \mid n > \; = \; & \frac{\beta}{2}(\delta_{n'n+1}[(n-1)(\alpha+n-1)]^{\frac{1}{2}} \\ & -\delta_{n'n-1}[(n-2)(\alpha+n-2)]^{\frac{1}{2}}). \end{aligned} \tag{2.34}$$

There is no simple closed form for the matrix elements over $r^{-1}$ or $r^{-2}$. The usual procedure is to use Gauss–Laguerre integration.

In this case of spherical oscillator functions all the kinetic energy matrix

elements can be evaluated analytically[37]:

$$< n \mid \frac{\partial^2}{\partial r^2} \mid n' >= \frac{\beta^{\frac{1}{2}}}{2} \left( \delta_{n'n}(2n + \alpha + \frac{3}{2}) + \delta_{n'\pm 1,n} \left[ \frac{n + \frac{1}{2} \mp \frac{1}{2}}{n + \alpha + 1 \mp \frac{1}{2}} \right]^{\frac{1}{2}} \right) + < n \mid r^{-2} \mid n' > \tag{2.35}$$

$$< n \mid r^{-2} \mid n' >= \frac{\beta^{\frac{1}{2}}}{2} \left[ \frac{n!}{n'!} \frac{\Gamma(n' + \alpha + \frac{3}{2})}{\Gamma(n + \alpha + \frac{3}{2})} \right]^{\frac{1}{2}} \sum_{\sigma=0}^{n'} \frac{n'!}{\sigma!} \frac{\Gamma(\sigma + \alpha + \frac{1}{2})}{\Gamma(n' + \alpha + \frac{3}{2})} \qquad n' \leq n \tag{2.36}$$

where the numerical reason for the apparently inefficient grouping of the factorial and Γ-function terms in Equation (2.36) will be explained in the following section.

The radial integrals over the potential energy are performed using a Gaussian quadrature also. The accuracy of the quadrature integrations can be checked at an early stage in a particular calculation by altering the number of integration points for different runs. The Gaussian quadrature integration schemes used in the computer codes developed for this work are based on those given by Stroud and Secrest[77].

## 2.5 Symmetry

It is not strictly necessary to use the full symmetry of a system when performing variational calculations. However doing so not only makes the calculations computationally more efficient, but also eases the task of making suitable assignments to calculated states.

In considering the symmetries involved in the ro-vibrational wavefunction it is necessary to consider both the permutation symmetry of the atoms in the molecule and the symmetry of the rotational portion of the wavefunction. The group theory involved is this problem has been described by Bunker[78] and Ezra[79].

For the triatomics $A_3$, $AB_2$ and ABC, permutation symmetry groups $S_3$, $S_2$ and $S_1$ apply respectively. In the coordinate system used here it is not possible

to adapt the wavefunction *a priori* to $S_3$ symmetry[80]. $S_1$ has no permutation symmetry; so this discussion of symmetry is restricted to $AB_2$ systems.

In the flexible coordinates of Figure 2.1, the interchange symmetry can be carried by the angular or the radial coordinates depending on the choice of $(g_1, g_2)$. In scattering coordinates, $(g_1 = 0.5, g_2 = 0.0)$ for an atom-diatom system with a homonuclear diatomic, interchanging the like atoms is equivalent to changing $\theta \rightarrow \pi - \theta$ . In a FBR, this symmetry is naturally carried by Legendre polynomials which have the property that even polynomials are symmetric (denoted $q = 0$) with respect to interchange of the two like atoms and odd polynomials are antisymmetric $(q = 1)$.

If coordinates are chosen in which $g_1 = g_2$ (these include both Radau and bondlength-bondangle coordinates provided that the odd atom is chosen as the central atom), then interchanging the atoms is equivalent to the exchange $r_1 \leftrightarrow r_2$. Symmetrization in this case requires the selection of identical functions, $| m >$, to carry the $r_1$ motions to those, $| n >$, used for the $r_2$ coordinate. In this case the functions can be written, for $q = 0$ or 1, as

$$| m, n, q >= 2^{-\frac{1}{2}}(1 + \delta_{mn})^{-\frac{1}{2}}(| m >| n > +(-1)^q | n >| m >) \qquad m \geq n + q. \tag{2.37}$$

However, whereas the angular symmetrisation is consistent with embedding the body-fixed z-axis along either $r_1$ or $r_2$, the radial symmetrisation is only achieved with the z-axis embedded along the bisector of $r_1$ and $r_2$. This means that for calculations involving rotationally excited states the Hamiltonian used in this work cannot be fully symmetrised for coordinates with $g_1 = g_2$.

For each embedding the rotational functions are symmetrised by considering the behaviour of the projection of the total angular momentum on the body-fixed z-axis, k, for the combined rotational and bending functions. The symmetrised

functions take the form, for $k \geq p$,

$$| j,k,p >= 2^{-\frac{1}{2}}(1+\delta_{k0})^{-\frac{1}{2}}[\Theta_{jk}(\theta)D^J_{Mk}(\alpha,\beta,\gamma) + (-1)^p\Theta_{j-k}(\theta)D^J_{M-k}(\alpha,\beta,\gamma)]. \tag{2.38}$$

The total parity is given by $(-1)^{J+p}$ with p = 0 or 1. States with p = 0 and 1 are conventionally labelled e and f states respectively[81].

This rotational symmetrisation does not affect the effective vibrational kinetic energy operators, $\hat{K}_V^{(1)}$ and $\hat{K}_V^{(2)}$, and potential energy term given above. It modifies the $\hat{K}_{VR}$ terms by introducing a factor of $\sqrt{2}$ into terms coupling $p = 0, k = 0$ to $p = 0, k = 1$. Of course, in this symmetrized basis, basis functions differing in $p$ are decoupled. Furthermore for each block it is necessary only to consider $k$ values running from $p$ to $J$.

In fact the observation that the $p = 1$ secular matrix is simply a sub-matrix of the $p = 0$ secular matrix (with the rows and columns involving $k = 0$ removed) means that this matrix need not be explicitly calculated.

## 2.6 Rotational Excitation

The previous section discussed methods for calculating vibrational wavefunctions of triatomic systems. In fact the formalism is presented in a sufficiently general manner that it could be used directly to perform fully ro-vibrational calculations. Indeed, until 1986, this was how calculations which included full ro-vibrational or Coriolis coupling were performed.

Analysis of the angular basis functions given previously shows that for a direct solution of the ro-vibrational problem the size of the secular problem increases as (2J+1). Symmetrisation reduces this to two separate secular matrices increasing as J and J+1, but does not solve the basic difficulty with large J calculations. The result of this is that this approach has never been used for calculations with

J larger than 4.

A way round this problem, using a two-step variational procedure, was suggested by Tennyson and Sutcliffe[48]. The first step of this procedure is to solve the 'vibrational' problem obtained by ignoring the off-diagonal Coriolis coupling terms. This approximation is equivalent to assuming k, the projection of the total angular momentum on the body-fixed z-axis, is a good quantum number. For certain systems this approximation is very accurate[69,82,83].

Ignoring rotational symmetry, the eigenfunctions of the effective, Coriolis decoupled Hamiltonian

$$\hat{H}^k(r_1,r_2) = \hat{K}_V^{(1)} + \hat{K}_V^{(2)} + \delta_{k'k}\left(\hat{K}_{VR}^{(1)} + \hat{K}_{VR}^{(2)}\right) + < j',k \mid V(r_1,r_2,\theta) \mid j,k >_\theta \tag{2.39}$$

can be written

$$\mid i,k >= \sum_{jmn} c_{jmn}^{Jki} \mid j,k > \mid m > \mid n > \tag{2.40}$$

with corresponding eigenenergy $\epsilon_i^{Jk}$. The second step of the procedure then consists of using these eigenfunctions, symmetrised, as a basis for the exact effective Hamiltonian. This gives a Hamiltonian matrix of the form

$$< i',k' \mid \hat{H} \mid i,k >= \delta_{k'k}\delta_{i'i}\epsilon_i^{Jk} + \delta_{k'k\pm1}(1+\delta_{k0}+\delta_{k'0})^{\frac{1}{2}} < i',k' \mid \hat{K}_{VR}^{(1)} + \hat{K}_{VR}^{(2)} \mid i,k > \tag{2.41}$$

where symmetrising the rotational basis set introduces a factor of $\sqrt{2}$ in off-diagonal terms involving $k = 0$.

The form of this Hamiltonian is further simplified in orthogonal coordinates where $\hat{K}_{VR}^{(2)} = 0$ and the off-diagonal element is given by

$$< i',k\pm1 \mid \hat{K}_{VR}^{(1)} \mid i,k >= - < i',k\pm1 \mid \delta_{j'j}\delta_{n'n} C_{Jk}^{\pm} C_{jk}^{\pm} \frac{\hbar^2}{2\mu_1 r_1^2} \mid i,k > \tag{2.42}$$

$$= -C_{Jk}^{\pm} \sum_{jmn} C_{jk}^{\pm} c_{jmn}^{Jki} \sum_{m'} c_{jmm'}^{Jk\pm1i'} < m' \mid \frac{\hbar^2}{2\mu_1 r_1^2} \mid m > .$$

This expression is valid when the body-fixed $z$-axis is embedded parallel to $r_1$. Solving the rotational problem in this fashion has major advantages. Firstly it is not necessary to include all the solutions of the first step to obtain converged solutions for the second. The best algorithm for this[84] is to select the intermediate basis functions according to an energy ordering criteria i.e. according to the $\epsilon_i^{Jk}$. This results in a greatly reduced final secular matrix. This reduction in size is particularly drastic for the case where $k$ is a nearly good quantum number, hence the importance of selecting the best embedding.

Secondly, the secular matrix constructed for the second step has a characteristic sparse structure, see Figure 2.2. All the elements are zero with the exception of the diagonal elements and one off-diagonal block linking $k$ with $k \pm 1$. Thus it is only necessary to store the non-zero elements, reducing the core requirement by a factor of approximately J[85]. Furthermore this sparse matrix can be rapidly diagonalized using an iterative technique to obtain the eigenenergies and wavefunctions of interest. This diagonalisation is so efficient it is actually quicker to solve the full problem, the one obtained by not truncating the intermediate basis, in two steps than directly in one step[85] !

Finally, within the symmetrised rotational basis, the secular matrix for p = 1 is simply a sub-matrix of that for p = 0. The solution to both problems can thus be obtained using the same matrix by simply removing the portion of the p = 0 matrix involving k = 0[86].

For this symmetrised problem, the $s^{th}$ solution of the second step can be written

$$\Psi_s^{Jp} = \sum_{ik} b_{ik}^{Jps} \mid i,k,p > \tag{2.43}$$

with corresponding eigenenergy $E_s^{Jp}$. The coefficient vectors $\mathbf{b}^{Jps}$ can then be back transformed to yield coefficients of the wavefunction in terms of the original

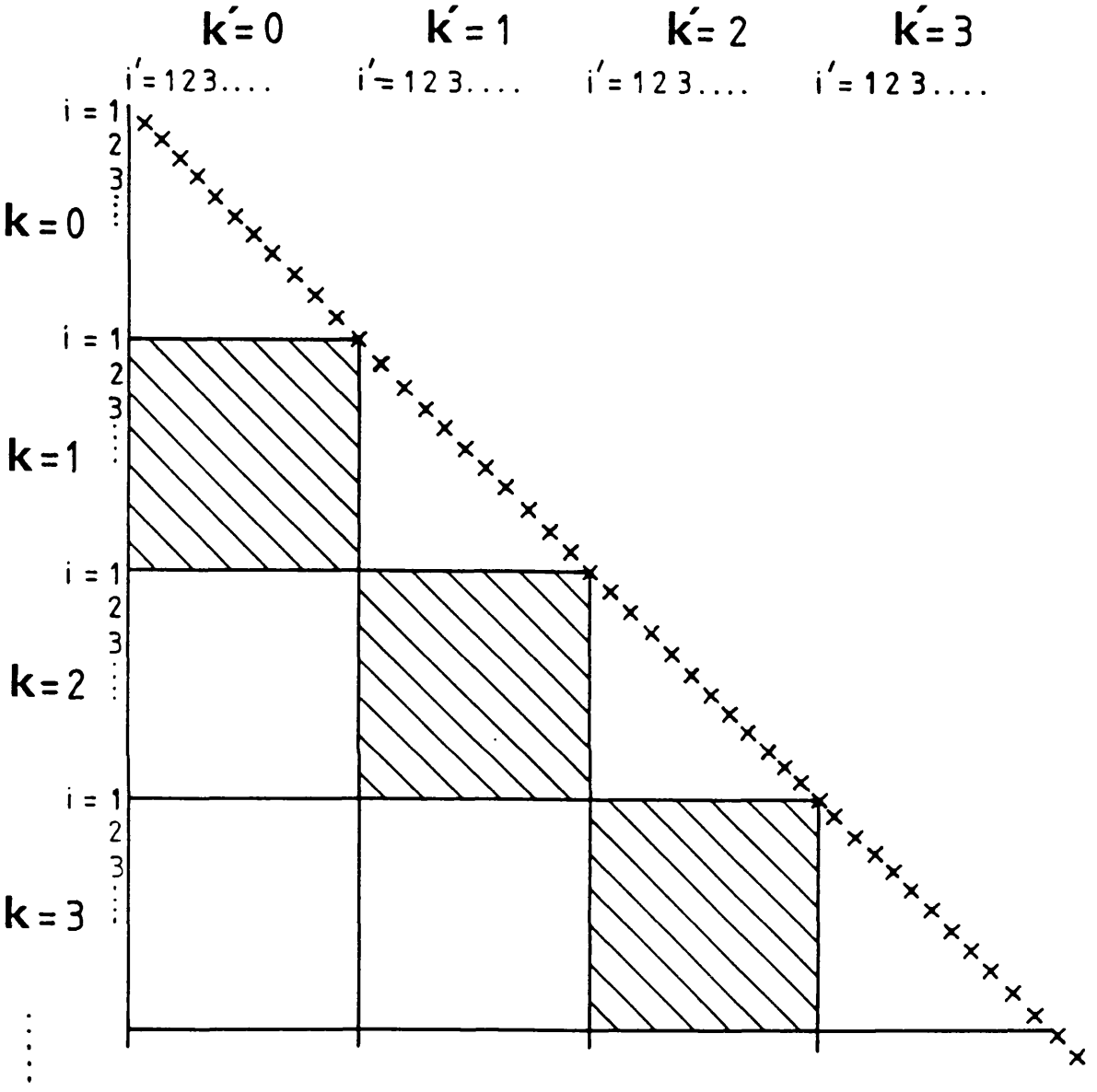


Figure 2.2: Structure of the secular matrix for the second variational step (see text).

basis functions

$$d^{Jps}_{kjmn} = \sum_i b^{Jps}_{ik} c^{Jki}_{jmn}. \tag{2.44}$$

These coefficients are important for calculating properties of the wavefunction and in particular transition intensities.

There is one important difference between the two-step procedure outlined above and that proposed by Chen *et al* [50]. Whereas this one solves a new 'vibrational' problem for each $(J, \mid k \mid)$ combination, that of Chen *et al* simply uses the solutions of the $J = 0$ problem to expand all rotationally excited problems of interest. This obviously leads to a substantial saving in the number of vibrational problems that have to be solved. The problem with Chen *et al* 's method is that the intermediate basis functions do not allow for rotational distortion effects and, more seriously, the method fails for bent molecules when they start sampling linear geometries. This means that for studies involving any large amplitude vibrations or extreme rotational motion, the method of Tennyson and Sutcliffe needs to be employed.

## 2.7 Problems in an FBR

As mentioned earlier, when using FBR techniques a point of prime importance (obviously) is to choose functions which offer the best representation for the wavefunction, so that the size of the basis set and hence the secular matrix can be kept to a minimum. The practical limitation here of course is that one is often restricted in computer time and memory. It is usually the available in-core memory that is limiting in these calculations. Nearly all of the cpu time (for a well written code) will be spent in the diagonalisation of the final Hamiltonian matrix.

The size of the basis can become excessively large for two main reasons.

Firstly, it is clear that if very high energy states are to be sought then one must introduce more functions into the basis set to converge the higher levels. The situation is certainly not helped by the (sometimes) dramatic increase in density of states. Secondly, the basis set can demand a very large amount of functions if the molecule in question has a very complicated potential energy surface and can undergo very large amplitude, erratic and coupled motions.

Although, as shown §2.1.3, one can attempt to reduce the size of the basis in an FBR calculation, this still does not solve the second problem mentioned above.

## 2.8 A Case Study: The Lithium Trimer Cation

This section contains an account of some investigations made into the two most abundant isotopomers of the metal cluster ion $^7Li_3^+$ using a Finite Basis Representation in all three internal co-ordinates. This investigation is presented by way of a case study of the FBR methods for the calculation of ro-vibrational wavefunctions. Computed dipole transition intensities are also presented for this system.

Understanding simple alkali metal clusters, such as $Li_3^+$, gives important insight into the nucleation processes from free atom to metallic state. It has also been suggested that alkali cluster ions may be important in the next generation of lamps and tunable lasers[87]. The spectrum of $Li_3^+$ has yet to be observed, but Searles, Dunne and von Nagy-Felsobuki (SDF)[88,89,90] performed a series of *ab initio* studies aimed at elucidating its vibrational spectrum to facilitate laboratory observation of this species. The FBR studies described here are aimed to corroborate their findings and to extend their work in two important aspects.

Firstly, SDF mainly considered vibrational motion in their studies, rotations

being only considered through the vibrational averaging of certain matrix elements. A knowledge of the rotational constants of the system is important for any observational study. Secondly, SDF studied only the symmetric isotopomers $^7Li_3^+$ and $^6Li_3^+$. As exemplified by Tennyson and Sutcliffe[91] on the $H_3^+$ molecular ion, the study of the asymmetric isotopomer(s) is at least as important as the purely symmetric species. In particular the symmetric ions studied by SDF do not have any dipole allowed pure rotational transitions.

It is estimated that $^7Li_3^+$ has a natural abundance of about 80% and $^7Li_2\,^6Li^+$ of about 18% in any sample of $Li_3^+$. A spectroscopic analysis of both these isotopomers is therefore presented to aid the observation of $Li_3^+$.

In this work, ro-vibrational energy levels and wave functions are calculated using the two-step variational method described earlier, and the analytic $5^{th}$-order exponential Dunham expansion potential energy surface used by SDF[89] to represent their Configuration Interaction (CISD) data. Dipole transition intensities are also calculated using the dipole surface given by SDF[90].

The method of solution is that described above. This FBR method has been employed by Tennyson and co-workers for a series of studies on the $H_3^+$ system (see, for example, references [83,92,93,94,95]), and has led to thorough theoretical understanding of the spectroscopy of the low-lying states of this system and its deuterated isotopomers. In particular, the rotational constants obtained for the ground state and fundamentals of $H_3^+$, $H_2D^+$, $D_2H^+$ and $D_3^+$ are competitive in accuracy with those obtained experimentally.

### 2.8.1 Computational Details

The vibration-only (J=0) problem was solved in body-fixed scattering coordinates. These coordinates represent the interaction between an atom at distance $r_2$ and angle $\theta$ from the centre of mass of a diatom whose bondlength is $r_1$.

Scattering co-ordinates are precisely those shown in Figure 2.1, when point $R$ coincides with atom $A_1$ and point $P$ is at the centre of mass of the diatom $A_2A_3$ ( $g_1 = \frac{m_2}{m_2+m_3}$, $g_2 = 0$ ). These orthogonal coordinates are particularly suitable for atom-diatom systems that tend to be 'floppy' and/or isomerise. Scattering co-ordinates are actually found also to be very useful in the study of van der Waals complexes where an atom may be very loosely bound to a diatomic molecule. They have proved so successful for studies on $H_3^+$ and thus a natural choice for $^7Li_3^+$ . The body-fixed z axis was taken parallel to the $r_2$ coordinate. Associated Legendre functions were used to carry the angular coordinate and the Morse oscillator-like functions defined previously to carry the two radial coordinates[34].

The parameters in the Morse oscillator-like functions ($r_e$,$D_e$,$\omega_e$) were adjusted variationally to yield the best radial basis. The parameters for the calculations presented here are given in Table 2.1. These parameters were found to give a good representation for both ions considered and so could be kept the same for the asymmetric species.

In test calculations basis functions were pre-selected for the calculation according to a number of criteria (given in §2.3)[76]. For this system the most efficient method proved to be selection by weighted quantum numbers. As shown earlier, this meant that all products of the one-dimensional basis functions were included that satisfied the condition

$$Q \geq m + n + \frac{j}{6} \tag{2.45}$$

for a given value of $Q$. In Equation (2.43) m, n and j are the number of quanta in the basis function representing the $r_1, r_2$ and $\theta$ coordinates respectively. Note that in each expansion the first function has quantum number zero. Tables 2.1 and 2.2 demonstrate the convergence of the $^7Li_3^+$ and $^7Li_2{}^6Li^+$ band origins as a function of $Q$. In both cases the fundamentals were converged to 0.01 $cm^{-1}$ for $Q$ =9, an accuracy very much higher than one might expect for the potential.

Table 2.1: Parameters used for Morse oscillator-like functions (in atomic units):

| co-ordinate | $r_e$ | $D_e$ | $\omega_e$ |
|---|---|---|---|
| $r_1$ | 5.85 | 0.046 | 0.001302 |
| $r_2$ | 5.01 | 0.040 | 0.001300 |

Table 2.2: Calculated vibrational band origins for $^7Li_3^+$ in $cm^{-1}$.

| $\nu_1\nu_2\ell$ | symmetry | parity[a] | $Q$=6 | $Q$=7 | $Q$=8 | $Q$=9 | SDF[89] |
|---|---|---|---|---|---|---|---|
| 0 1 1 | E | e | 226.27 | 226.04 | 226.01 | 225.99 | 225.98 |
| | | o | 225.94 | 225.89 | 225.77 | 225.98 | |
| 1 0 0 | $A_1$ | e | 298.92 | 298.79 | 298.78 | 298.77 | 298.76 |
| 0 2 0 | $A_1$ | e | 449.01 | 448.35 | 447.93 | 447.80 | 447.76 |
| 0 2 2 | E | e | 453.86 | 451.83 | 451.32 | 451.10 | 451.05 |
| | | o | 451.95 | 451.15 | 450.97 | 451.07 | |
| 1 1 1 | E | e | 522.58 | 521.00 | 520.67 | 520.57 | 520.54 |
| | | o | 521.16 | 520.52 | 520.37 | 520.55 | |
| 2 0 0 | $A_1$ | e | 596.80 | 595.67 | 595.53 | 595.48 | 595.47 |

[a] Parity of Legendre functions used in the basis:

e = even; o = odd.

The first step of the rotationally excited calculations involves diagonalising a series of vibrational calculations in which it is assumed that the projection of the total angular momentum onto the body-fixed z-axis, k, is a good quantum number. These results are then energy ordered and the lowest $I$ eigenvectors used as a basis for the fully-coupled problem. It was found that the rotational calculations converged rapidly with $I$. For all the results presented here the first step was solved with N=8 and $I$ taken as 25 $\times$ (J+1-p). This gave rotational levels converged to better than 0.01 $cm^{-1}$ relative to the appropriate band origin.

The calculations used the programs SELECT, TRIATOM and ROTLEV[96] which have been updated to drive a new program DIPOLE[97]. This allows for the calculation of transition dipole moments, the theory of which can be found elsewhere[98,99].

### 2.8.2 Results and Discussion

Table 2.2 presents results for the vibrational band origins of $^7Li_3^+$ as a function of $Q$. The slight splitting between the even and odd components of the degenerate E states is caused by the failure of the method to allow for the full $D_{3h}$ symmetry of the system. This splitting can provide a useful indication of convergence. The results are well converged for $Q$=8 and agree closely with those of SDF, which are presented for comparison.

Table 2.3 presents the analogous results for $^7Li_2{}^6Li^+$ . Again the results are well converged at the $Q$=8 level. It may be interesting to note that the splitting between $\nu_2$ and $\nu_3$ caused by lowering the symmetry of the system by isotopic substitution is only 0.5 $cm^{-1}$, in contrast to $H_2D^+$ where it is 130 $cm^{-1}$[100].

Rotational calculations were performed for values of the total angular momentum, J, $\leq$ 4. Rather than presenting the individual levels, the results of least squares fits to the more compact parameterised Hamiltonians due to Watson *et*

Table 2.3: Calculated vibrational band origins for $^{7}Li_2\,^{6}Li^{+}$ in $cm^{-1}$.

| $\nu_1\nu_2\nu_3$ | symmetry | $Q$=7 | $Q$=8 | $Q$=9 | SF[109] |
|---|---|---|---|---|---|
| 0 1 0 | $A_1$ | 231.44 | 231.41 | 231.40 | 231.40 |
| 0 0 1 | $B_2$ | 231.93 | 231.93 | 231.93 | 231.92 |
| 1 0 0 | $A_1$ | 307.31 | 307.30 | 307.30 | 307.29 |
| 0 2 0 | $A_1$ | 459.16 | 458.88 | 458.80 | 458.76 |
| 0 0 2 | $A_1$ | 462.35 | 462.11 | 462.06 | 462.04 |
| 0 1 1 | $B_2$ | 462.92 | 462.83 | 462.81 | 462.80 |
| 1 0 1 | $B_2$ | 534.34 | 534.28 | 534.28 | 534.27 |
| 1 1 0 | $A_1$ | 535.17 | 534.92 | 534.86 | 534.84 |
| 2 0 0 | $A_1$ | 612.50 | 612.36 | 612.34 | 612.33 |

*al* [101,102] are given. For a full discussion of assigning and parameterising the levels of $X_3$ systems see Watson[103]. Note however that K in Tables 2.4 and 2.6 refers to the projection of J along the $C_3$ symmetry axis of $^7Li_3^+$ . It was found that including up to quartic terms gave a very good representation of the data as can be judged by the standard deviations given in Tables 2.4 and 2.5.

$^7Li_2\,^6Li^+$ is an asymmetric top with $\kappa \simeq 0.62$. One feature of the results for $^7Li_2\,^6Li^+$ presented in Table 2.5 is the very strong Coriolis interaction between the nearby $\nu_2$ and $\nu_3$ fundamentals. Because the rotational manifolds of the two states not only overlap but are also strongly coupled, they were fitted simultaneously with no attempt at vibrational pre-assignment. Instead, the vibrational states were assigned by analysis of the eigenvectors produced by the fitting procedure. Even for J=1 there was up to 20% mixing between the levels. As in the equivalent bands of $H_2D^+$ [104], any experimental analysis of these fundamentals will undoubtedly prove difficult.

Tables 2.6 and 2.7 present dipole allowed transitions for $^7Li_3^+$ and $^7Li_2\,^6Li^+$. Only transitions involving the vibrational ground state where $J$ equals 0 or 1 for either level are given. These give a representative sample of the transition intensities to be expected for this system.

For $^7Li_3^+$ the only allowed transitions involve excitation of the $\nu_2$ fundamental. For the $\nu_2$ state the $\ell$ doubling introduces the extra quantum numbers G (=K+U) and U (=$\pm$ 1) [103]. For this band there is the additional selection rule G=K.

In contrast, for $^7Li_2\,^6Li^+$ all three fundamentals are infrared red active and the ion also has a pure rotational spectrum as a result of its permanent dipole along the b axis (our z-axis). If $Li_3^+$ was a rigid system, the transition dipole for the $1_{11} - 0_{00}$ transition would be equal to the permanent dipole of $^7Li_2\,^6Li^+$ . In fact this transition gives a value of $\mu$ of 0.4172 D in very close agreement with the value calculated for the equilibrium geometry at the centre of mass of 0.4157

Table 2.4: Rotational constants[103] for $^7Li_3^+$ in $cm^{-1}$.

| Parameter | Ground state | $\nu_1$ | $\nu_2$ |
|---|---|---|---|
| B | 0.5319 | 0.5260 | 0.5321 |
| C | 0.2641 | 0.2603 | 0.2629 |
| $10^5 D^{JJ}$ | 0.9 | -9.9 | 2.6 |
| $10^5 D^{JK}$ | -1.4 | 2.6 | 1.4 |
| $10^5 D^{KK}$ | 0.6 | -0.7 | -0.7 |
| $C\zeta$ | | | -0.2588 |
| $10^5 \eta^J$ | | | -4.4 |
| $10^5 \eta^K$ | | | 2.5 |
| $10^2 q$ | | | -1.007 |
| $10^5 q^J$ | | | 1.0 |
| $10^5 q^K$ | | | -16.5 |
| No. [a] | 16 | 16 | 32 |
| $10^3 \sigma^b$ | 0.01 | 4.1 | 1.2 |

[a] Number of levels fitted

[b] Standard deviation on fits

Table 2.5: Rotational constants[103] for $^{7}Li_2\,^{6}Li^{+}$ in $cm^{-1}$.

| Parameter | Ground state | $\nu_1$ | $\nu_2$ | $\nu_3$ |
|---|---|---|---|---|
| A | 0.5908 | 0.5867 | 0.6030 | 0.5777 |
| B | 0.5320 | 0.5293 | 0.5206 | 0.5406 |
| C | 0.2779 | 0.2763 | 0.2173 | 0.3343 |
| $10^5\Delta^{JJ}$ | 0.5 | -0.1 | -185.1 | 224.2 |
| $10^5\Delta^{JK}$ | -0.1 | 1.3 | 443.7 | -876.6 |
| $10^5\Delta^{KK}$ | 0.8 | -0.2 | -182.0 | 708.6 |
| $10^3\delta^{J}$ | | | 1.10 | -0.91 |
| $10^3\delta^{K}$ | | | -1.88 | 1.78 |
| $\varsigma_{23}$ | | | -0.5003 | |
| $10^3\varsigma^{J}$ | | | 2.61 | |
| $10^3\varsigma^{K}$ | | | -3.16 | |
| $10^3\alpha_{23}$ | | | -8.09 | |
| No. [a] | 24 | 24 | 48 | |
| $10^3\sigma^{b}$ | 0.0 | 0.0 | 6.9 | |

[a] Number of levels fitted.

[b] Standard deviation on fits.

Table 2.6: Dipole allowed ro-vibrational transitions for $^7Li_3^+$ . All transitions are for the $\nu_2$ fundamental. The energy levels are given relative to the J=0 state of the vibrational ground state. (Powers of ten in brackets).

| $J'G'_U$–$J''K''$ | E' ($cm^{-1}$) | E'' ($cm^{-1}$) | $\omega_{if}$ ($cm^{-1}$) | S(f-i) ($Debye^2$) |
|---|---|---|---|---|
| $0\ 1_{+1}\ 1\ 1$ | 225.986 | 0.796 | 225.190 | 0.661(-3) |
| $1\ 0_{-1}\ 1\ 0$ | 227.291 | 1.064 | 226.227 | 0.195(-2) |
| $1\ 1_{+1}\ 1\ 1$ | 227.053 | 0.796 | 226.256 | 0.977(-3) |
| $1\ 1_{-1}\ 1\ 1$ | 227.291 | 0.000 | 227.291 | 0.132(-2) |

Table 2.7: Dipole allowed rotational and ro-vibrational transitions from the vibrational ground state of $^7Li_2\,^6Li^+$ . The energy levels are given relative to the J=0 state of the vibrational ground state. (Powers of ten in brackets).

| $\nu'$ | $J'_{K_{-1}K_{+1}}$–$J''_{K_{-1}K_{+1}}$ | Type | E′ ($cm^{-1}$) | E″ ($cm^{-1}$) | $\omega_{if}$ ($cm^{-1}$) | S(f-i) ($Debye^2$) |
|---|---|---|---|---|---|---|
| 0 | $1_{10}\ 1_{01}$ | b | 1.123 | 0.810 | 0.3130 | 0.261(0) |
| 0 | $1_{11}\ 0_{00}$ | b | 0.869 | 0.0 | 0.8690 | 0.174(0) |
| 2 | $0_{00}\ 1_{11}$ | b | 231.400 | 0.869 | 230.531 | 0.151(-3) |
| 2 | $1_{01}\ 1_{10}$ | b | 231.888 | 1.123 | 230.765 | 0.165(-3) |
| 3 | $0_{00}\ 1_{01}$ | a | 231.925 | 0.810 | 231.115 | 0.169(-2) |
| 2 | $1_{10}\ 1_{01}$ | b | 232.527 | 0.810 | 231.717 | 0.231(-3) |
| 2 | $1_{11}\ 0_{00}$ | b | 231.917 | 0.0 | 231.917 | 0.152(-3) |
| 3 | $1_{11}\ 1_{10}$ | a | 233.105 | 1.123 | 231.982 | 0.259(-2) |
| 3 | $1_{10}\ 1_{11}$ | a | 233.047 | 0.869 | 232.178 | 0.251(-2) |
| 3 | $1_{01}\ 0_{00}$ | a | 233.100 | 0.0 | 233.100 | 0.168(-2) |
| 1 | $0_{00}\ 1_{11}$ | b | 307.299 | 0.869 | 306.430 | 0.126(-3) |
| 1 | $1_{01}\ 1_{10}$ | b | 308.106 | 1.123 | 306.983 | 0.187(-3) |
| 1 | $1_{10}\ 1_{01}$ | b | 308.416 | 0.810 | 307.606 | 0.186(-3) |
| 1 | $1_{11}\ 0_{00}$ | b | 308.163 | 0.0 | 308.163 | 0.122(-3) |

D. For the ro-vibrational transitions, the $\nu_3$ a-type transitions are roughly an order of magnitude stronger than the $\nu_1$ and $\nu_2$ b-type lines.

In conclusion, results have been presented for those ro-vibrational transitions of $Li_3^+$ which would appear to be most promising for a laboratory observation of the system. As the ro-vibrational calculations are of proven accuracy it is necessary to concentrate on the potential energy surface in estimating any errors in the results. Error estimates for the potential are difficult. However, the rotational constants obtained for the vibrational ground state of $^7Li_3^+$ agree not only with SDF's estimates using the same potential, but also those of Martins *et al* [105] obtained from a pseudo-potential calculation.

Finally, it should be noted that since these studies were made, Searles and von Nagy-Felsobuki (SF)[106] have made some further investigations – including the other $C_{2v}$ species $^6Li_2\,^7Li^+$.

There were two motives for their further calculations. Firstly they were simply supplying more data to assist the observation of the system. Secondly, they were wanting know if the excellent agreement between their previous work and this work, for the $D_{3h}$ case, could be reproduced for the $C_{2v}$ case. As can be seen in Table 2.3, and also in reference [106], excellent agreement was indeed obtained.

The solution algorithm used by SDF (and SF) essentially employs the perturbative vibrational Hamiltonian of Carney *et al* [107] in space-fixed co-ordinates. The excellent agreement between the two methods (to within 0.04 $cm^{-1}$ for $^7Li_2\,^6Li^+$ ) is in some ways surprising. Clearly though, if higher energies are to be calculated the use of the approximate Hamiltonian of SDF will become unrealistic.

# Chapter 3

# The Discrete Variable Representation

## 3.1 Introduction

The recent employment of the Discrete Variable Representation (DVR) has greatly increased our power and ability to deal with the spectroscopy and molecular dynamics of small molecules. For the calculation of significant numbers of ro-vibrational levels it is proving to be the method of choice in many cases. The conventional FBR method often converges less than 5% of the levels given as eigenvalues of the Hamiltonian matrix; with DVR techniques this number can be as large as 40%.

The difference between the two methods is clear cut and simple. In the FBR the solutions are expressed as coefficients of basis functions; in the DVR the solutions are expressed as the amplitudes of approximate solutions at a well defined set of grid points. Finite difference and finite element methods such as this have been used for many years but have never really been favoured in the field of bound state calculations since very much larger numbers of grid points

than basis functions have usually been required.

The DVR however, is isomorphic to an FBR of the same order and where matrix elements are evaluated using the appropriate quadrature on the DVR points. The two are related by a similarity transformation – a property first exploited in the 1960's[55,56]. Harris *et al* [55] used a DVR-type method for a 1-dimensional problem, but it has not been until recently that the power of the DVR method for quantum mechanical problems be fully explored.

The method relies on successive diagonalisation and truncation in co-ordinate (or point) space; the FBR method is always in function space. As mentioned in Chapter 1, the method of Carter and Handy[57] uses the diagonalisation-truncation technique, though they still work in function space. This technique is extremely effective in supplying very representative intermediate bases. The DVR however has one more advantage. By working in point space the method actually 'scans' the potential energy surface during the calculation and so provides the best possible basis all over the regions of interest on the surface. For complicated and strongly coupled surfaces this is very useful and is exactly where the method of Carter and Handy is less powerful.

The next section formally defines the DVR, and the transformation from function-space to point-space. The following two sections show how to construct the Hamiltonian in two different representations of the DVR.

## 3.2 Definition of the DVR in 1 Dimension

The formal properties of the DVR are given here, one dimension being used for clarity and simplicity. It must be said from the beginning that the method is not *strictly* variational, but often *behaves* variationally. This will be explained later.

Consider a set of basis functions $\{\phi(r)\} = \{\phi\}$. The usual definition of inner

product and overlap matrix apply:

$$\begin{aligned} S_{ij} &= < \phi_i \mid \phi_j > \\ &= \int \phi_i^*(r)\phi_j(r)dr \qquad i,j = 1,2,3 \ .... \end{aligned} \tag{3.1}$$

It is known that if the basis is orthormal on its range then **S** is simply the unit matrix. The matrix representation of a Hamiltonian operator $\hat{H}$ in a truncated basis $\{\phi\}$ is then given by

$$H_{ij} = \int \phi_i^*(r)\hat{H}\phi_j(r)dr \qquad i,j = 1,...,N. \tag{3.2}$$

If the integrals in this basis function representation are evaluated using an appopriate quadrature at a set of points $\{r\}$ then we simply have defined an FBR. Note that this FBR is strictly only variational if the quadrature is exact. The DVR corresponding to this FBR is an approximate pointwise representation at the $N$ points. It is obtained by a unitary transformation of the FBR; the two representations are then isomorphic.

It was shown by Dickinson and Certain[56] that an orthogonal transformation exists between representaions in the $N$ orthogonal polynomials $\{P_0,.....P_{N-1}\}$ and representations at the $N$ associated Gaussian quadrature points, given by the zeroes of $P_N$. The transformation is defined by

$$T_{j\alpha} = \phi_j(r_\alpha)\omega_\alpha^{1/2}, \tag{3.3}$$

where $\{r\}$ and $\{\omega\}$ are the points and weights respectively for the quadrature associated with the functions $\{\phi\}$. Dickinson and Certain also showed that the discrete analogue of orthogonality can be given;

$$(\mathbf{T}\mathbf{T}^\dagger)_{ij} = \delta_{ij} = \sum_{\alpha=1}^{N} \phi_i(r_\alpha)\omega_\alpha\phi_j(r_\alpha). \tag{3.4}$$

Matrix elements in the DVR are evaluated by using the transformation matrix **T**. For a given operator $\hat{M}$, with FBR matrix elements $(M^{FBR})_{ij} \equiv < \phi_i \mid M \mid$

$\phi_j >$, we have

$$\mathbf{M}^{DVR} = \mathbf{T}(\mathbf{M}^{FBR})\mathbf{T}^{\dagger}. \tag{3.5}$$

This is used to evaluate a kinetic energy operator, for example, in its DVR from the matrix elements of the FBR.

An important feature of the DVR is the way in which the potential energy function V is dealt with. The potential is approximated by its value at the DVR points. So we have,

$$(\mathbf{T}(\mathbf{V}^{FBR})\mathbf{T}^{\dagger})_{\alpha\alpha'} \approx V(r_\alpha)\delta_{\alpha\alpha'} = (V^{DVR})_{\alpha\alpha'}. \tag{3.6}$$

The same result is arrived at as follows. Consider alternatively the direct transformation if V were evaluated in the FBR;

$$(\mathbf{T}(\mathbf{V}^{FBR})\mathbf{T}^{\dagger})_{\alpha\alpha'} = \sum_{ij} T_{i\alpha} < \phi_i \mid V \mid \phi_j > T_{j'\alpha'}. \tag{3.7}$$

The rule for the Gaussian quadrature associated with these basis functions is

$$\begin{aligned} < \phi_i \mid V \mid \phi_j > &\approx \sum_{\alpha''} \phi_i(r_{\alpha''})V(r_{\alpha''})\phi_j(r_{\alpha''})\omega_{\alpha''} \\ &= \sum_{\alpha''} T_{i\alpha''}T_{j\alpha''}V(r_{\alpha''}). \end{aligned} \tag{3.8}$$

Substitution of this into Equation (3.7) and making use of the orthonormality of $\mathbf{T}$ leads directly the statement of V being diagonal on the DVR points as in Equation (3.6). This shows that the approximation is simply a quadrature approximation.

It is well known that integrals of polynomials of order $2n-1$ can be computed exactly using an $n$-point quadrature[77]. Due to the isomorphism the FBR-DVR transformation only effectively allows for an $n$ - point quadrature. Overlap integrals can thus be calculated exactly but higher order operators will demand truncation. This then means that the DVR method is not strictly variational. The method does indeed behave variationally though when $n$ is sufficiently large.

The formal properties of the transformation in 1-D have been given in this section. The procedure of intermediate contraction and the recoupling of the lower dimensions is to be discussed in the remaining sections of this chapter.

## 3.3 DVR in the Angular Co-ordinate

### 3.3.1 The Hamiltonian

We are now able to take the generalised Hamiltonian operator of chapter 2 and transform it to a DVR in the generalised co-ordinates. This section describes the theory for the angular co-ordinate, $\theta$, being treated in a DVR, whilst $r_1$ and $r_2$ remain untransformed in an FBR. This representation is applied to LiNC/LiCN in chapter 4 and to $H_3^+$ in chapter 5. This discretisation of the angular co-ordinate was found to be useful by Light, Bačić, Whitnell and co-workers in their studies on LiCN/LiNC and HNC/HCN[108,109], $Na_3$[110] and $H_2O$[111].

As explained at the beginning of chapter 2, the close-coupling method is used[65], along with the approach of Tennyson and Sutcliffe[34]. This results in an effective radial Hamiltonian of the form

$$\hat{H}(r_1, r_2) = \hat{K}_V^{(1)} + \hat{K}_V^{(2)} + \hat{K}_{VR}^{(1)} + \hat{K}_{VR}^{(2)} + \delta_{k'k} < j'k \mid V(r_1, r_2, \theta) \mid jk >_\theta, \quad (3.9)$$

with all terms as those in chapter 2.

The above close-coupled equations are in an FBR labelled by $j$, corresponding to the associated Legendre functions forming the angular basis for any particular $(J, k)$. We now transform them to a DVR labelled by a finite set of angles. As stated in chapter 2, the angular basis functions are of the form $\mid j, k >= \Theta_{j,k}(\theta) D^J_{Mk}(\alpha, \beta, \gamma)$. Then, from Equation (3.3), the DVR transformation is given by

$$T^k_{j\alpha} = N_{jk} \omega^{1/2}_{k\alpha} \Theta_{j,k}(\theta_{k\alpha}), \quad (3.10)$$

where $N_{jk}$ normalises $\Theta_{jk}$. Note that the discretisation procedure depends on $k$. Note that the DVR points now depend on $k$.

One can now transform the effective Hamiltonian operator in the FBR to yield

$$\begin{aligned}
\hat{H}_{k'\alpha',k\alpha} &= \sum_{j=k}^{N+k-1} \sum_{j'=k'}^{N'+k'-1} T^{k'}_{j'\alpha'} \hat{H}(r_1,r_2) T^{k}_{j\alpha} \\
&= \delta_{k'k}\delta_{\alpha'\alpha}\left[-\frac{\hbar^2}{2\mu_1}\frac{\partial^2}{\partial r_1^2} - \frac{\hbar^2}{2\mu_2}\frac{\partial^2}{\partial r_2^2} + \frac{\hbar^2}{2\mu_1 r_1^2}[J(J+1)-2k^2] + V(r_1,r_2,\theta_{k\alpha})\right] \\
&\quad +\delta_{k'k}\frac{\hbar^2}{2}\left(\frac{1}{\mu_1 r_1^2}+\frac{1}{\mu_2 r_2^2}\right) L^k_{\alpha'\alpha} \\
&\quad -\delta_{k'k}\frac{\hbar^2}{2\mu_{12}}\left[M^{(1)k}_{\alpha'\alpha}\frac{\partial^2}{\partial r_1 \partial r_2} - M^{(2)k}_{\alpha'\alpha}\left(\frac{1}{r_1}\frac{\partial}{\partial r_2}+\frac{1}{r_2}\frac{\partial}{\partial r_1}\right) + M^{(3)k}_{\alpha'\alpha}\frac{1}{r_1 r_2}\right] \\
&\quad -\delta_{k'k\pm1}\frac{\hbar^2}{2\mu_1 r_1^2} C^{\pm}_{Jk} Q^{k\pm}_{\alpha'\alpha} \\
&\quad -\delta_{k'k\pm1}\frac{\hbar^2}{2\mu_{12} r_1} C^{\pm}_{Jk}\left[R^{(1)k\pm}_{\alpha'\alpha}\frac{\partial}{\partial r_2} + R^{(2)k\pm}_{\alpha'\alpha}\frac{1}{r_2}\right]. \qquad (3.11)
\end{aligned}$$

The new, transformed matrices that are diagonal in $k$ are given by

$$L^k_{\alpha'\alpha} = \sum_{j=k}^{N+k-1} T^k_{j\alpha'} j(j+1) T^k_{j\alpha} \qquad (3.12)$$

$$M^{(i)k}_{\alpha'\alpha} = \sum_{j=k}^{N+k-1} T^k_{j+1,\alpha'}\left[(j+1)^{i-1} d_{jk} + (j)^{i-1} d_{j-1,k}\right] T^k_{j\alpha}. \qquad (3.13)$$

The off-diagonal, Coriolis matrices are given by

$$Q^{k\pm}_{\alpha'\alpha} = \sum_j T^{k\pm1}_{j\alpha'} C^{\pm}_{jk} T^k_{j\alpha} \qquad (3.14)$$

$$R^{(i)k\pm}_{\alpha'\alpha} = \sum_j T^{k\pm1}_{j+1,\alpha'}\left[(j+1)^{(i-1)} a_{j,\pm k} + (-1)^i (j)^{(i-1)} b_{j,\pm k}\right] T^k_{j\alpha}. \qquad (3.15)$$

where the sum goes from $\max(k, k\pm1)$ to $\min(N+k-1, N'+k\pm1-1)$. Again, the constants used above are defined in chapter 2. Note that for convenience the DVR superscript is dropped from the matrices. Each of these transformed matrices is effectively formed by the same operation and so all of them can be computed at the same time.

In a more compact notation Equation (3.11) can be written

$$\hat{\mathbf{H}} = \hat{\mathbf{H}}^k + \hat{\mathbf{K}}^{VR}, \tag{3.16}$$

where

$$\hat{\mathbf{H}}^k = \hat{\mathbf{h}}^k(r_1, r_2)\mathbf{I} + w_0(r_1, r_2)\mathbf{L}^k + \sum_{i=1}^{3}(-1)^i w_i(r_1, r_2)\mathbf{M}^{(i)k} \tag{3.17}$$

$$\hat{\mathbf{K}}^{VR} = -u_0(r_1, r_2)\mathbf{Q}^{k\pm} - \sum_{i=1}^{2} u_i(r_1, r_2)\mathbf{R}^{(i)k}, \tag{3.18}$$

where the matrix indices are $\alpha$ and $\alpha'$.

In deriving Equation (3.11) we have used the approximation mentioned earlier, i.e. made the potential diagonal in the angular grid points;

$$\sum_{j,j'=k}^{N+k-1} T^k_{j'j\alpha} < j'k \mid V(r_1, r_2, \theta) \mid jk >_\theta T^k_{j\alpha} \simeq \delta_{\alpha\alpha'} V(r_1, r_2, \theta_{k\alpha}). \tag{3.19}$$

Consequently the only angular-coupling is provided by the transformed kinetic energy matrices which are relatively simple to evaluate.

The DVR procedure then is to solve the two-dimensional (2D) Hamiltonian $\hat{\mathbf{h}}^k$, contained in $\hat{\mathbf{H}}^k$, for each different angle $\alpha$. This can be thought of as finding solutions at various 2D 'cuts' across the potential energy surface. The 2D eigenvectors obtained can then be used as a well adapted basis in which to represent the fully coupled problem. The major benefit is that not all the solutions of these lower-dimensional problems are required to converge the desired states of $\hat{\mathbf{H}}$. One can select a subset of each of the 2D solutions at each angle according to an energy cut-off criterion, then the final basis constructed from these will be of reduced size and hence offer great computational savings.

The elements of $\hat{\mathbf{h}}^k$ are block-diagonal in angle, with all other terms spanning the whole of $\hat{\mathbf{H}}^k$. Clearly one could either include the diagonal contributions from the angular-coupling matrices in the 2D calculations or in the final, 3D calculation. It is generally better to include them in the 3D calculation as one can

then assign a physical meaning to the 2D solutions, as eigenvalues of the stretching vibrations (rather like an adiabatic approximation). Essentially, by taking this option, the 2D eigenvalues are independent of the number of DVR points and faster convergence of final solutions is achieved. The faster convergence is achieved because the diagonal angular coupling tends to distort the intermediate results and produce a basis which is not so meaningful physically.

The full expression for $\hat{\mathbf{H}}$ in a DVR has been given for completeness, and indeed it is possible to go ahead from this and obtain ro-vibrational solutions entirely in a DVR in the generalised coordinates. For vibrational problems ($J = 0$) it is seen that $\hat{\mathbf{K}}^{VR} = 0$ and so one purely solves $\hat{\mathbf{H}}^{k}$ in the DVR for $k = 0$ only. To account for rotational excitation ($J > 0$), $\hat{\mathbf{H}}^{VR}$ can also be solved in a DVR, for all $k$.

A preferred alternative however, partly due to computational considerations, is to treat the non-Coriolis coupled ($\hat{\mathbf{H}}^{k}$ only) problem in a DVR, for each $k$. Take the lowest of these solutions (for each $k$) and back-transform to an FBR. Then couple the $k$'s to solve the full Coriolis-coupled Hamiltonian, using the solutions of each $k$ calculation, expressed in an FBR, as a basis to solve the final $\hat{\mathbf{H}}$. The advantage here again is that not all of the non-Coriolis solutions are required. This is an efficient way of performing ro-vibrational calculations utilising both a DVR and the two-step variational approach of Tennyson and Sutcliffe[48]. It is this hybrid algorithm which is used for the $H_3^+$ ro-vibrational calculations in chapter 5.

The rotation-vibration Hamiltonian has been presented for a DVR in the angular co-ordinate of a very generalised set of co-ordinates, which clearly has simplified special cases. All DVR calculations presented in this thesis have been performed in orthogonal co-ordinates. Not presented in this thesis, but reported elsewhere[112], are DVR-in-$\theta$ calculations on the sodium trimer. $Na_3$ is extremely

difficult to study because of its highly complex potential energy surface. It was found that best results were obtained using a DVR in the orthogonal Radau co-ordinates, described in chapter 2. These co-ordinates in a DVR were used by Bačić *et al* [111] for their calculations on the water molecule.

For orthogonal co-ordinate systems we know from §2.1 that $\mu_{12}^{-1} = 0$ and so $\hat{K}_V^{(2)} = \hat{K}_{VR}^{(2)} = 0$. The effective radial Hamiltonian thus has a much simplified form for the calculations presented in this thesis.

Using the DVR transformation matrix to transform the simplified Hamiltonian we obtain

$$\hat{H}^k_{\alpha\alpha'} = \delta_{\alpha\alpha'}\left[\frac{-\hbar^2}{2\mu_1}\frac{\partial^2}{\partial r_1^2} - \frac{\hbar^2}{2\mu_2}\frac{\partial^2}{\partial r_2^2} + \frac{\hbar^2}{2\mu_1 r_1^2}[J(J+1) - 2k^2] + V(r_1, r_2, \theta_{k\alpha})\right] + \frac{\hbar^2}{2}\left(\frac{1}{\mu_1 r_1^2} + \frac{1}{\mu_2 r_2^2}\right) L^k_{\alpha\alpha'}. \tag{3.20}$$

This can be compactly expressed in matrix notation as

$$\hat{\mathbf{H}}^k = \hat{\mathbf{h}}^k(r_1, r_2)\mathbf{I} + w(r_1, r_2)\mathbf{L}^k. \tag{3.21}$$

The coupling between $\alpha$ blocks is provided by the angular kinetic energy term as expressed by the term involving the **L** matrix of Equation (3.12).

### 3.3.2 Wavefunctions

An FBR is used to expand the solutions of the 2D Hamiltonian, $\hat{h}^k_\alpha$. The $r^{th}$ wavefunction, with eigenenergy $\epsilon^k_{\alpha r}$, can then be written

$$\phi^{Jk}_{\alpha r}(r_1, r_2; \theta_{k\alpha}) = \sum_{m,n} a^{Jkr}_{mn\alpha} H_m(r_1) H'_n(r_2) D^J_{Mk}(\Omega). \tag{3.22}$$

The radial functions, $H_m$ and $H'_n$, are orthogonal polynomials based on the solutions of model potentials, as described in chapter 2.

Solutions of the Hamiltonian $\hat{\mathbf{H}}^k$ are then expressed in terms of the $\phi^{Jk}$:

$$\begin{aligned}\Psi_s^{Jk}(r_1,r_2,\theta_{k\alpha}) &= \sum_r b_{\alpha r}^{Jks}\phi_{\alpha r}^{Jk} \\ &= \sum_{m,n} c_{mn\alpha}^{Jks} H_m(r_1)H_n'(r_2)D_{Mk}^J(\Omega), \end{aligned} \tag{3.23}$$

where

$$c_{mn\alpha}^{Jks} = \sum_r a_{mn\alpha}^{Jkr} b_{\alpha r}^{Jks}. \tag{3.24}$$

For the second variational step it is desirable to have wavefunctions expressed in an FBR expansion. This is because the off-diagonal Coriolis coupling terms, in orthogonal co-ordinates, are diagonal in $j$ but off-diagonal in $\alpha$. So writing

$$\Psi_s^{Jk}(r_1,r_2,\theta) = \sum_{j,m,n} d_{jmn}^{Jks} H_m(r_1)H_n'(r_2)\Theta_{jk}(\theta)D_{Mk}^J(\Omega) \tag{3.25}$$

one obtains the coefficients of the FBR by back transforming

$$d_{jmn}^{Jks} = \sum_\alpha T_{\alpha j}^k c_{mn\alpha}^{Jks} = \sum_\alpha N_{jk}\omega_{k\alpha}^{1/2}\Theta_{jk}(\theta_{k\alpha})c_{mn\alpha}^{Jks} \tag{3.26}$$

As $\hat{\mathbf{H}}^k$ depends only on $k^2$, the $\mathbf{d}^{Jks}$ depend only on $\mid k \mid$. The $\mathbf{d}^{Jks}$ form the input for the second variational step yielding a final ro-vibrational wavefunction:

$$\begin{aligned}\Psi_t^{Jp}(r_1,r_2,\theta) &= \delta_{k0}\delta_{p0}\sum_s e_{ks}^{Jpt}\psi_s^{Jk} + \sum_{k=1}^{J}\sum_s e_{ks}^{Jpt}2^{-1/2}[\psi_s^{Jk} + (-1)^p\psi_s^{J-k}] \\ &= \delta_{k0}\delta_{p0}\sum_{jkmn} f_{jmn}^{Jpt} H_m(r_1)H_n'(r_2)\Theta_{jk}(\theta)D_{Mk}^J(\Omega) \\ &+ \sum_{k=1}^{J}\sum_s f_{jkmn}^{Jpt} H_m(r_1)H_n'(r_2)2^{-1/2}\left[\Theta_{jk}(\theta)D_{Mk}^J(\Omega) + (-1)^p\Theta_{j-k}(\theta)D_{M-k}^J(\Omega)\right], \end{aligned} \tag{3.27}$$

where

$$f_{jkmn}^{Jpt} = \sum_s d_{jmn}^{Jks} e_{ks}^{Jpt} \tag{3.28}$$

and $p$ equals 0 or 1. The total parity of the wavefunction is given by $(-1)^{J+p}$.

### 3.3.3 Symmetry

Whitnell and Light were able to make use of symmetry in a DVR[113] for their studies on $H_3^+$ in hyperspherical co-ordinates. In this subsection a slightly different, and computationally more efficient, procedure is proposed for symmetry adapting the DVR for systems with at least $C_{2v}$ symmetry.

In an FBR the symmetry of an $AB_2$ system is carried naturally by associated Legendre polynomials. Functions with $j$ even are symmetric and those with $j$ odd antisymmetric with respect to reflection in the molecular plane about $\theta = 90^o$. In this case the symmetry of the Gauss-associated Legendre quadrature about $\chi = \cos\theta = 0$ means that all the unique problems lie in the half range $0 \leq \chi_{k\alpha} < 1$. It is then possible to symmetrise the DVR wavefunction $\phi_{\alpha r}^{Jk}$ by writing

$$\phi_{\alpha r}^{Jkq}(r_1, r_2; \chi_{k\alpha}) = 2^{-1/2}\left[\phi_{\alpha r}^{Jk}(r_1, r_2; \chi_{k\alpha}) + (-1)^q \phi_{\alpha r}^{Jk}(r_1, r_2; -\chi_{k\alpha})\right] \qquad (3.29)$$

$$q = 0, 1; \qquad \chi_{k\alpha} > 0$$

where the restriction to an even number of DVR points, $N$, is simply to avoid the special case of $\chi_{k\alpha} = 0$.

Transforming $\hat{H}_{\alpha\alpha'}^k$ to this symmetrised basis gives

$$\hat{\mathbf{H}}^{kq} = \hat{\mathbf{h}}^k \mathbf{I} + w(r_1, r_2)\mathbf{L}^{kq} \qquad (3.30)$$

where

$$L_{\alpha\alpha'}^{kq} = 2 \sum_{\ell=k}^{N/2+k-1} T_{2\ell+q,\alpha'}^k (2\ell + q)(2\ell + q + 1) T_{2\ell+q,\alpha}^k \qquad (3.31)$$

This means that in the symmetrised DVR only the term which differs between even ($q = 0$) and odd ($q = 1$) calculations is provided by the $\mathbf{L}^{kq}$ matrix.

The matrix elements of $\hat{\mathbf{H}}^{kq}$ can be expressed as

$$< \alpha' r' \mid \hat{\mathbf{H}}^{kq} \mid \alpha r >= \delta_{\alpha\alpha'}\delta_{rr'}\epsilon_{\alpha r}^k + \tilde{W}_{\alpha' r' \alpha r} L_{\alpha'\alpha}^{kq} \qquad (3.32)$$

where

$$\tilde{W}_{\alpha' r' \alpha r} = \sum_{m,n} \sum_{m',n'} a^{Jkr}_{mn\alpha} a^{Jkr'}_{m'n'\alpha'} < m'n' \mid w(r_1, r_2) \mid mn > \qquad (3.33)$$

The orthogonal co-ordinates used here simplify this transformation as:

$$< m'n' \mid w(r_1, r_2) \mid mn >= \delta_{nn'} < m' \mid \frac{\hbar^2}{2\mu_1 r_1^2} \mid m > \qquad (3.34)$$

$$+\delta_{mm'} < n' \mid \frac{\hbar^2}{2\mu_2 r_2^2} \mid n >$$

The advantage of this method of symmetrisation is now clear. Not only does one solve on a reduced DVR grid for a given symmetry block, but also if both symmetry blocks are required, the results for the second can be computed at relatively small extra cost. Doing this requires simply saving the eigenvalues and eigenvectors of the $\hat{h}^k_\alpha$ and the transformed matrix $\tilde{\mathbf{W}}$.

## 3.4 Multidimensional DVR: $\mathbf{r}_1$, $\mathbf{r}_2$ and $\theta$

Clearly, it is possible to develop a method which treats 2 degrees of freedom in a DVR and leaves 1 in an FBR, and indeed it is possible to treat all co-ordinates in a DVR. This section presents the theory for such a 3-dimensional (3D) DVR.

A multidimensional DVR is a direct product DVR as a transformation of direct product FBRs in 1D basis functions. The required transformation is a direct product of three 1D DVR transformation matrices.

A 3D DVR is attractive. Firstly it is a totally pointwise representation and hence only those DVR points which lie in relevant parts of the potential need be selected. This is a zeroth order truncation and can give an immediate saving, essentially before the calculation has begun. Secondly, there are no numerical integrals at all. And the potential matrix elements simply take the value at each of the grid points.

The DVR-in-$\theta$ algorithm from the previous section showed how the initial 3D Hamiltonian was reduced to a set of 2D Hamiltonians at the associated DVR points. In a 3D DVR one takes those 2D Hamiltonians and evaluates a set of 1D Hamiltonians at each of a set of grid points of those 2D Hamiltonians. The procedure is to solve all the 1D matrices and select a subset of the eigenvectors. These vectors are used as a very physical basis to solve all of the 2D matrices, the solutions of which will be used similarly to couple the kinetic energy and solve the final 3D matrix. The advantage is that this final matrix will be much reduced in size and be of high information content. The computational expense of evaluating and solving the 1D and 2D matrices is negligible.

### 3.4.1 The Composite Transformation

Only the vibrational ($J = 0$) problem is considered here. Further, for convenience the theory is only presented for orthogonal co-ordinates. Inspection of Equation (3.20) shows that we need to transform the following matrix elements:

$$\begin{aligned}
h^{(1)}_{jj'mm'nn'} &\equiv < m' \mid -\frac{\hbar^2}{2\mu_1}\frac{\partial^2}{\partial r_1^2} \mid m > \delta_{jj'}\delta_{nn'} \\
h^{(2)}_{jj'mm'nn'} &\equiv < n' \mid -\frac{\hbar^2}{2\mu_2}\frac{\partial^2}{\partial r_2^2} \mid m > \delta_{jj'}\delta_{mm'} \\
G^{(1)}_{jj'mm'nn'} &\equiv < m' \mid \frac{\hbar^2}{2\mu_1 r_1^2} \mid m > j(j+1)\delta_{jj'}\delta_{nn'} \qquad (3.35) \\
G^{(2)}_{jj'mm'nn'} &\equiv < n' \mid \frac{\hbar^2}{2\mu_2 r_2^2} \mid n > j(j+1)\delta_{jj'}\delta_{mm'} \\
V_{jj'mm'nn'} &\equiv < j'm'n' \mid V(r_1, r_2, \theta) \mid jmn > . \qquad (3.36)
\end{aligned}$$

The required transformation matrix will be of the form

$$\mathbf{T} = \mathbf{T}^{(r_1)}\mathbf{T}^{(r_2)}\mathbf{T}^{(\theta)}. \qquad (3.37)$$

Let the notation for the different sets of DVR points be defined as follows:

$$(r_1)_\gamma \equiv \rho^{(1)}_\gamma, \quad (r_2)_\beta \equiv \rho^{(2)}_\beta, \quad (\theta)_\alpha \equiv \chi_\alpha, \qquad (3.38)$$

and label the different matrices as

$$\mathbf{T}^{(r_1)} \equiv \mathbf{T}^{(1)}, \quad \mathbf{T}^{(r_2)} \equiv \mathbf{T}^{(2)}, \quad \mathbf{T}^{(\theta)} \equiv \mathbf{T}^{(\theta)}. \tag{3.39}$$

The composite can now be written as

$$T^{\alpha\beta\gamma}_{jmn} = T^{(1)}_{m\gamma} T^{(2)}_{n\beta} T^{(\theta)}_{j\alpha}, \tag{3.40}$$

where

$$\begin{aligned} T^{(1)}_{m\gamma} &= N^{(1)}_m \omega^{(1)\frac{1}{2}}_m H_m(\rho^{(1)}_\gamma), \\ T^{(2)}_{n\beta} &= N^{(2)}_n \omega^{(2)\frac{1}{2}}_n H'_n(\rho^{(2)}_\beta), \\ T^{(\theta)}_{j\alpha} &= N^{(\theta)}_j \omega^{(\theta)\frac{1}{2}}_j \Theta_{j0}(\chi_\alpha). \end{aligned} \tag{3.41}$$

The angular functions $\Theta_{j0}$ and the radial functions $H_m$ and $H'_n$ are those defined in chapter 2, although of course the theory is still general enough for any uncoupled orthogonal polynomial functions to be used.

We can now transform the various matrix elements, making use of the orthogonality of the components of $\mathbf{T}$ where appropriate.

$$\begin{aligned} (T(h^{(1)})T^\dagger)_{\alpha\alpha'\beta\beta'\gamma\gamma'} &= K^{(1)}_{\alpha\alpha'\beta\beta'\gamma\gamma'} \\ &= \sum_{jj'}\sum_{mm'}\sum_{nn'} T^{\alpha\beta\gamma}_{jmn} < m' \mid -\frac{\hbar^2}{2\mu_1}\frac{\partial^2}{\partial r_1^2} \mid m > T^{\alpha'\beta'\gamma'}_{j'm'n'} \delta_{jj'}\delta_{nn'} \\ &= \sum_{j}\sum_{mm'}\sum_{n} T^{\alpha\beta\gamma}_{jmn} < m' \mid -\frac{\hbar^2}{2\mu_1}\frac{\partial^2}{\partial r_1^2} \mid m > T^{\alpha'\beta'\gamma'}_{jm'n} \\ &= \delta_{\alpha\alpha'}\delta_{\beta\beta'} \sum_{mm'} T^{(1)}_{m\gamma} < m' \mid -\frac{\hbar^2}{2\mu_1}\frac{\partial^2}{\partial r_1^2} \mid m > T^{(1)}_{m'\gamma'}. \end{aligned} \tag{3.42}$$

The symmetry in $r_1$ and $r_2$ gives, similarly,

$$\begin{aligned} (T(h^{(2)})T^\dagger)_{\alpha\alpha'\beta\beta'\gamma\gamma'} &= K^{(2)}_{\alpha\alpha'\beta\beta'\gamma\gamma'} \\ &= \delta_{\alpha\alpha'}\delta_{\gamma\gamma'} \sum_{nn'} T^{(2)}_{n\beta} < n' \mid -\frac{\hbar^2}{2\mu_2}\frac{\partial^2}{\partial r_2^2} \mid n > T^{(2)}_{n'\beta'}. \end{aligned} \tag{3.43}$$

$$
\begin{aligned}
(T(G^{(1)})T^{\dagger})_{\alpha\alpha'\beta\beta'\gamma\gamma'} &= L^{(1)}_{\alpha\alpha'\beta\beta'\gamma\gamma'} \\
&= \sum_{jj'}\sum_{mm'}\sum_{nn'} T^{\alpha\beta\gamma}_{jmn} < m' \mid \frac{\hbar^2}{2\mu_1 r_1^2} \mid m > T^{\alpha'\beta'\gamma'}_{j'm'n'} j(j+1)\delta_{jj'}\delta_{nn'} \\
&= \sum_{j}\sum_{mm'}\sum_{n} T^{\alpha\beta\gamma}_{jmn} < m' \mid \frac{\hbar^2}{2\mu_1 r_1^2} \mid m > T^{\alpha'\beta'\gamma'}_{jm'n} j(j+1) \\
&= L_{\alpha\alpha'}\sum_{mm'} T^{(1)}_{m\gamma} < m' \mid \frac{\hbar^2}{2\mu_1 r_1^2} \mid m > T^{(1)}_{m'\gamma'}\delta_{\beta\beta'} \\
&= L_{\alpha\alpha'}\frac{\hbar^2}{2\mu_1(\rho^{(1)}_{\gamma})^2}\delta_{\gamma\gamma'}\delta_{\beta\beta'}, \qquad (3.44)
\end{aligned}
$$

where **L** is that defined in Equation (3.12). Note also that the DVR quadrature approximation has been used in that the operator is simply evaluated at its DVR grid points. Once again the symmetry between the two radial co-ordinates leads to

$$
\begin{aligned}
(T(G^{(2)})T^{\dagger})_{\alpha\alpha'\beta\beta'\gamma\gamma'} &= L^{(2)}_{\alpha\alpha'\beta\beta'\gamma\gamma'} \\
&= L_{\alpha\alpha'}\frac{\hbar^2}{2\mu_2(\rho^{(2)}_{\beta})^2}\delta_{\gamma\gamma'}\delta_{\beta\beta'}. \qquad (3.45)
\end{aligned}
$$

$$
\begin{aligned}
(T(V)T^{\dagger})_{\alpha\alpha'\beta\beta'\gamma\gamma'} &= V_{\alpha\alpha'\beta\beta'\gamma\gamma'} \\
&= V(\rho^{(1)}_{\gamma}, \rho^{(2)}_{\beta}, \chi_{\alpha})\delta_{\alpha\alpha'}\delta_{\beta\beta'}\delta_{\gamma\gamma'}. \qquad (3.46)
\end{aligned}
$$

The full 3D DVR (J=0) Hamiltonian can be written down:

$$
\begin{aligned}
H_{\alpha\alpha'\beta\beta'\gamma\gamma'} &= K^{(1)}_{\alpha\alpha'\beta\beta'\gamma\gamma'} + K^{(2)}_{\alpha\alpha'\beta\beta'\gamma\gamma'} \\
&+ L^{(1)}_{\alpha\alpha'\beta\beta'\gamma\gamma'} + L^{(2)}_{\alpha\alpha'\beta\beta'\gamma\gamma'} \\
&+ V_{\alpha\alpha'\beta\beta'\gamma\gamma'}. \qquad (3.47)
\end{aligned}
$$

The problem can now be solved in a reduction–truncation manner for some permutation of the DVR point sets.

### 3.4.2 Solution Strategy

The problem of determining in which order the coordinates should be treated in the successive diagonalisation and truncation procedure has been discussed by Light *et al* [114]; the objective is to minimize the CPU time (and memory) required by obtaining the smallest possible final Hamiltonian matrix. This is done by treating the coordinate with the smallest density of states last. Clearly then the choice will be different for different systems. For $H_3^+$, in Jacobi coordiates, the highest density of states is in the dissociating $r_2$ coordinate and the lowest in the $\theta$ coordinate. For the calculations presented in chapter 6 the coordinates were therefore treated in the order $r_2 \rightarrow r_1 \rightarrow \theta$, although others were tested. It is this order of solution which is given below.

Firstly note that the notation in the final Hamiltonian can be simplified by removing the redundant subscripts. For example, it can be seen from Equation (3.42) that $\mathbf{K}^{(1)}$ is a function of $\gamma$ only. This contribution to the Hamiltonian can thus be written $K^{(1)}_{\gamma\gamma'}\delta_{\alpha\alpha'}\delta_{\beta\beta'}$, with similar properties holding for the other terms in Equation (3.48).

The Hamiltonian can then be written

$$\begin{aligned} H_{\alpha\alpha'\beta\beta'\gamma\gamma'} &= K^{(1)}_{\gamma\gamma'}\delta_{\alpha\alpha'}\delta_{\beta\beta'} + K^{(2)}_{\beta\beta'}\delta_{\alpha\alpha'}\delta_{\gamma\gamma'} \\ &+ L^{(1)}_{\alpha\alpha'}\delta_{\beta\beta'}\delta_{\gamma\gamma'} + L^{(2)}_{\alpha\alpha'}\delta_{\beta\beta'}\delta_{\gamma\gamma'} \\ &+ V_{\alpha\beta\gamma}\delta_{\alpha\alpha'}\delta_{\beta\beta'}\delta_{\gamma\gamma'} \end{aligned} \tag{3.48}$$

We now wish to solve this in the order $r_2 \rightarrow r_1 \rightarrow \theta$ ($\beta \rightarrow \gamma \rightarrow \alpha$). The first step is to construct, for each $\gamma$ and $\alpha$, one-dimensional Hamiltonian matrices $\mathbf{H}^{1D}$ which are indexed on $\beta$:

$$(H^{1D})^{\gamma\alpha}_{\beta\beta'} = K^{(2)}_{\beta\beta'} + V(\rho^{(1)}_{\gamma}, \rho^{(2)}_{\beta}, \chi_{\alpha})\delta_{\beta\beta'}. \tag{3.49}$$

$\mathbf{H}^{1D}$ is then diagonalised to yield eigenvectors $\mathbf{C}^{1D}$ and eigenvalues $\mathbf{E}^{1D}$.

The truncation technique necessitates defining some cut-off energy $\epsilon^{1D}$. All the $(n^{1D})^{\gamma\alpha}$ eigenvectors with $(E^{1D})_i^{\gamma\alpha} \leq \epsilon^{1D}$ are selected. The cut-off must be chosen such that $0 < N^{1D} \leq N^{DVR}$, where $N^{1D} = \sum_{\gamma\alpha}(n^{1D})^{\gamma\alpha}$ and $N^{DVR}$ is the number of DVR points in $r_1$ multiplied by the number in $r_2$ multiplied by the number $\theta$. Solutions which are of the form $(E^{1D})_i^{\gamma\alpha}$ and $(C^{1D})_\beta^{\gamma\alpha i}$, where $i$ runs from 1 to $(n^{1D})^{\gamma\alpha}$ (*ie.* the number of vectors chosen for a particular 'ray') are thus retained.

The next step is to form the 2D matrices. That is, we need to construct $\mathbf{H}^{2D}$ for each $\alpha$, indexed on $\beta$ and $\gamma$.

$$(H^{2D})^{\alpha}_{\beta\beta'\gamma\gamma'} = (H^{1D})^{\gamma\alpha}_{\beta\beta'}\delta_{\gamma\gamma'} + K^{(1)}_{\gamma\gamma'}\delta_{\beta\beta'}. \tag{3.50}$$

This matrix is transformed using the 1D eigenvectors labelled by $i$. This gives a contracted 2D Hamiltonian

$$(H^{2D})^{\alpha}_{\gamma\gamma' ii'} = (E^{1D})_i^{\gamma\alpha}\delta_{ii'}\delta_{\gamma\gamma'} + K^{(1)}_{\gamma\gamma'}\sum_{\beta}(C^{1D})_\beta^{\gamma\alpha i}(C^{1D})_\beta^{\gamma'\alpha i'}. \tag{3.51}$$

Diagonalisation gives eigenvectors $\mathbf{C}^{2D}$ and eigenvalues $\mathbf{E}^{2D}$. A cut-off energy $\epsilon^{2D}$ is then defined. All the $(n^{2D})^{\alpha}$ eigenvectors with $(E^{2D})_j^{\alpha} \leq \epsilon^{2D}$ are selected. So the cut-off must be chosen such that $0 < N^{2D} \leq N^{1D}$, where $N^{2D} = \sum_{\alpha}(n^{2D})^{\alpha}$ and $N^{1D}$ is the size of the contracted basis formed from the 1D solutions. So we obtain solutions of the form $(E^{2D})_j^{\alpha}$ and $(C^{2D})_{\gamma i}^{\alpha j}$. Here $j$ runs from 1 to $(n^{2D})^{\alpha}$.

This set of 2D vectors is now a very well adapted basis in which to form the 3D Hamiltonian. Transforming to a representation in the $j$-basis we obtain;

$$(H^{3D})_{\alpha\alpha' jj'} = (E^{2D})_j^{\alpha}\delta_{\alpha\alpha'}\delta_{jj'} + \sum_{\beta\gamma}[(L^{(1)}_{\alpha\alpha'} + L^{(2)}_{\alpha\alpha'})C^{\alpha j}_{\beta\gamma}C^{\alpha' j'}_{\beta\gamma}], \tag{3.52}$$

where we have defined

$$C^{\alpha j}_{\beta\gamma} = \sum_i (C^{2D})^{\alpha j}_{\gamma i}(C^{1D})^{\gamma\alpha i}_{\beta}. \tag{3.53}$$

Diagonalisation of the 3D Hamiltonian matrix yields the final wavefunction coefficients and eigenvalues. Note that there are five other possible orders of dealing with the co-ordinates. Note though that it is trivial to switch the order of the radial co-ordinates ($r_1 \leftrightarrow r_2$) as the symmetry between $r_1$ and $r_2$ in the Hamiltonian operator is preserved by the DVR. It is straightforward to derive the solution algorithm for any of the other orders, indeed a generalised computer program has been developed to treat four of the six possible orders.

The previous section discussed the exploitation of $C_{2v}$ symmetry in DVR-in-$\theta$ calculations. The very same use of symmetry in the angular co-ordinate can be made in the 3D DVR. The only important matrix, as before, is the L-matrix. Note that if the $\theta$ co-ordinate is treated last then little computational advantages appear in calculating both odd and even symmetry blocks in the same computer run. If however it is treated first then savings can be made, somewhat similar to those described in §3.3.3.

We now have a 3D Hamiltonian in a basis of very representative 2D eigenfunctions, with exact coupling to the lower dimension. Typically we select between 20 and 50% of the vectors to be used as a basis and recoupled to the next higher dimension. Chapter 6 reports 3D DVR calculations on the $H_3^+$ system. The largest Hamiltonian constructed was of dimension 3,300; the uncontracted equivalent dimension would have been 23,040 in each symmetry block. Note also that these calculations are computationally fairly modest. For example a calculation on $H_3^+$ with a final Hamiltonian of dimension 2400 took 2 minutes to perform all the steps up to and including constructing the final Hamiltonian matrix and 22 minutes to diagonalise this matrix, all timings are for a single processor of a Cray–XMP.

# Chapter 4

# Very Highly Excited States of the LiNC/LiCN system

## 4.1 Introduction

'Floppy' molecules, capable of executing very large amplitude motions and with interesting potential energy surfaces, have stimulated much experimental and theoretical interest in the past few years. A recent review by Bačić and Light[115] gives an excellent account of the theoretical progress in the study of these systems.

The LiNC/LiCN isomerising system in particular has been the focus of many studies[53,69,98,116,117,118,119,120] of its bound state nuclear motion dynamics. All except the earliest of these studies[116] employed the 2D, CN bondlength frozen, SCF potential energy surface of Essers *et al* [121], see Figure 4.1. This surface has features which lead to interesting dynamics which is thought to be typical of many triatomic systems[118] but are encountered for LiCN at lower energies than other isomerising systems. The surface predicts a linear LiNC absolute minimum, in agreement with experiment[122], and a metastable linear

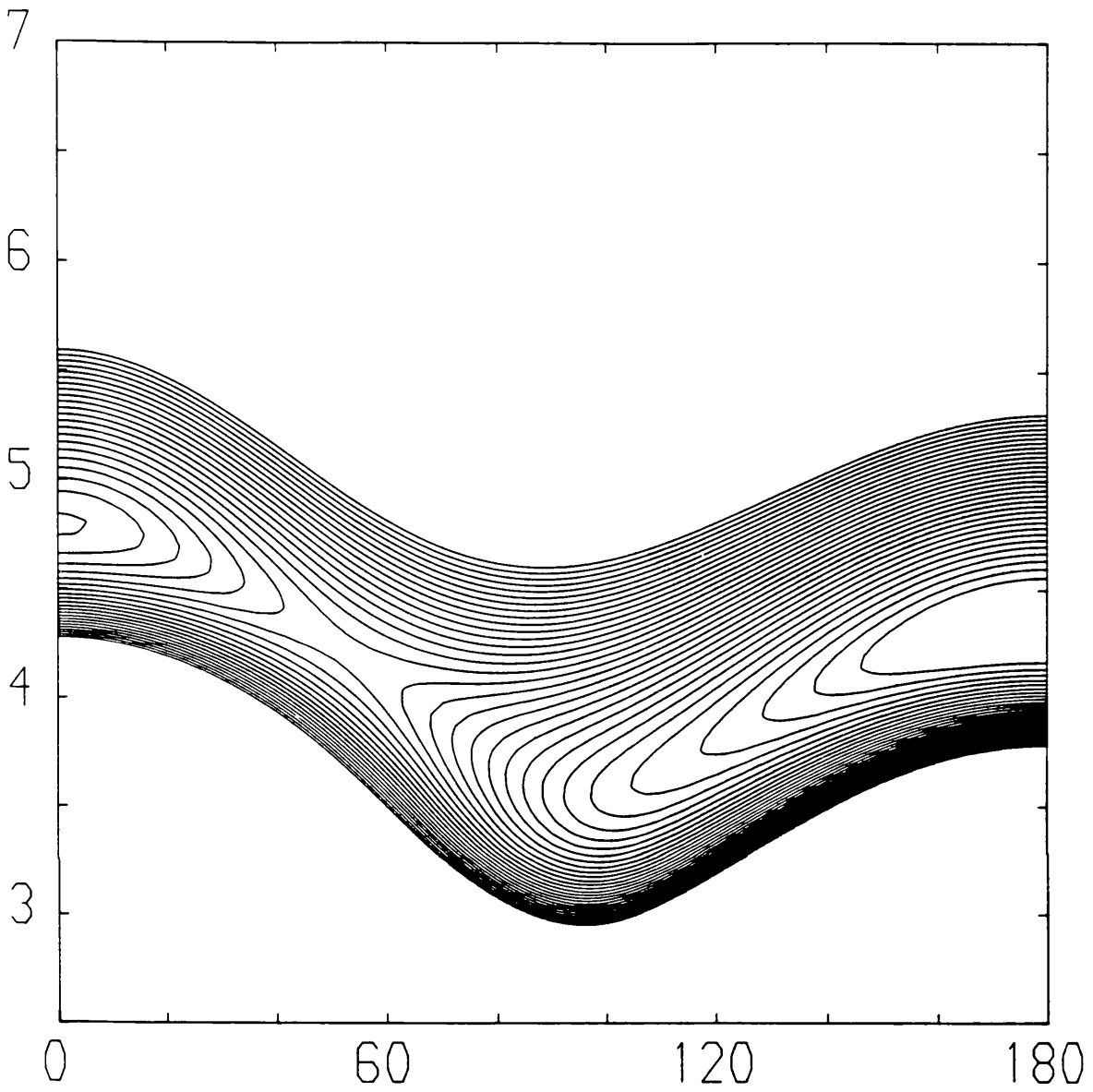


Figure 4.1: Co ntour plots of the potential energy surface for LiNC/LiCN. The vertical axis represents $r_2$ in $a_0$, and the horizontal axis show $\theta$ in degrees. The contours are given at intervals of 240 $cm^{-1}$.

LiCN minimum at 2281 $cm^{-1}$ above LiNC. The minima are separated by a barrier of 3455 $cm^{-1}$ from LiNC. Classical calculations[117] show an onset of chaos approximately halfway to this barrier.

Although there has been a gradual improvement in the methods used to treat the vibrational states of LiCN, all the works cited above concentrated only on the lowest 131 states of the system. Few of these states lie above the barrier to isomerisation of the system; the behaviour of the system well above this barrier thus remains an open question. It is the power of the DVR which allows this question to be addressed in this chapter.

## 4.2 Calculations

Convenient coordinates to represent LiCN are $r_{CN}$, here fixed at 2.186 $a_0$, $r_2$, the distance of Li to the CN centre of mass, and $\theta$, the angle between $r_{CN}$ and $r_2$. These are scattering co-ordinates. $\theta$ runs from $0^o$ for linear LiCN to $180^o$ for linear LiNC. Bačić and Light[53] were the first to employ a discrete variable representation (DVR) of the $\theta$ coordinate for LiCN, although that particular study is limited compared to that presented here.

Reported here are calculations on LiNC/LiCN using the surface of Essers *et al* , see Figure 4.1, and the DVR programs developed from the theory in chapter 2.

Final calculations were performed using a DVR grid in $\theta$ based on 80 Gauss-Legendre quadrature points and 56 previously optimised Morse oscillator-like functions[117] to carry the radial motions. The final Hamiltonian matrix was diagonalised using the $L = 1870$ lowest solutions of the 1D hamiltonians diagonalised for each of the angular quadrature points or 'rays'[53]. This selection criterion is equivalent to choosing all solutions of the 1D problem with energy less

than $E_{RAY} = 13866\ cm^{-1}$. This basis converged the lowest 700 vibrational states of LiCN to within 0.5 $cm^{-1}$; the next 150 states were converged to 2 – 5 $cm^{-1}$; the highest states presented here are only converged to about 10 $cm^{-1}$. Table 4.1 demonstrates convergence of a selection of levels with respect to changing the parameters of the calculation.

In order to analyse the results of this calculation the wavefunctions of the lowest 900 states of the system have been plotted. This method of analysing the system was used by Tennyson and Farantos[117,118] to study the lowest 80 vibrational states of the system. They were able to characterise (a) regular states localised about the LiNC minimum, (b) regular states localised about the LiCN minimum, (c) irregular states localised about the LiNC minimum, (d) irregular delocalised states and possibly (e) two states which had a free rotor-like character. In their work the distinction between regular and irregular states was made according to whether approximate quantum numbers could be assigned on the basis of the observed nodal structure.

In the present calculations the majority of the states are found to be irregular in structure and delocalised. However, inspection of the wavefunctions revealed regular states corresponding to normal modes of LiNC, normal modes of LiCN and free rotor states. These correspond to classes (a), (b) and (e) above. Details of these states are given in Tables 4.2, 4.3 and 4.4 respectively. Tabulation of a complete set of normal mode states is given as no tabulation of these appears to have been given previously. Above the barrier there are very few spatially localised irregular states. Figures 4.2 to 4.5 show typical wavefunctions for the system of type (a), (b), (d) and (e) respectively. These contour plots were obtained using the same coordinate range as the plot of the potential, Figure 4.1, and also have a contour denoting the classical turning point for the state in question. This allows judgements to be made about how individual wavefunctions

Table 4.1: Convergence of the LiCN band origins as a function of parameters used in the calculations. $N_R$ gives the number of Morse oscillator-like functions used for the $r_2$ coordinate. $N_\theta$ gives the number of discrete points used in the angular coordinate, $\theta$. $E_{RAY}$ gives the cut-off energy for solutions of the 1-D radial problem in $cm^{-1}$ relative to the LiNC minimum of the potential yielding a final Hamiltonian matrix of dimension $L$. All band origins are given in $cm^{-1}$ relative to the LiNC ground state at 512.4 $cm^{-1}$. Comparison of levels below level 500 showed them all to be converged to within 0.1 $cm^{-1}$ by the calculations presented here.

| $N_R$ | 56 | 56 | 46 | 51 | 56 | 56 | 56 | 56 |
|---|---|---|---|---|---|---|---|---|
| $N_\theta$ | 70 | 80 | 90 | 90 | 90 | 80 | 80 | 80 |
| $E_{RAY}$ | 13866 | 13866 | 14042 | 13950 | 13866 | 12613 | 13866 | 15231 |
| L | 1455 | 1661 | 1870 | 1870 | 1870 | 1470 | 1661 | 1870 |
| Level | | | | | | | | |
| 500 | 9425.4 | 9425.4 | 9425.4 | 9425.4 | 9425.4 | 9425.6 | 9425.4 | 9425.3 |
| 500 | 9941.2 | 9941.2 | 9941.2 | 9941.2 | 9941.2 | 9941.3 | 9941.2 | 9941.2 |
| 600 | 10442.1 | 10442.1 | 10442.1 | 10442.1 | 10442.1 | 10443.2 | 10442.1 | 10441.9 |
| 650 | 10912.5 | 10912.4 | 10912.7 | 10912.4 | 10912.4 | 10914.4 | 10912.4 | 10912.2 |
| 700 | 11387.8 | 11387.8 | 11390.9 | 11389.4 | 11387.8 | 11390.9 | 11387.8 | 11387.2 |
| 750 | 11816.3 | 11814.6 | 11829.9 | 11815.0 | 11814.6 | 11840.2 | 11814.6 | 11813.2 |
| 800 | 12250.9 | 12250.6 | 12265.4 | 12258.6 | 12250.1 | 12322.6 | 12250.6 | 12247.4 |
| 820 | 12432.8 | 12432.5 | 12453.0 | 12432.3 | 12432.5 | 12541.7 | 12432.5 | 12430.3 |
| 840 | 12596.7 | 12597.6 | 12623.7 | 12602.3 | 12597.5 | 12732.6 | 12597.6 | 12592.2 |
| 860 | 12766.7 | 12765.6 | 12796.7 | 12773.8 | 12765.3 | 12978.6 | 12765.6 | 12758.5 |
| 880 | 12938.0 | 12928.0 | 12978.2 | 12940.8 | 12927.7 | 13205.5 | 12928.0 | 12916.3 |
| 900 | 13109.7 | 13108.7 | 13138.1 | 13113.4 | 13108.7 | 13452.8 | 13108.7 | 13086.5 |

Table 4.2: Assignments to LiNC 'normal mode' states. States are assigned by inspection of the wavefunction (see fig. 4.2) quanta of Li – NC stretch, $\nu_s$, and bend, $\nu_b$. States for which the nodal structures are greatly distorted are denoted by a ?.

| Level | Frequency | Assignment | | Level | Frequency | Assignment | |
|---|---|---|---|---|---|---|---|
| no. | $cm^{-1}$ | $\nu_s$ | $\nu_b$ | no. | $cm^{-1}$ | $\nu_s$ | $\nu_b$ |
| 1 | 0.0 | 0 | 0 | 19 | 1738.7 | 2 | 2 |
| 2 | 247.2 | 0 | 2 | 20 | 1786.6 | 1 | 12? |
| 3 | 469.0 | 0 | 4 | 21 | 1874.8 | 0 | 22? |
| 4 | 665.6 | 0 | 6 | 22 | 1919.2 | 1 | 14? |
| 5 | 754.4 | 1 | 0 | 23 | 1946.4 | 2 | 4 |
| 6 | 836.8 | 0 | 8 | 24 | 2036.8 | 0 | 24? |
| 7 | 982.3 | 0 | 10 | 26 | 2118.1 | 2 | 6 |
| 8 | 998.1 | 1 | 2 | 28 | 2231.8 | 3 | 0 |
| 9 | 1111.7 | 0 | 12 | 29 | 2244.9 | 0 | 26? |
| 10 | 1212.8 | 1 | 4 | 30 | 2246.8 | 2 | 8? |
| 11 | 1245.3 | 0 | 14 | 32 | 2340.4 | 2 | 10? |
| 12 | 1390.3 | 0 | 16 | 34 | 2418.2 | 0 | 28? |
| 13 | 1397.7 | 1 | 6 | 35 | 2452.3 | 2 | 12? |
| 14 | 1498.4 | 2 | 0 | 36 | 2469.0 | 3 | 2 |
| 15 | 1545.4 | 0 | 18 | 37 | 2531.3 | 0 | 30? |
| 16 | 1550.4 | 1 | 8 | 41 | 2669.1 | 3 | 4 |
| 17 | 1671.5 | 1 | 10 | 44 | 2761.8 | 0 | 32? |
| 18 | 1708.4 | 0 | 20 | 45 | 2825.4 | 3 | 6 |

Table 4.2: (continued)

| Level no. | Frequency $cm^{-1}$ | Assignment $\nu_a$ | Assignment $\nu_b$ | Level no. | Frequency $cm^{-1}$ | Assignment $\nu_a$ | Assignment $\nu_b$ |
|---|---|---|---|---|---|---|---|
| 49 | 2918.4 | 0 | 34? | 199 | 5740.6 | 8 | 0 |
| 48 | 2918.3 | 3 | 8? | 213 | 5964.4 | 8 | 2 |
| 51 | 2954.8 | 4 | 0 | 245 | 6410.6 | 9 | 0 |
| 53 | 2995.5 | 3 | 10? | 262 | 6632.2 | 9 | 2 |
| 54 | 3025.0 | 0 | 36? | 272 | 6780.3 | 9 | 4 |
| 57 | 3112.8 | 3 | 12? | 294 | 7070.0 | 10 | 0 |
| 59 | 3188.8 | 4 | 2? | 347 | 7718.6 | 11 | 0 |
| 68 | 3382.0 | 4 | 4 | 365 | 7935.9 | 11 | 2 |
| 75 | 3565.5 | 4 | 6? | 400 | 8356.6 | 12 | 0 |
| 81 | 3667.1 | 5 | 0 | 457 | 8984.2 | 13 | 0 |
| 91 | 3898.5 | 5 | 2 | 515 | 9601.4 | 14 | 0 |
| 93 | 3921.5 | 3 | 14? | 536 | 9814.7 | 14 | 2 |
| 100 | 4083.5 | 5 | 4 | 575 | 10208.0 | 15 | 0 |
| 117 | 4368.9 | 6 | 0 | 598 | 10418.8 | 15 | 2 |
| 128 | 4597.6 | 6 | 2 | 638 | 10804.4 | 16 | 0 |
| 139 | 4775.9 | 6 | 4 | 701 | 11390 | 17 | 0 |
| 144 | 4874.8 | 6 | 8 | 725 | 11597 | 17 | 2 |
| 156 | 5060.1 | 7 | 0 | 767 | 11965 | 18 | 0 |
| 169 | 5286.3 | 7 | 2 | 832 | 12531 | 19 | 0 |
| 180 | 5455.0 | 7 | 4 | 900 | 13086 | 20 | 0 |

Table 4.3: Assignments to LiCN 'normal mode' states. States are assigned by inspection of the wavefunction (see Figure 4.3) quanta of Li – CN stretch, $\nu_s$, and bend, $\nu_b$. States for which the nodal structures are greatly distorted are denoted by a ?. Frequencies are relative to the LiCN (0,0) state which lies 2286.6 $cm^{-1}$ above the LiNC (0,0) state.

| Level | Frequency | Assignment | | Level | Frequency | Assignment | |
|---|---|---|---|---|---|---|---|
| no. | $cm^{-1}$ | $\nu_s$ | $\nu_b$ | no. | $cm^{-1}$ | $\nu_s$ | $\nu_b$ |
| 31 | 0.0 | 0 | 0 | 171 | 3034.7 | 4 | 2 |
| 40 | 323.0 | 0 | 2 | 192 | 3345.5 | 5 | 0 |
| 47 | 610.1 | 0 | 4 | 206 | 3573.4 | 4 | 6 |
| 52 | 689.1 | 1 | 0 | 215 | 3687.7 | 5 | 2 |
| 58 | 853.7 | 0 | 6 | 234 | 3978.5 | 6 | 0 |
| 64 | 1016.2 | 1 | 2? | 236 | 3991.2 | 5 | 4 |
| 76 | 1306.3 | 1 | 4 | 253 | 4229.9 | 5 | 6 |
| 80 | 1368.0 | 2 | 0 | 260 | 4267.7 | 6 | 2 |
| 88 | 1550.6 | 1 | 6 | 281 | 4608.8 | 7 | 0 |
| 96 | 1700.0 | 2 | 2 | 284 | 4638.2 | 6 | 4? |
| 111 | 1992.2 | 2 | 4 | 302 | 4875.6 | 6 | 6 |
| 113 | 2055.7 | 3 | 0 | 309 | 4963.3 | 7 | 2 |
| 123 | 2234.2 | 2 | 6 | 330 | 5228.8 | 8 | 0 |
| 131 | 2372.4 | 3 | 2 | 335 | 5271.9 | 7 | 4 |
| 148 | 2666.8 | 3 | 4 | 353 | 5516.6 | 7 | 6 |
| 151 | 2695.6 | 4 | 0 | 360 | 5585.2 | 8 | 2 |
| 163 | 2912.3 | 3 | 6 | 381 | 5836.9 | 9 | 0 |

Table 4.3: (continued)

| Level no. | Frequency $cm^{-1}$ | Assignment $\nu_s$ | $\nu_b$ | Level no. | Frequency $cm^{-1}$ | Assignment $\nu_s$ | $\nu_b$ |
|---|---|---|---|---|---|---|---|
| 413 | 6199.8 | 9 | 2? | 603 | 8177.4 | 13 | 0 |
| 433 | 6435.5 | 10 | 0 | 663 | 8739.4 | 14 | 0 |
| 468 | 6802.8 | 10 | 2 | 723 | 9205 | 15 | 0 |
| 489 | 7026.3 | 11 | 0 | 785 | 9842 | 16 | 0 |
| 525 | 7398.8 | 11 | 2 | 854 | 10421 | 17 | 0 |
| 545 | 7606.3 | 12 | 0 | | | | |

Table 4.4: Assignments to LiCN 'free rotor' states. States are assigned by inspection of the wavefunction (see Figure 4.5) quanta of Li – CN stretch, $\nu_s$, and bend (or free rotation), $m$. States for which the nodal structures are greatly distorted are denoted by a ?. Frequencies are relative to the LiNC (0,0) state.

| Level | Frequency | Assignment | | Level | Frequency | Assignment | |
|---|---|---|---|---|---|---|---|
| no. | $cm^{-1}$ | $\nu_s$ | $m$ | no. | $cm^{-1}$ | $\nu_s$ | $m$ |
| 65 | 3311.3 | 0 | 24 | 366 | 7938.3 | 0 | 53? |
| 71 | 3474.8 | 0 | 26 | 375 | 8055.2 | 2 | 48? |
| 74 | 3552.1 | 0 | 27? | 382 | 8141.9 | 0 | 54 |
| 82 | 3671.8 | 0 | 28 | 399 | 8349.5 | 0 | 55? |
| 87 | 3819.4 | 0 | 29? | 409 | 8454.9 | 1 | 52? |
| 94 | 3968.4 | 0 | 30? | 459 | 8989.7 | 0 | 58 |
| 110 | 4275.1 | 0 | 33? | 499 | 9418.6 | 0 | 60 |
| 145 | 4896.6 | 1 | 31? | 519 | 9634.0 | 0 | 61? |
| 150 | 4971.9 | 0 | 37? | 563 | 10075.7 | 0 | 63 |
| 160 | 5139.7 | 1 | 33? | 586 | 10299.5 | 0 | 64? |
| 181 | 5468.6 | 0 | 40 | 609 | 10520.5 | 0 | 65 |
| 191 | 5623.3 | 0 | 41? | 682 | 11197.5 | 0 | 66? |
| 237 | 6295.2 | 0 | 45? | 732 | 11652 | 0 | 68? |
| 333 | 7539.8 | 0 | 51 | 783 | 12108 | 0 | 70? |
| 349 | 7737.1 | 0 | 52 | 810 | 12337 | 0 | 73 |

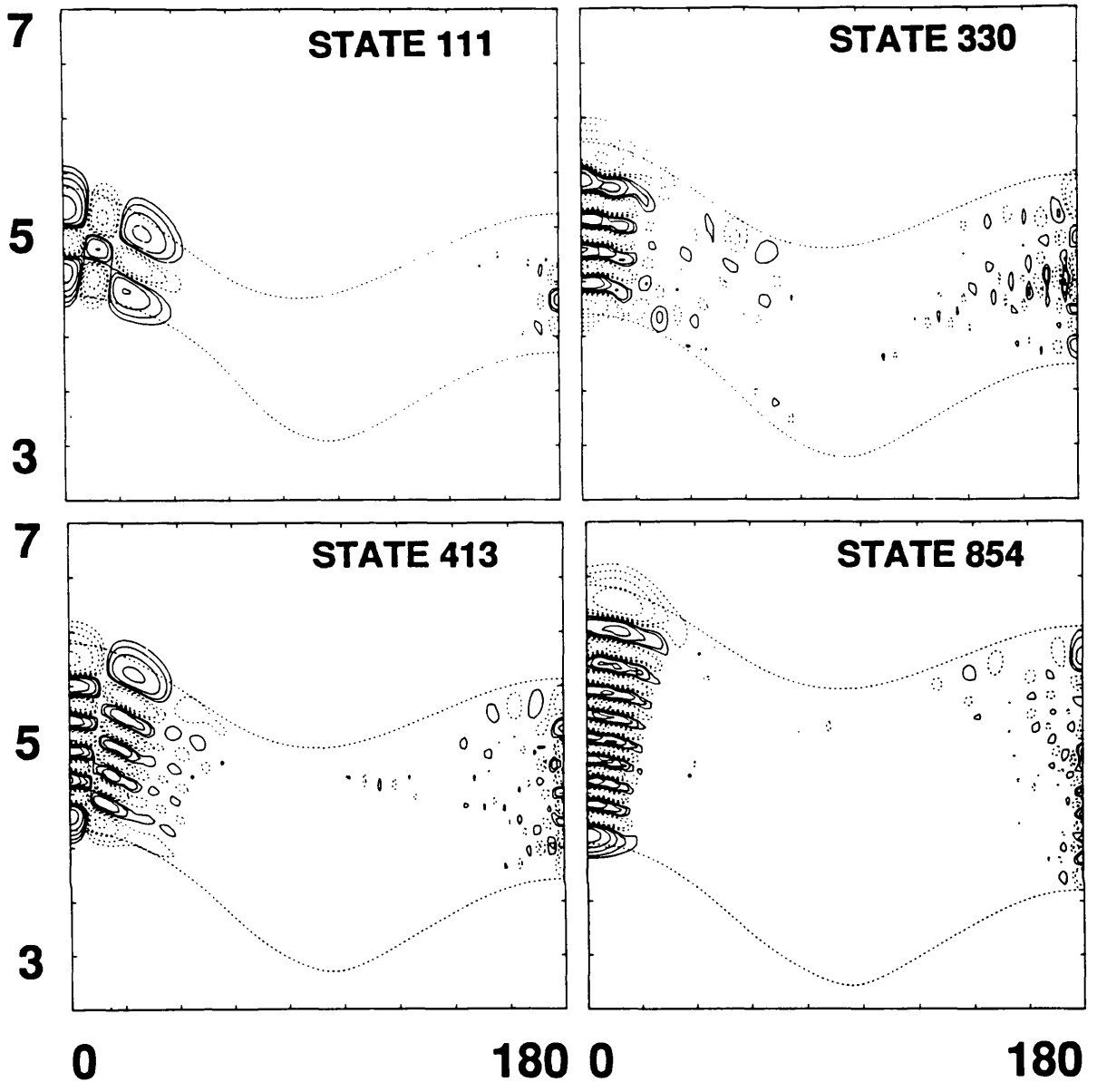


Figure 4.2: Co ntour plots of 4 typical LiCN normal mode states. The vertical axes represent $r_2$ in $a_0$, and the horizontal axes show $\theta$ in degrees. Solid (dashed) contours enclose regions where the wavefunction has positive (negative) amplitude. Contours are drawn at 4%, 8%, 16%, 32% and 64% of the maximum ampliude of the wavefunction. The outer dashed contours represent the classical turning point of the potential for the associated eigenvalue.

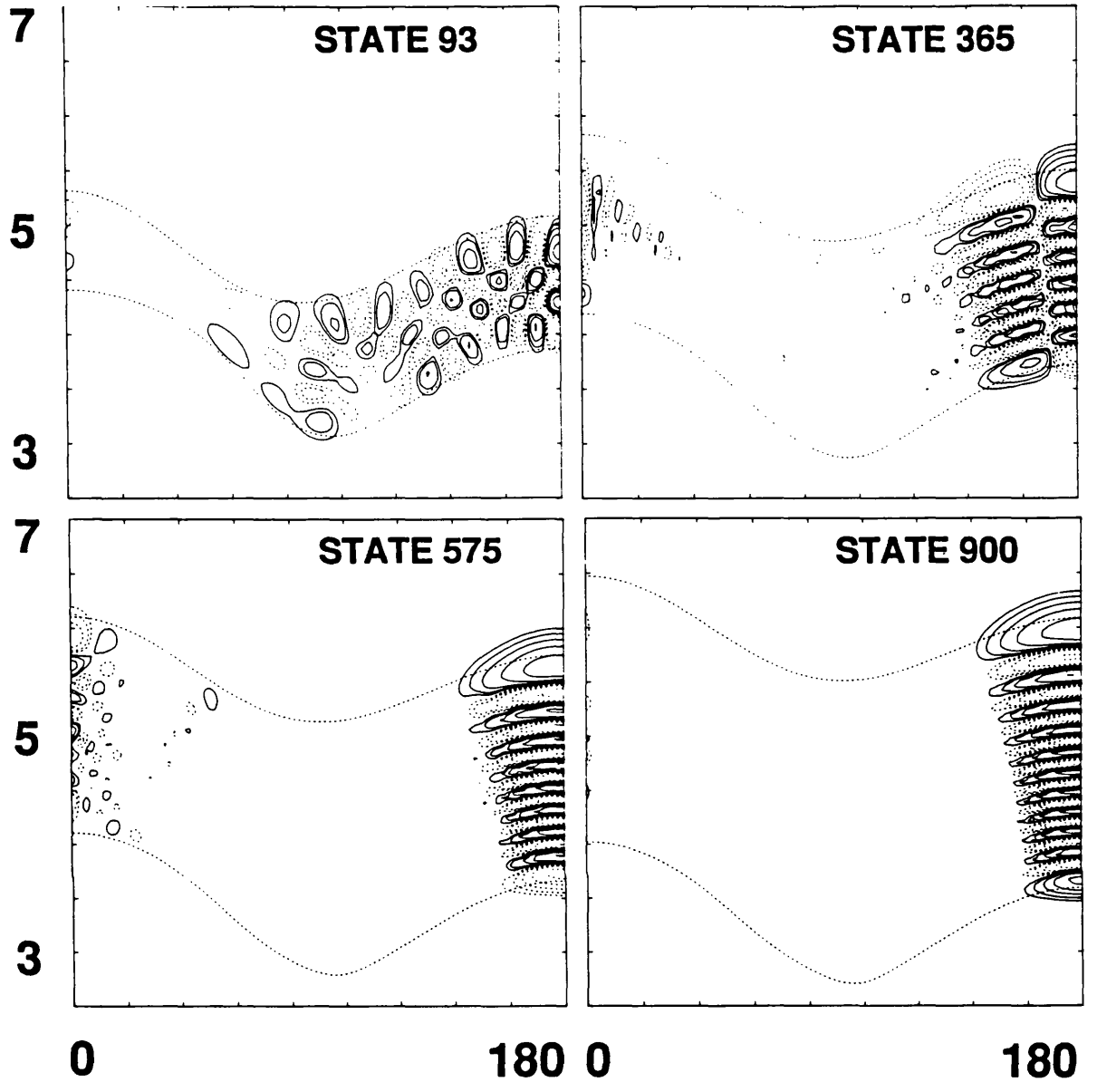


Figure 4.3: Co ntour plots of 4 typical LiNC normal mode states. Contours and axes as in Figure 4.2.

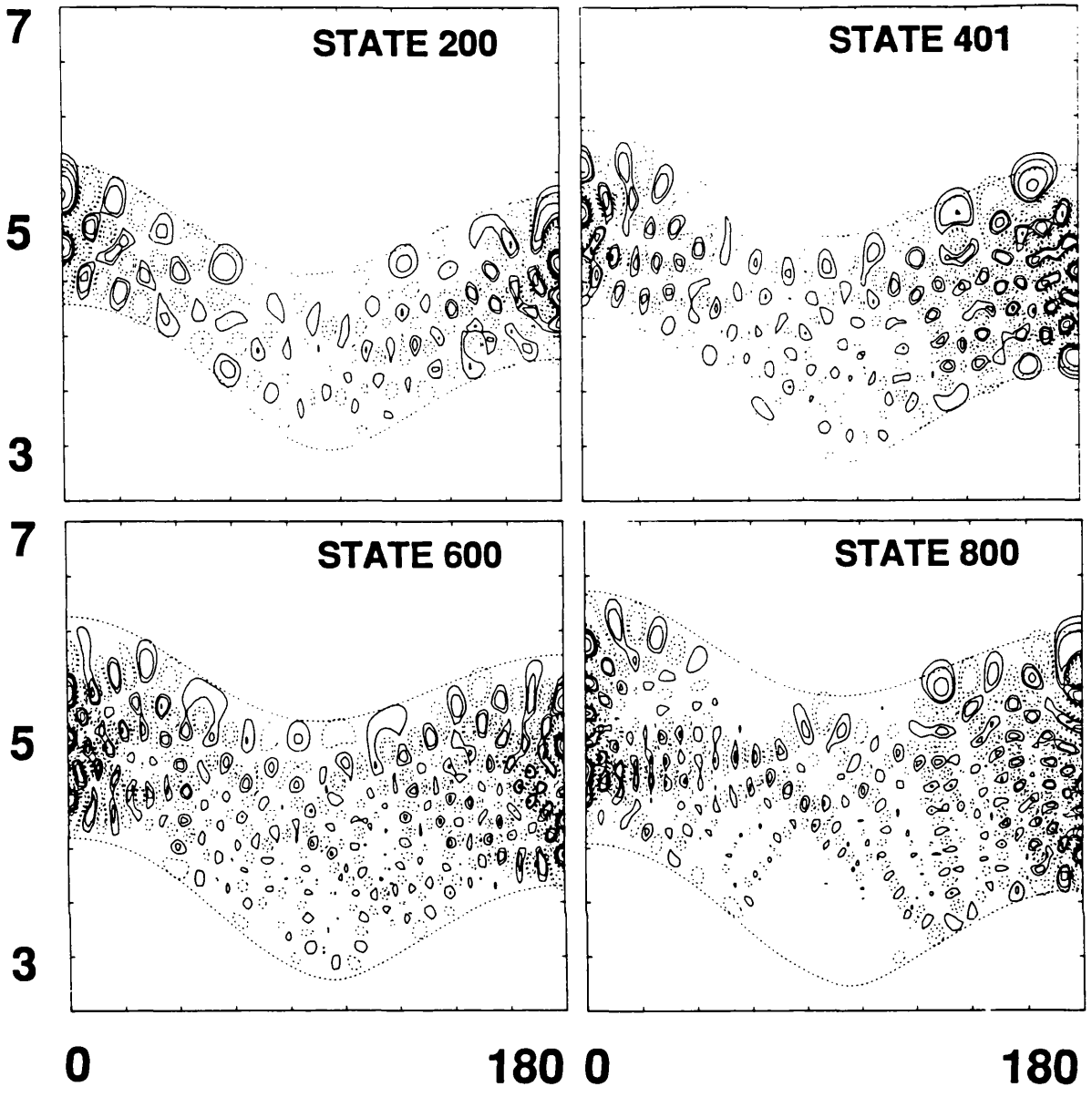


Figure 4.4: Co ntour plots of 4 typical unassignable states. Contours and axes as in Figure 4.2.

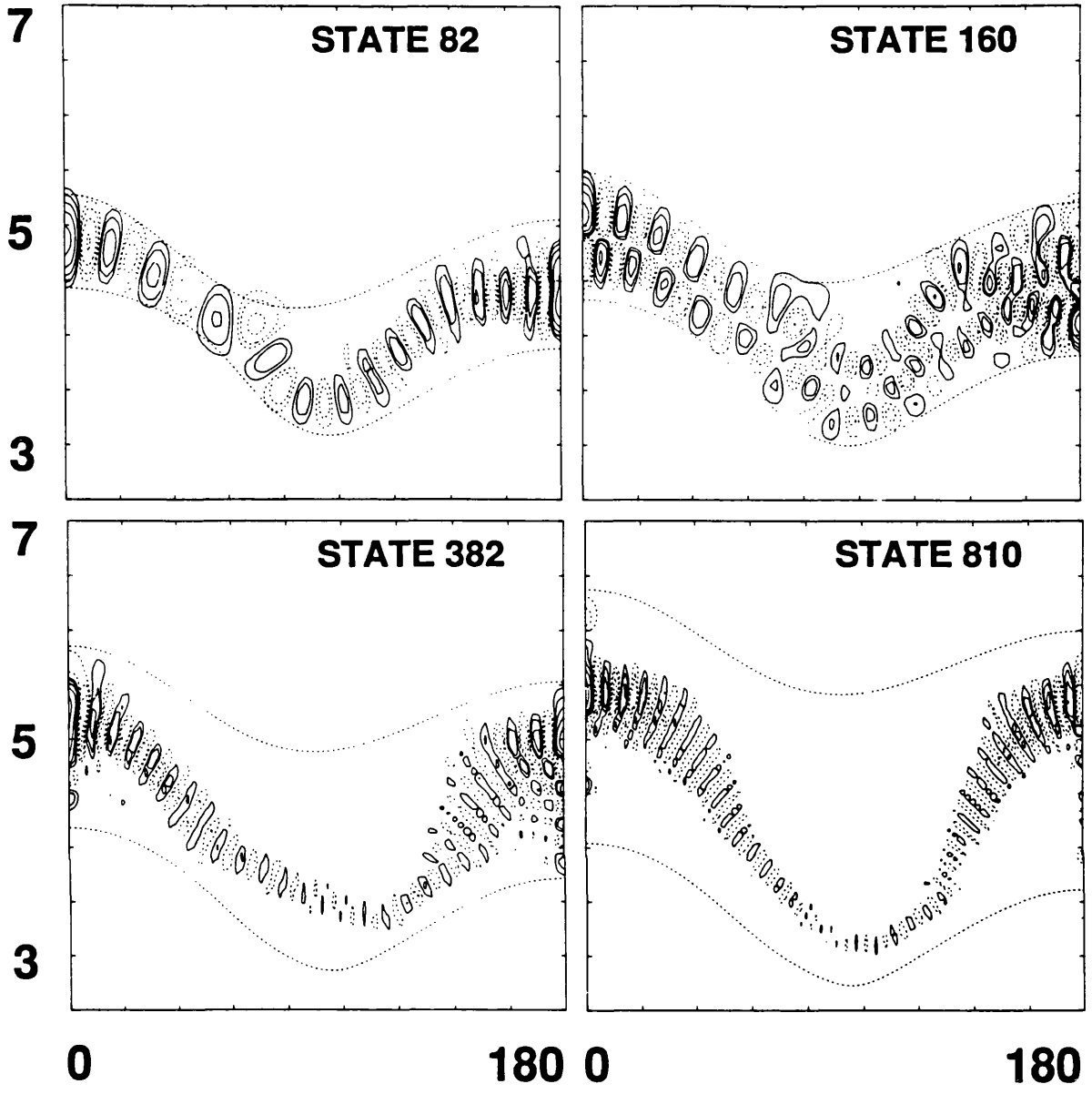


Figure 4.5: Co ntour plots of 4 typical free rotor states. Contours and axes as in Figure 4.2.

reflect the shape of the underlying potential function and the degree to which these wavefunctions sample the available coordinate space.

Another tool that has been used to analyse the behaviour of quantum mechanical systems in regions where their classical analog is chaotic is the distribution of spacings between neighbouring levels. This distribution should tend to a Poisson-type distribution for regular states[123] and a Wigner distribution for irregular ones[124]. Farantos and Tennyson[117] looked at the distribution of the lowest 80 energy levels of LiCN using these ideas but their analysis was inconclusive because of the poor statistics involved.

An investigation was made into the behaviour of the levels using a Brody distribution[125,126]:

$$P_q(S) = \alpha S^q \exp(-\beta S^{1+q}) \tag{4.1}$$

where

$$\alpha = (1+q)\beta, \qquad \beta = \left[\bar{S}^{-1}\Gamma\left(\frac{2+q}{1+q}\right)\right]^{1+q} \tag{4.2}$$

where S is the spacing between neighbouring levels. The Brody distribution is a generalisation which gives a Poisson distribution for $q = 0$ and a Wigner distribution for $q = 1$. In practice the parameter $q$ is least-squares fitted to the nearest neighbour distribution in question. For more details see Haller *et al* [126].

One difficulty with the present results, and possibly with any attempt to analyse the level spacing distributions of molecules, is that the density of states increases with energy. This has a tendency to distort the idealised distributions. Although unfolding procedures have been proposed to circumvent this problem[127], it was decided to analyse small portions of the spectrum consisting of up to 200 levels at one time. Table 4.5 presents a summary of the results and Figure 4.6 shows some of the resulting distributions.

Table 4.5: Level spacing distribution Brody parameter[125,126], $q$, for the levels of LiCN presented here. Fits to level 101 upwards were to distributions obtained by binning the level spacings in 25 bins 2 $cm^{-1}$ wide. Levels 1-30 were placed in 12 bins of width 20 $cm^{-1}$ and levels 31-100 in 14 bins of width 5 $cm^{-1}$. The average level spacing, $\bar{S}$, in $cm^{-1}$ and the standard deviation, $\sigma$, of the fit in units of probability as well as the percentage of unassigned states, u, in each fit are also given.

| Levels | $\bar{S}$ | q | $\sigma$ | u |
|---|---|---|---|---|
| 1–30 | 77.5 | 0.154 | 0.034 | 7% |
| 31–100 | 26.0 | 0.588 | 0.030 | 44 |
| 101–300 | 15.3 | 0.785 | 0.012 | 81 |
| 201–400 | 13.0 | 0.798 | 0.015 | 85 |
| 301–500 | 11.4 | 0.764 | 0.017 | 88 |
| 401–600 | 10.5 | 0.794 | 0.013 | 91 |
| 501–700 | 9.8 | 0.859 | 0.011 | 93 |
| 601–800 | 9.0 | 0.830 | 0.012 | 94 |
| 701–900 | 8.6 | 1.049 | 0.011 | 95 |

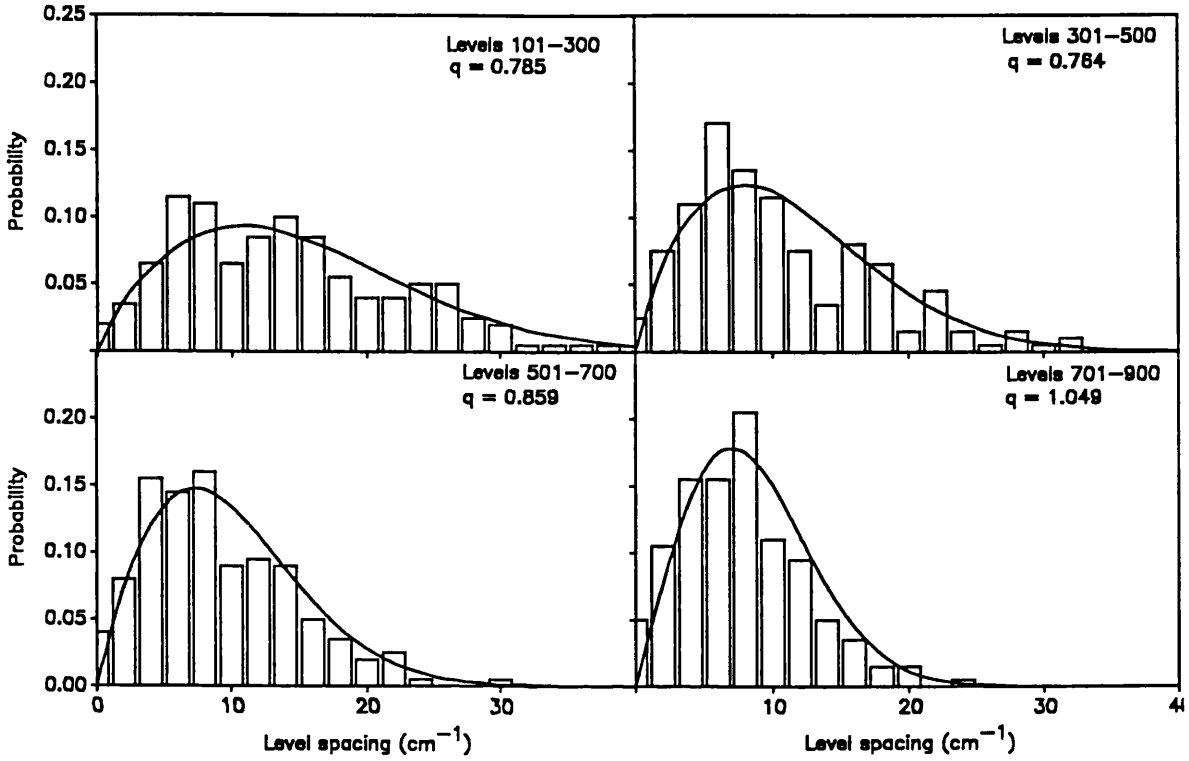


Figure 4.6: Sample nearest-neighbour level spacing distributions for blocks of 200 levels. The solid line is the curve given by the best fit to a Brody distribution with $q$ as indicated.

## 4.3 Discussion and Conclusions

As observed previously[117,118], the study of the nodal structure of the wavefunction is highly informative. In the region above the barrier regular states were identified which stem from the zeroth-order hamiltonians for LiNC normal modes, LiCN normal modes and the free rotation of $Li^+$ about $CN^-$. These states should be associated with stable periodic orbits in the corresponding classical problem although free rotor periodic orbits have yet to be identified. The systematic absences in the assignable free rotor states probably correlate with energy regions where the classical free rotor periodic orbit is unstable. Similar behaviour has recently been noted in 2D studies of the vibrational states of $H_3^+$[72]. Another indicator that the free rotor states do not all correspond to a uniform series of states is given by the failure to fit the energy levels of these states to a model free rotor Hamiltonian.

Corresponding to the classically chaotic sea are the many irregular, delocalised states which are visibly ergodic in the sense that their wavefunctions sample all of coordinate space – see Figure 4.4 for example. An estimate of the proportion of unassignable states as a function of energy is given by Table 4.5. This shows that above the barrier to isomerisation, which is reached at about state 70, only a small proportion of the states can even be approximately assigned. This change in behaviour is reflected by the Brody parameter which shows a rapid change from a near-regular (Poisson) distribution for the lowest levels to a chaotic (Wigner) distribution for levels above the barrier. The use of level spacing distributions as a measure of 'quantum chaos' has proved controversial[128]. However, for the results given here these distributions appear to give a true reflection of the underlying nature of the system.

In summary, a discrete variable representation in one internal co-ordinate has been used to substantially extend our knowledge of the high lying vibrational

levels of the 2D Li – CN system. Above the barrier to isomerisation this system displays a large proportion of states that cannot be assigned. However, regular states corresponding to LiNC normal modes, LiCN normal modes and free-rotor states all exist over the entire frequency range studied.

Since the above analysis a further inspection has been made of some of the wavefunction plots. This was inspired by the suggestion that there may be some interesting features corresponding to islands of stability in the classical dynamics[120,129]. An interesting such feature is shown in Figure 4.7a for vibrational state number 304. It can be seen that there exists a localised circular-type 'whirl' in the wavefunction centered at about $\theta = 100^o$ and $r_2 = 3.8a_0$; this wavefunction is otherwise totally irregular and delocalised.

It would be interesting to know if this intriguing feature were simply an artefact of a particular solution of a particular potential surface, or perhaps is a manifestation of some more general property. One method to indicate whether this curiousity be worth pursuing is to determine if this small localisation is stable with respect to small perturbations in the potential. This test was used by Farantos and Tennyson in an earlier study of LiCN/LiNC[117].

The third term in the 9-term potential Legendre expansion was perturbed by 1% and 2% and the wavefunction for state 304 was calculated. The two wavefunctions of the perturbed system are shown in Figures 4.7b and 4.7c. It can be seen that the general shape of this feature still remains, indicating that it may well be stable. If it were not stable then the perturbations enforced should easily be strong enough to destroy it. Farantos and Tennyson[117] also perturbed this term, and showed that even at very much lower energies these perturbations were enough to totally disrupt the energy pattern.

Classical trajectory calculations are currently underway to investigate this further[129].

Figure 4.7:(overleaf) Countour plots of vibrational state 304 for perturbations of a) 0%, b) 1% and c) 2% of the potential. The 'whirl' in the wavefunction (see text) is centered at about $\theta = 100^o$ and $r_2 = 3.8a_0$. Contours and axes are as in Figure 4.2.

Fig 4.7

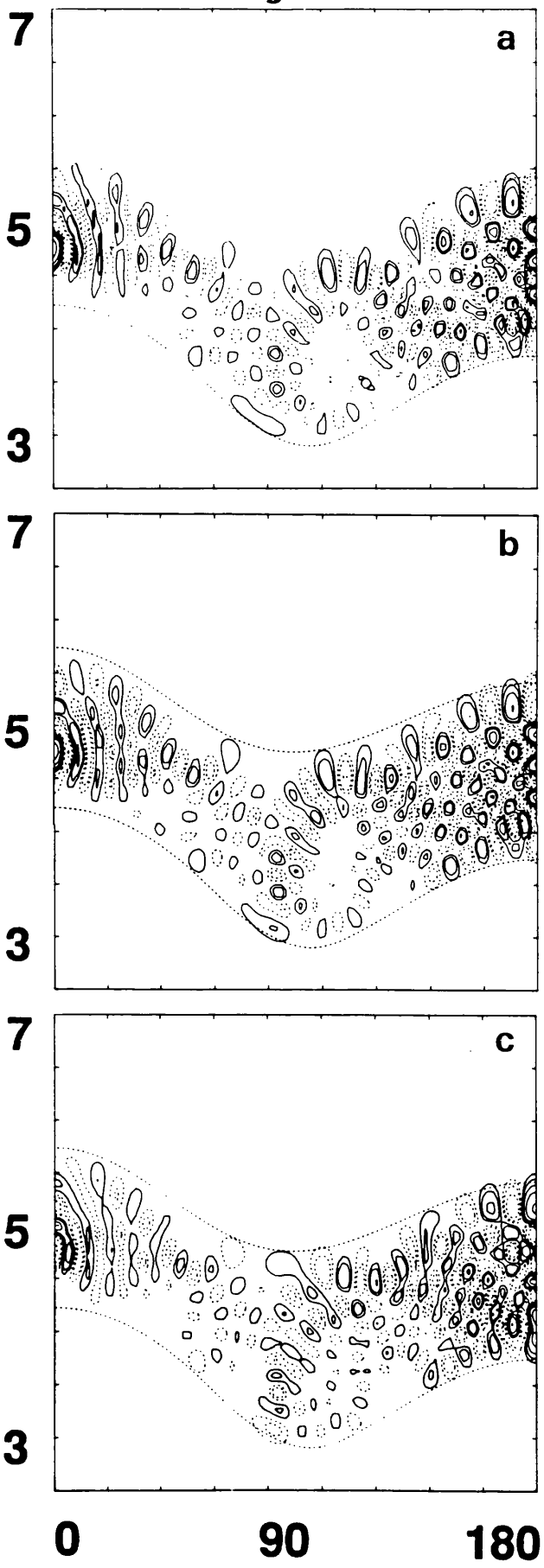

# Chapter 5

# $H_3^+$: A DVR in $\theta$

## 5.1 Introduction

The unassigned, near-dissociation, infrared spectrum of $H_3^+$ recorded by Carrington and Kennedy[1,2] has given rise to much interest and speculation. The generally accepted explanation of these extremely rich spectra is that high angular momentum states are being observed with the final state undergoing rotational predissociation[130,131,132,133]. However, coarse grained versions of these spectra display regular features which has been attributed to underlying regular features in the classical motions of the system. An example of this motion is the 'horseshoe' periodic orbit of Gomez Llorrente and Pollak[134]. This is when one proton vibrates rapidly in and out through the other two, forcing these two to vibrate in and out themselves as it does so. This can be interpreted as the very highly excited bending motion of a quasi-linear molecule. Gomez Llorrente and Pollak[134] propose that this motion, in the Carrington Kennedy spectrum, is rotating about it's $C_{2v}$ axis of symmetry. A major support for this theory is that the rotational constant of the 'horseshoe' orbit is in good agreement with the spacings of the clumps in the low resolution spectrum. Until now these classical

investigations have awaited confirmation from fully quantum mechanical studies.

Limited quantum mechanical calculations[72,135,136] have been made which suggest that the 'horseshoe' orbit should be found at high energies in *fully coupled* quantum calculations. No-one has yet been successful in performing these calculations. It is this problem for which the power of the DVR is used in this chapter and the next. It is well known[80] that FBR methods become inappropriate for this system at or about when it becomes linear (about one third of the way to dissociation).

In this chapter results are presented for $H_3^+$ using a DVR in $\theta$ and an FBR in $r_1$ and $r_2$, the theory for this being given in §3.3. It is found that this approach enables accurate calculations to be made about two thirds of the way to dissociation.

## 5.2 Calculations

### 5.2.1 J = 0

In a recent study of near-dissociating states of $H_3^+$, Tennyson, Brass and Pollak (TBP)[72] performed a series of reduced dimensionality calculations on the system in the $C_{2v}$ subspace obtained by freezing $\theta$ at 90°. By using basis sets composed of 23 Morse oscillator-like functions for the $r_1$ co-ordinate and 29 spherical oscillators for the $r_2$ co-ordinate, they were able to obtain converged solutions for the system up to dissociation. These calculations correspond closely to the first step in the DVR-in-$\theta$ approach and involved simply the solution of $\hat{h}_\alpha^k$ for $\chi_{k\alpha} = 0$.

Test calculations at other angles showed that TBP's basis was flexible enough to give a good representation of the system for a range of $\theta$ values. It was therefore decided to use this basis to represent the solutions of $\hat{h}_\alpha^k$.

Table 5.1: $H_3^+$ vibrational band origins, in $cm^{-1}$, as a function of DVR points, $N_\theta$, size of the final Hamiltonian matrix, $L$, and cut-off energy, in $cm^{-1}$, relative to the lowest 2D solution, $\epsilon^{2D}$.

| $L$ | 2000 | 2222 | 2657 | 2400 | 2800 |
|---|---|---|---|---|---|
| $N_\theta$ | 36 | 40 | 48 | 36 | 36 |
| $\epsilon^{2D}$ | 34930 | 34930 | 34930 | 37390 | 39669 |
| level | | | | | |
| 21 | 10592.6 | 10592.6 | 10592.6 | 10592.4 | 10592.3 |
| 41 | 13582.1 | 13582.1 | 13582.1 | 13581.3 | 13580.9 |
| 61 | 15369.8 | 15369.9 | 15370.0 | 15368.9 | 15368.3 |
| 81 | 17219.1 | 17219.1 | 17219.2 | 17217.7 | 17217.0 |
| 101 | 18435.0 | 18435.1 | 18435.1 | 18433.7 | 18433.1 |
| 121 | 19514 | 19514 | 19514 | 19511 | 19509 |
| 141 | 20498 | 20498 | 20498 | 20495 | 20493 |
| 161 | 21433 | 21433 | 21434 | 21429 | 21428 |
| 180 | 22215 | 22215 | 22215 | 22209 | 22206 |

Table 5.1 shows the convergence characteristics of a selection of states as a function of changing the size of final basis $L$, and DVR grid, $N_\theta$. Demonstrating convergence with the DVR method is not as straightforward as with FBR calculations. Firstly, the DVR method is not variational and therefore convergence is not necessarily obtained from above and secondly because increasing the DVR grid can actually make a calculation worse unless some means is devised of keeping the number of functions per grid point approximately constant. This is further complicated by the fact that the grid points move when the number of points is changed.

As explained in chapter 3, we include in the final problem all the 2D solutions

whose eigenenergies lie below some energy cut-off, $\epsilon^{2D}$. The first three columns of Table 5.1 demonstrate the effect of increasing the number of DVR points with a constant cut-off energy. The final columns show convergence for a constant grid as the energy cut-off or total number of functions, $L$, included in the final problem is increased.

The final column of Table 5.1 gives the best results obtained, which are presented in full in Table 5.2. For $E$ symmetry states only the lower component of each doublet is shown. For comparison the results of Whitnell and Light[45] and Miller and Tennyson[137] are also given. Assignments are given where possible. These assignments were obtained by plotting cuts through the wavefunctions for $\theta = 90^o$ and confirmed by inspecting other cuts with $\theta = 80^o, 70^o$ and $0^o$. This method of assignment, as used in chapters 4 and 6 also, is necessarily approximate and was only attempted for even q = 0 ($A_1$ or $E_e$) states as the odd q = 1 ($A_2$ or $E_o$) states have a node at $\theta = 90^o$. The assignment of a vibrational angular momentum quantum number, $\ell$, to excitations of the degenerate $\nu_2$ bending mode is not possible by visual inspection of the plots and has not been attempted.

### 5.2.2 J = 1

Calculations for the first rotationally-excited state of $H_3^+$ were performed using the $N_\theta = 36$, $L = 2800$ basis used for the $J = 0$ results presented above. Table 5.3 shows the convergence of the lowest 151 $J = 1, p = 0, q = 0$ states as a function of the number of functions, $I$, included in the final step of the calculation. The levels span the rotational manifold of the lowest 102 vibrational states.

Table 5.4 gives all the $J = 1$ levels of $H_3^+$ for the lowest vibrational states. The results are only presented in this form for the lowest 41 states as analysis of the higher states becomes increasingly difficult. This is because the increased density of states makes the assignment of rotational levels to a particular vibrational state

Table 5.2: Band origins, in $cm^{-1}$, for the lowest 180 states of $H_3^+$ calculated using $L = 2800$, $N_\theta = 36$. Results due to Whitnell and Light[45] and Miller and Tennyson[137] are shown for comparison. Tentative assignments are given where possible.

| Level | Symmetry | $(\nu_1, \nu_2^\ell)$ | This work | WL | MT |
|---|---|---|---|---|---|
| 1 | $A_1$ | $(0,0^0)$ | [4363.5][b] | [4364.0][b] | [4363.5][b] |
| 2 | E | $(0,1^1)$ | 2521.3 | 2521.5 | 2521.3 |
| 3 | $A_1$ | $(1,0^0)$ | 3178.4 | 3178.7 | 3178.4 |
| 4 | $A_1$ | $(0,2^0)$ | 4777.1 | 4777.5 | 4777.0 |
| 5 | E | $(0,2^2)$ | 4997.4 | 4997.6 | 4997.4 |
| 6 | E | $(1,1^1)$ | 5553.7 | 5554.2 | 5553.7 |
| 7 | $A_1$ | $(2,0^0)$ | 6262.0 | 6262.6 | 6262.0 |
| 8 | E | $(0,3^1)$ | 7003.5 | 7003.9 | 7003.4 |
| 9 | $A_1$ | $(0,3^3)$ | 7282.6 | 7283.2 | 7282.5 |
| 10 | $A_2$ | $(0,3^3)$ | 7492.7 | 7493.3 | 7492.7 |
| 11 | $A_1$ | $(1,2^0)$ | 7769.2 | 7770.0 | 7769.2 |
| 12 | E | $(1,2^2)$ | 7868.7 | 7869.1 | 7868.8 |
| 13 | E | $(2,1^1)$ | 8487.0 | 8487.7 | 8487.1 |
| 14 | $A_1$ | $(0,4^0)$ | 8996.8 | 8997.6 | |
| 15 | E | $(0,4^2)$ | 9107.7 | 9108.2 | |
| 16 | $A_1$ | (3,0) | 9251.6 | 9252.6 | 9251.6 |
| 17 | E | (1,3)? | 9650.7 | 9651.1 | |
| 18 | $A_1$ | (1,3) | 9964.2 | 9965.0 | |
| 19 | E | (1,3)? | 9996.6 | 9997.5 | |
| 20 | $A_2$ | | 10208.6 | 10209.5 | |

Table 5.2:(continued)

| Level | Symmetry | $(\nu_1, \nu_2^\ell)$ | This work | WL | MT |
|---|---|---|---|---|---|
| 21 | $A_1$ | (2,2)? | 10592.3 | 10593.3 | |
| 22 | E | (2,2)? | 10642.8 | 10643.3 | |
| 23 | E | (0,5) | 10853.5 | 10854.1 | |
| 24 | $A_1$ | (0.5) | 10913.4 | 10914.4 | |
| 25 | E | (3,1) | 11321.6 | 11322.5 | |
| 26 | $A_2$ | | 11525.8 | 11526.4 | |
| 27 | E | (1,4)? | 11651.4 | 11652.6 | |
| 28 | $A_1$ | (1,4)? | 11809.6 | 11811.0 | |
| 29 | E | u | 12073.5 | 12074.2 | |
| 30 | $A_1$ | (4,0) | 12146.0 | 12417.4 | |
| 31 | E | (0,6) | 12294.5 | 12295.5 | |
| 32 | $A_1$ | (0,6) | 12363.8 | 12365.2 | |
| 33 | E | (0,6)? | 12467.8 | 12469.0 | |
| 34 | $A_1$ | (2,3)? | 12584.7 | 12585.8 | |
| 35 | E | (2,3)? | 12694.3 | 12695.8 | |
| 36 | $A_2$ | | 12828.6 | 12829.5 | |
| 37 | $A_1$ | u | 13285.1 | 13286.8 | |
| 38 | E | (4,1)? | 13313.7 | 13314.9 | |
| 39 | E | (1,5)? | 13385.6 | 13387.6 | |
| 40 | $A_1$ | (1,4)? | 13392.2 | 13395.6 | |
| 41 | E | (1,5)? | 13581.0 | 13582.7 | |
| 42 | E | (0,7) | 13681.3 | 13684.7 | |

Table 5.2:(continued)

| Level | Symmetry | $(\nu_1, \nu_2^\ell)$ | This work | WL | MT |
|---|---|---|---|---|---|
| 43 | $A_1$ | (0,7)? | 13706.0 | 13708.3 | |
| 44 | $A_2$ | | 13747.3 | 13747.9 | |
| 45 | E | (4,1) | 14052.5 | 14053.4 | |
| 46 | $A_1$ | u | 14186.1 | 14191.6 | |
| 47 | E | (2,4)? | 14211.5 | 14216.7 | |
| 48 | E | (2,4)? | 14465.2 | 14471.7 | |
| 49 | $A_2$ | | 14564.4 | 14566.2 | |
| 50 | $A_1$ | (2,4)? | 14663.4 | 14666.6 | |
| 51 | E | (1,6)? | 14878.7 | 14888.6 | |
| 52 | $A_1$ | u | 14886.2 | 14902.9 | |
| 53 | E | u | 14886.4 | 14890.9 | |
| 54 | $A_1$ | (5,0) | 14939.0 | 14940.9 | |
| 55 | $A_1$ | (0,8)? | 15062.0 | 15067.1 | |
| 56 | E | (0,8) | 15103.8 | 15108.3 | |
| 57 | $A_1$ | u | 15158.3 | 15160.3 | |
| 58 | $A_2$ | | 15179.1 | 15180.1 | |
| 59 | E | (3,3)? | 15203.3 | 15206.3 | |
| 60 | E | (3,3)? | 15325.2 | 15332.0 | |
| 61 | $A_2$ | | 15368.3 | 15369.6 | |
| 62 | E | u | 15772.0 | | |
| 63 | $A_1$ | u | 15868.5 | 15878.2 | |
| 64 | E | (5,1)? | 15881.6 | | |

Table 5.2:(continued)

| Level | Symmetry | $(\nu_1, \nu_2^\ell)$ | This work | WL | MT |
|---|---|---|---|---|---|
| 65 | $A_1$ | u | 15909.3 | 15936.4 | |
| 66 | $A_2$ | | 15952.0 | 15955.1 | |
| 67 | E | (2,5)? | 16006.6 | | |
| 68 | $A_1$ | (1,7)? | 16195.6 | 16223.3 | |
| 69 | E | (1,7)? | 16243.8 | | |
| 70 | E | u | 16442.9 | | |
| 71 | $A_1$ | u | 16444.2 | 16457.4 | |
| 72 | E | u | 16546.3 | | |
| 73 | $A_2$ | | 16580.7 | 16583.3 | |
| 74 | E | (5,1)? | 16667.3 | | |
| 75 | $A_1$ | (0,9) | 16695.6 | 16706.2 | |
| 76 | E | (0,9)? | 16713.2 | | |
| 77 | E | u | 16859.3 | | |
| 78 | E | u | 16910.5 | | |
| 79 | $A_1$ | u | 17061.4 | 17118.1 | |
| 80 | $A_2$ | | 17078.7 | 17084.6 | |
| 81 | E | u | 17217.0 | | |
| 82 | $A_1$ | u | 17273.9 | 17332.7 | |
| 83 | E | (2,6)? | 17386.6 | | |
| 84 | $A_1$ | u | 17429.2 | 17459.6 | |
| 85 | E | u | 17440.8 | | |
| 86 | $A_1$ | (6,0) | 17586.1 | 17588.6 | |

Table 5.2:(continued)

| Level | Symmetry | $(\nu_1, \nu_2^\ell)$ | This work | WL | MT |
|---|---|---|---|---|---|
| 87 | E | u | 17601.7 | | |
| 88 | $A_2$ | | 17672.3 | 17688.0 | |
| 89 | $A_1$ | (6,0) | 17681.0 | 17689.5 | |
| 90 | E | u | 17692.3 | | |
| 91 | $A_1$ | (1,8)? | 17746.3 | 17779.9 | |
| 92 | $A_2$ | | 17809.5 | 17826.6 | |
| 93 | E | u | 17847.2 | | |
| 94 | $A_2$ | | 17858.1 | 17856.5 | |
| 95 | E | u | 17957.4 | | |
| 96 | E | u | 18210.3 | | |
| 97 | $A_1$ | u | 18226.6 | 18353.7 | |
| 98 | $A_2$ | | 18319.6 | 18328.6 | |
| 99 | E | $12^c$ | 18346.4 | | |
| 100 | $A_1$ | u | 18360.8 | | |
| 101 | E | (0,10) | 18433.1 | | |
| 102 | $A_1$ | (0,10)? | 18456.8 | | |
| 103 | E | u | 18568.1 | | |
| 104 | $A_1$ | u | 18584.2 | | |
| 105 | E | (2,7)? | 18711.4 | | |
| 106 | $A_1$ | u | 18794.6 | | |
| 107 | E | u | 18795.7 | | |
| 108 | $A_2$ | | 18869.4 | 18911.3 | |

Table 5.2:(continued)

| Level | Symmetry | $(\nu_1, \nu_2^\ell)$ | This work | WL | MT |
|---|---|---|---|---|---|
| 109 | E | 13[c]? | 18915.3 | | |
| 110 | E | 13[c]? | 19039.0 | | |
| 111 | E | (1,9)? | 19079.5 | | |
| 112 | $A_1$ | (2,8)? | 19098.5 | | |
| 113 | $A_2$ | | 19180.0 | 19197.3 | |
| 114 | E | (2,8)? | 19209 | | |
| 115 | $A_2^d$ | 13[c]? | 19255 | 19335.6[d] | |
| 116 | E | u | 19272 | | |
| 117 | $A_1$ | u | 19300 | | |
| 118 | $E^d$ | | 19301 | | |
| 119 | E | u | 19411 | | |
| 120 | $A_1$ | u | 19414 | | |
| 121 | E | u | 19509 | | |
| 122 | $A_2$ | | 19726 | | |
| 123 | E | u | 19754 | | |
| 124 | $A_1$ | u | 19761 | | |
| 125 | $A_1$ | u | 19805 | | |
| 126 | E | u | 19828 | | |
| 127 | E | u | 19863 | | |
| 128 | E | u | 20047 | | |
| 129 | $A_2$ | | 20048 | | |
| 130 | $A_1$ | 14[c] | 20068 | | |

Table 5.2:(continued)

| Level | Symmetry | $(\nu_1, \nu_2^\ell)$ | This work | WL | MT |
|---|---|---|---|---|---|
| 131 | E | (2,8)? | 20091 | | |
| 132 | $A_1$ | (0,11)? | 20178 | | |
| 133 | $A_1$ | (7,0)? | 20206 | | |
| 134 | E | (0,11)? | 20211 | | |
| 135 | E | (0,11) | 20241 | | |
| 136 | $A_2$ | | 20277 | | |
| 137 | $A_1$ | u | 20336 | | |
| 138 | $A_2$ | | 20362 | | |
| 139 | E | u | 20426 | | |
| 140 | $A_1$ | u | 20490 | | |
| 141 | E | u | 20493 | | |
| 142 | E | u | 20596 | | |
| 143 | $A_1$ | u | 20613 | | |
| 144 | $E^d$ | u | 20764 | | |
| 145 | $E^d$ | | 20771 | | |
| 146 | E | u | 20777 | | |
| 147 | $A_2$ | | 20814 | | |
| 148 | $A_1$ | u | 20832 | | |
| 149 | E | (1,10) | 20854 | | |
| 150 | $A_1 + A_2^d$ | u | 20925 | | |
| 151 | E | u | 20974 | | |
| 152 | $A_1$ | u | 21026 | | |

Table 5.2:(continued)

| Level | Symmetry | $(\nu_1, \nu_2^\ell)$ | This work | WL | MT |
|---|---|---|---|---|---|
| 153 | E | u | 21106 | | |
| 154 | E | u | 21144 | | |
| 155 | $A_2$ | | 21179 | | |
| 156 | $A_1$ | u | 21206 | | |
| 157 | $A_1$ | u | 21220 | | |
| 158 | E | u | 21265 | | |
| 159 | E | u | 21311 | | |
| 160 | $A_2$ | | 21330 | | |
| 161 | E | u | 21428 | | |
| 162 | $A_1$ | u | 21465 | | |
| 163 | E | u | 21539 | | |
| 164 | $A_2$ | | 21585 | | |
| 165 | E | u | 21591 | | |
| 166 | $A_1$ | (2,9)? | 21629 | | |
| 167 | E | $15^c$? | 21663 | | |
| 168 | E | u | 21666 | | |
| 169 | $A_1$ | u | 21728 | | |
| 170 | E | u | 21762 | | |
| 171 | E | u | 21884 | | |
| 172 | $A_2$ | | 21892 | | |
| 173 | E | u | 21899 | | |
| 174 | $A_1$ | $15^c$? | 21992 | | |

Table 5.2:(continued)

| Level | Symmetry | $(\nu_1, \nu_2^\ell)$ | This work | WL | MT |
|---|---|---|---|---|---|
| 175 | $A_1$ | u | 22087 | | |
| 176 | E | (0,12)? | 22120 | | |
| 177 | $A_2$ | | 22144 | | |
| 178 | E | u | 22161 | | |
| 179 | $A_1$ | (0,12) | 22176 | | |
| 180 | E | (0,12)? | 22206 | | |

[a] ? denotes states with distorted nodal structures

[b] zero point energy

[c] states assigned to the 'inverted hyperspherical mode' (reference [72])

[d] symmetry re-assigned by Carter and Meyer (reference [59])

u denotes states that could not be assigned

Table 5.3: Convergence of $H_3^+$ $J = 1, p = 0, q = 0$ levels as a function of dimension of the final Hamiltonian, $I$. Frequencies, in $cm^{-1}$ are relative to the $J = 0$ ground state.

| Level | $I = 200$ | $I = 600$ | $I = 900$ | $I = 1200$ |
|---|---|---|---|---|
| 1 | 64.11 | 64.11 | 64.11 | 64.11 |
| 16 | 7876.07 | 7875.94 | 7875.94 | 7875.94 |
| 31 | 10659.40 | 10658.96 | 10658.95 | 10658.94 |
| 46 | 12381.25 | 12379.49 | 12379.46 | 12379.45 |
| 61 | 13722.25 | 13718.37 | 13718.21 | 13718.16 |
| 76 | 14939.1 | 14930.8 | 14930.6 | 14930.6 |
| 91 | 15912.1 | 15895.2 | 15893.9 | 15893.3 |
| 106 | 16714.8 | 16699.1 | 16698.0 | 16697.6 |
| 121 | 17494.9 | 17465.0 | 17463.3 | 17462.5 |
| 136 | 18073.7 | 17981.9 | 17968.4 | 17962.5 |
| 151 | 18743.4 | 18671.6 | 18669.2 | 18668.4 |

Table 5.4: $H_3^+$ $J = 1 \leftarrow 0$ rotational frequencies in $cm^{-1}$ and symmetry calculated using $L = 2800, N_\theta = 36, I = 1200$. Results due to Miller and Tennyson are shown for comparison.

| $J = 0$ | | | $J = 1$ | |
|---|---|---|---|---|
| Level | Symmetry | Band origin | $p = 0$ | $p = 1$ |
| 1 | $A_1$ | 0.0 | E 64.11 | $A_2$ 86.93 |
| | | | 64.10[a] | 86.93[a] |
| 2 | E | 2521.3 | E 26.76 $A_2$ 95.21 $A_1$ 105.90 | E 88.10 |
| | | | 26.76[a] 95.21[a] 105.90[a] | 88.09[a] |
| 3 | $A_1$ | 3178.4 | E 62.47 | $A_2$ 84.84 |
| | | | 62.47[c] | 84.84[a] |
| 4 | $A_1$ | 4777.1 | E 64.18 | $A_2$ 91.93 |
| | | | 64.1/64.2[a] | 91.8 |
| 5 | E | 4997.4 | $A_2$ -3.13 $A_1$ 0.98 E 127.06 | E 89.53 |
| | | | -3.2[a] 1.0[a] 127.0[a] | 89.6/89.3[a] |
| 6 | E | 5553.7 | E 30.05 $A_2$ 90.34 $A_1$ 100.01 | E 86.20 |
| | | | 30.0[a] 90.3[a] 100.0[a] | 85.9/86.3[a] |
| 7 | $A_1$ | 6262.0 | E 60.91 | $A_2$ 82.90 |
| | | | 60.9/60.8[a] | 82.8[a] |
| 8 | E | 7003.5 | E 40.74 $A_2$ 76.73 $A_1$ 103.91 | E 96.86 |
| 9 | $A_1$ | 7282.6 | E 40.15 | $A_2$ 82.90 |
| 10 | $A_2$ | 7492.7 | E 78.45 | $A_1$ 89.03 |
| 11 | $A_1$ | 7769.2 | E.70.79 | $A_2$ 88.63 |
| 12 | E | 7868.7 | $A_2$ 2.48 $A_1$ 7.22 E 118.96 | E 88.49 |
| 13 | E | 8487.0 | E 31.89 $A_2$ 81.14 $A_1$ 95.45 | E 84.64 |

Table 5.4:(continued)

| | $J = 0$ | | $J = 1$ | |
|---|---|---|---|---|
| Level | Symmetry | Band origin | $p = 0$ | $p = 1$ |
| 14 | $A_1$ | 8996.8 | E 67.41 | $A_2$ 107.86 |
| 15 | E | 9107.7 | $A_2$ 25.34 $A_1$ 57.07 E 98.48 | E 108.84 |
| 16 | $A_1$ | 9251.6 | E 66.67 | E 88.47 |
| 17 | E | 9650.7 | E 25.27 $A_2$ 95.39 $A_1$ 146.03 | E 91.73 |
| 18 | $A_1$ | 9964.2 | E 25.09[b] | $A_2$ 97.97 |
| 19 | E | 9996.6 | E 18.63[b] $A_2$ 133.45 $A_1$ 146.03 | E 91.73 |
| 20 | $A_2$ | 10208.6 | E 71.29 | $A_1$ 88.48 |
| 21 | $A_1$ | 10592.3 | E 66.67 | $A_2$ 88.47 |
| 22 | E | 10642.8 | $A_2$ 10.17 $A_1$ 15.71 E 109.90 | E 88.65 |
| 23 | E | 10853.5 | E 56.1 $A_2$ 60.7 $A_1$ 137.5 | E 141.4 |
| 24 | $A_1$ | 10913.4 | E 104.2 | $A_2$ 145.9 |
| 25 | E | 11321.6 | E 33.7 $A_2$ 81.8 $A_1$ 91.4 | E 83.6 |
| 26 | $A_2$ | 11525.8 | E 63.4 | $A_1$ 101.1 |
| 27 | E | 11651.4 | $A_2$ 35.7 $A_1$ 62.4 E 88.9 | E 113.9 |
| 28 | $A_1$ | 11809.6 | E 75.1 | $A_2$ 107.6 |
| 29 | E | 12073.5 | $A_2$ 27.4 $A_1$ 39.1 E 69.8 | E 103.4 |
| 30 | $A_1$ | 12146.0 | E 58.0 | $A_2$ 79.8 |
| 31 | E | 12294.5 | $A_2$ 40 $A_1$ 82 E 85 | E 140 |
| 32 | $A_1$ | 12363.8 | E 132 | $A_2$ 249 |
| 33 | E | 12467.8 | $A_2$ 44 E 156 $A_1$ 181 | E 210 |
| 34 | $A_1$ | 12584.7 | E 98 | $A_2$ 124 |

Table 5.4:(continued)

| | $J = 0$ | | $J = 1$ | |
|---|---|---|---|---|
| Level | Symmetry | Band origin | $p = 0$ | $p = 1$ |
| 35 | E | 12694.3 | E 28 $A_2$ 113 $A_1$ 145 | E 110 |
| 36 | $A_2$ | 12828.6 | E 67 | $A_1$ 89 |
| 37 | $A_1$ | 13285.1 | E 66 | $A_2$ 96 |
| 38 | E | 13313.7 | $A_2$ 21 $A_1$ 29 E 97 | E 92 |
| 39 | E | 13385.6 | $A_2$ 49 $A_1$ 72 E 81 | E 139 |
| 40 | $A_1$ | 13392.2 | E 119 | $A_1$ 133 |
| 41 | E | 13581.0 | E 72 $A_2$ 95 $A_1$ 137 | E 147 |

[a] ref. [137]

[b] These states are nearly degenerate

[c] This level is misprinted in ref. [137]

on energy criteria rather arbitrary. However, it should also be noted that in this region several 'degenerate' states began to show large splittings. These splittings were significantly larger than both those in the corresponding $J = 0$ calculations and the convergence suggested by Table 5.3. Analysis of the states showing large splittings clearly indicates that they are associated with states with appreciable amplitude at linear geometries and in particular the so-called 'horseshoe' states (see below). The onset of this behaviour appears very suddenly in the results.

In Table 5.4 no attempt has been made to assign quantum numbers to the rotational levels beyond symmetry designations. Watson[103] has suggested means of quantising and parameterising the rotational levels of $X_3$ systems. However, such schemes are only appropriate for molecules undergoing small amplitude vibrational motion. This is clearly not the case for the majority of states considered here.

The FBR results of Miller and Tennyson[93,138] are also given in Table 5.4. Detailed comparison with experiment can also be found in reference [93]. These results are in very good agreement with this study. Finally note that Table 5.4 includes results for $A_1$ states of $H_3^+$ which are forbidden by nuclear spin statistics. These results have been included as they yield useful data about the rotational structure of the system and can be compared with the results of other calculations.

## 5.3 Discussion

In appraising the validity of the results, it is important to have an assessment of convergence. This can be obtained by comparing results as a function of the parameters of the calculation, samples of which are presented in Tables 5.1 and 5.3 and also by monitoring the splitting between 'degenerate' states. These

tests suggest that the lowest 63 vibrational levels presented in Table 5.2 are converged to 1 $cm^{-1}$, the lowest 148 states to 5 $cm^{-1}$ and the remainder to 10 $cm^{-1}$. The convergence on these levels is greatly improved in the calculations presented in chapter 6. Carter and Meyer[59] have recently calculated the same number of levels using their diagonalisation-truncation technique in an FBR with hyperspherical co-ordinates; unique symmetry assigments are made possible in these co-ordinates. Their results are slightly better converged than those presented here. They confirmed that the original estimates on the convergence of these calculations were indeed correct. The very accurate results presented in the following chapter are superior however.

For the states common to both studies, the convergence here is similar to that claimed by WL[45]. However, comparison of the results show that the results presented here are consistently lower. A small systematic difference of approximately 1 $cm^{-1}$ was known previously and is believed to be due to the slightly less accurate constants employed by WL, but there are also very much larger discrepancies for the higher states. These discrepancies vary greatly from level to level and in many cases are more than 20 $cm^{-1}$. Furthermore, states with $A_2$ symmetry appear in general to be in better agreement than states with $A_1$ or E symmetry. It is our belief that these discrepancies are caused by incomplete convergence in WL's calculations.

Nonetheless, comparison with WL's calculations was useful. This is because they use the full $S_3$ symmetry of the $H_3^+$ system and thus obtained unique symmetry assignments. These calculations were performed in $S_2$ symmetry which means that an $A_1/A_2$ pair which is 'degenerate' to within the convergence limits is indistinguishable from a single E symmetry state. This consideration must be borne in mind when analysing the symmetry assignments to the higher states. In particular, states number 115 to 118 would have been assigned as three E states

if it had not been for WL's prediction of an $A_2$ state in this region. State 118, however, was wrongly assigned due to the poor convergence of WL's calculations. This level has now been re-assigned by Carter and Meyer[59]. State 115 in this group has also been re-assigned. The five re-assignments by Carter and Meyer are indicated in Table 5.2.

Table 5.2 also presents approximate assignments, where possible, to the 180 $q = 0$ states. Figures 5.1, 5.2 and 5.3 present illustrative contour plots for twelve of these states. While it is apparent that the majority of the states in the high-energy region are highly irregular in structure, there are some states which are spatially localised and for which assignments are possible. Noteworthy amongst these are regular states corresponding to highly-excited bending states, see Figure 5.2, state 86. Note that the state numbers given in the figures are for the *even* symmetry block - neglecting therefore the numbering from the $A_2$ (odd) states. The *actual* state number for Figure 5.2 state 86, for example, is 101. The 'horeshoe' states also exist with low degrees of stretching excitation, see state 125 of Figure 5.3 for example.

In the course of their 2D study of $H_3^+$, TBP[72] identified some periodic orbits in the high-energy regime that had not been previously observed. Although these orbits were found to be largely unstable in 3D, it is interesting to note that quantum states with this nature persist in these 3D calculations, see Figure 5.1, state 84. These states are described as being inverted hyperspherical modes in Table 5.2.

Table 5.3 shows that the convergence of the rotational portion of the calculation is very good and consistently better than for the corresponding vibrational levels. Therefore the occurrence of relatively large splittings in the degeneracies of a number of states was somewhat surprising. The comparison with the earlier FBR results suggest one possible explanation of this phenomenon. Several of

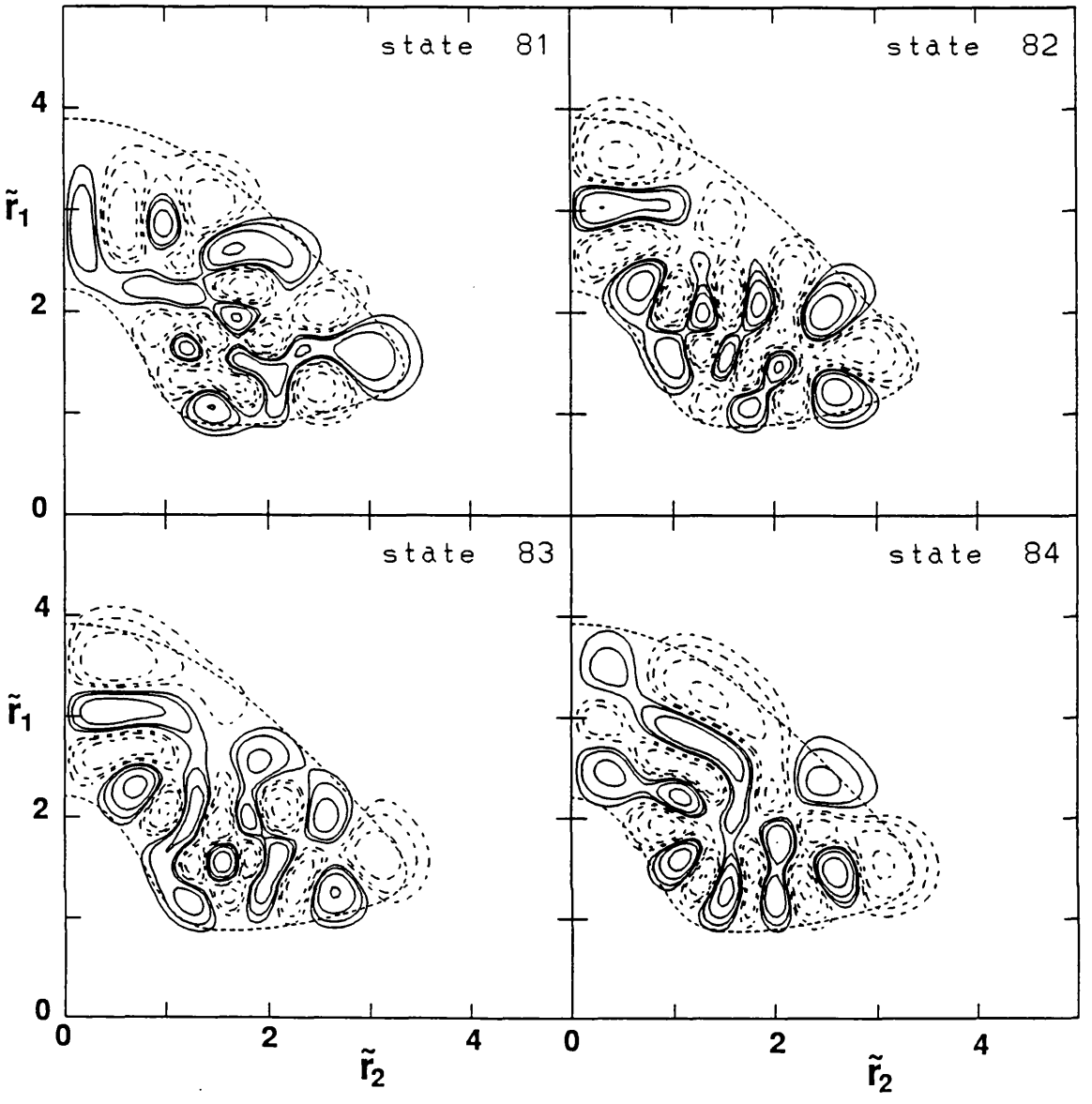


Figure 5.1: Cuts through the wavefunction of 4 even J = 0 states with $\theta = 90^o$. Contours are for 64%, 32%, 16% and 8% of the maximum amplitude with solid (dashed) curves enclosing regions of positive (negative) amplitude. The outer contour gives the classical turning point. The radial co-ordinates are mass weighted so that $\tilde{r}_1 = \alpha r_1$ and $\tilde{r}_2 = r_2/\alpha$ where $\alpha = (3/4)^{1/4}$. Note that the state numbering is for the even states.

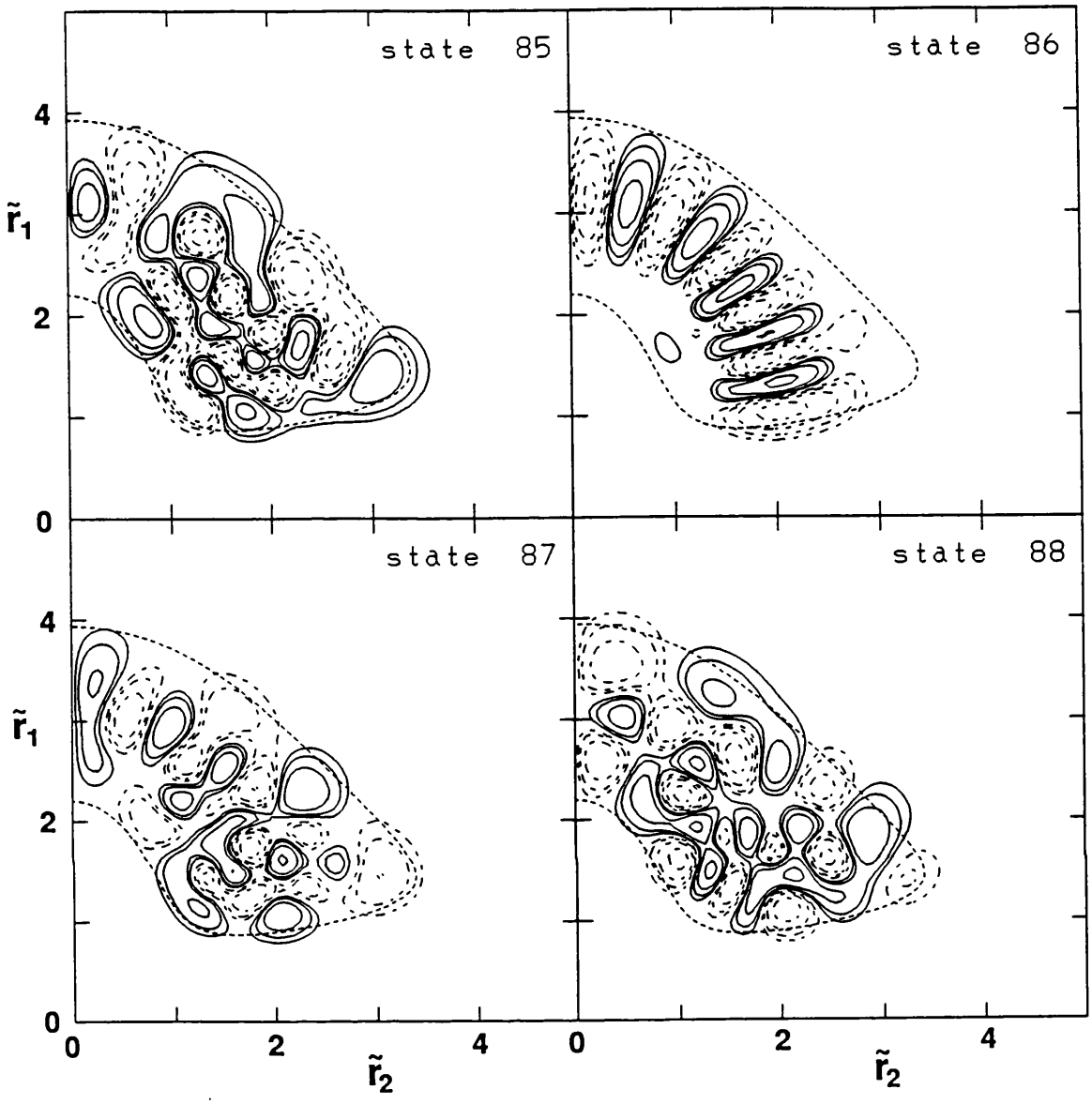


Figure 5.2: Cuts through the wavefunctions of 4 even $J = 0$ states with $\theta = 90°$. Contours and co-ordinates as in Figure 5.1.

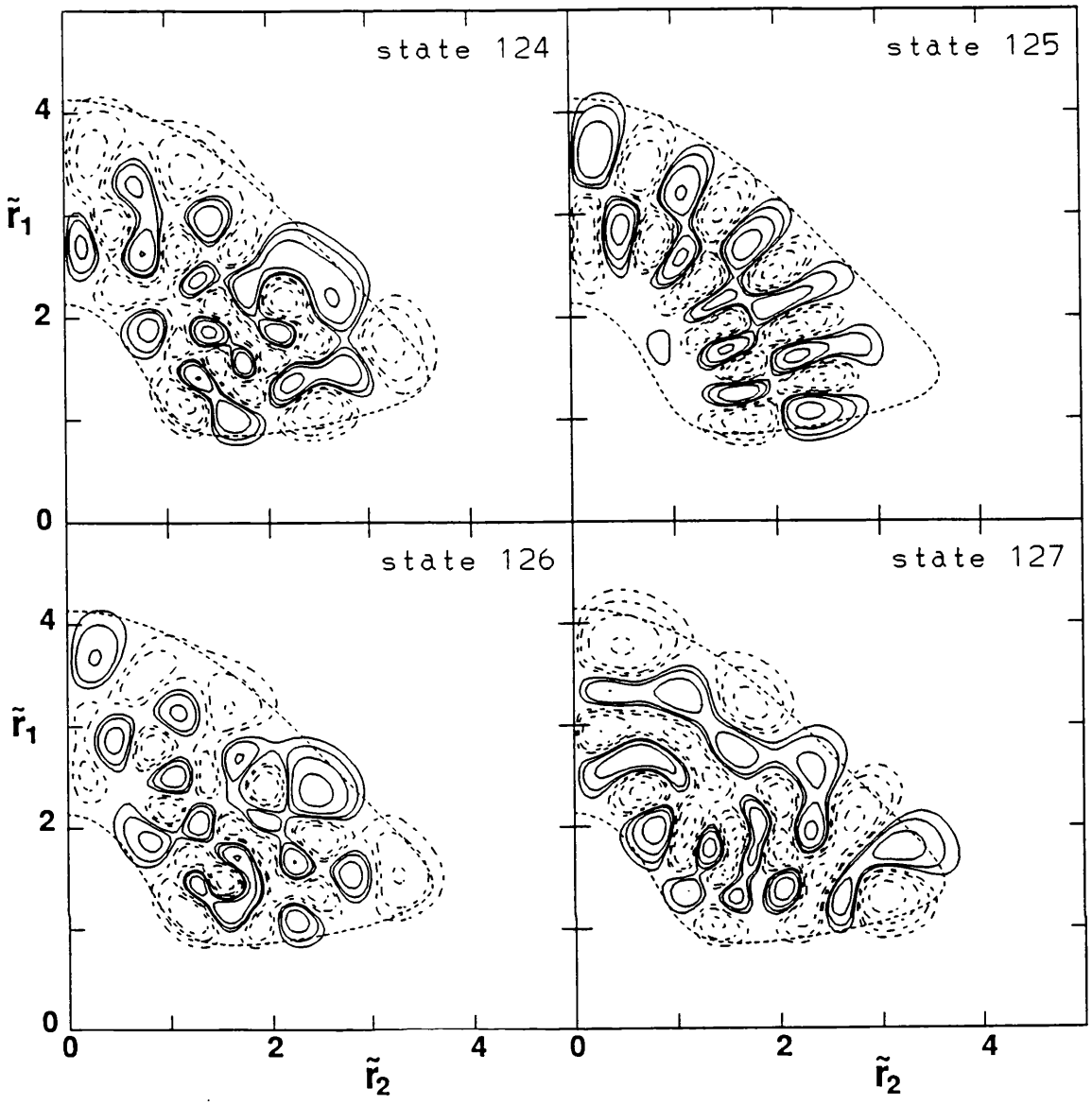


Figure 5.3: Cuts through the wavefunctions of 4 even $J = 0$ states with $\theta = 90°$. Contours and co-ordinates as in Figure 5.1.

the $p = 1$ states are slightly higher than the corresponding values of Miller and Tennyson. For $J = 1$ these results are simply the solutions of $\hat{H}^k$ for $k = 1$. It is possible that these results are not as well converged as the corresponding $k = 0$ ones and that this problem is worse for linear geometries — probably at the $\theta = 0^o$ limit.

Analysis of the $J = 1 \leftarrow 0$ excitation of the highly-excited bending or horseshoe states shows a rapid increase, particularly for the $J = 1, p = 1$ state. Such an increase is characteristic of the change from a bent to a quasi-linear molecule[136]. As such, the horseshoe states can be thought of as the large amplitude bending modes of a quasi-linear $H_3^+$.

## 5.4 Conclusions

We have used a discrete variable method, developed in chapter 3, for the study of ro-vibrational states of triatomic systems. This method is an extension of the earlier work of Bačic and Light[53,115,108], employing a two-step variational method[48] to treat rotationally excited states.

This method has been applied to $H_3^+$ yielding energies for the lowest 180 vibrational states of the system, covering two-thirds of the way to the dissociation limit. The accuracy has been confirmed by Carter and Meyer[59]. The efficient symmetrisation of the DVR, developed in §3.3.3, has been used. At this level the convergence and power of the 1D DVR approach is becoming suspect. It is necessary to make quantum investigations all the way to dissociation if a full understanding of the $H_3^+$ spectra is to be gained. It is the following chapter, employing a DVR in all 3 internal co-ordinates, which describes the success in stabilising *all* the vibrational bound states of the system.

# Chapter 6

# $H_3^+$: A DVR in $r_1, r_2$ and $\theta$

## 6.1 Introduction

In this chapter we further the investigations of chapter 5 by studying the $H_3^+$ system using a 3D DVR in scattering co-ordinates – the theory being given in §3.4. We obtain estimates, to within 10 $cm^{-1}$, of the positions of *all* the vibrational bound states of the system.

In this study three $H_3^+$ potential energy surfaces were used. The potential energy surface due to Meyer *et al* (MBB)[6] is of near spectroscopic accuracy at low energies[92]. However, although this surface is well behaved up to dissociation[59], it does not actually dissociate correctly. The less accurate *ab initio* potential due to Schinke *et al* (SDL)[139] was designed for scattering calculations and thus dissociating problems. However, in the course of this work, it was found that if one considers a coordinate where all 3 H atoms move apart symmetrically this potential actually becomes ill-behaved below the $H^+ - H_2$ dissociation limit. This problem was circumvented by forcing an artificially high energy in the region of poor behaviour. The diatoms-in-molecules (DIM) potential[140] has been used extensively for (semi)-classical calculations[132,134,135,141]. It is well behaved

over the entire energy range of concern but, at low energy, is significantly less accurate than the *ab initio* potentials. Although results are presented for all three potentials, most study is on the MBB potential because most earlier quantum calculations have employed this surface.

## 6.2 Calculations

As stated in §4.3, the order of solution used was $r_2 \rightarrow r_1 \rightarrow \theta$. As before, Morse oscillator-type functions were used in the $r_1$ co-ordinate and spherical oscillator functions in $r_2$. Both radial basis sets contain parameters which can be adjusted to give the variationally best functions for a given problem. The radial functions were optimised using a previously written[72] 2D ($\theta$ frozen) program working in a basis set rather than DVR. These tests ensured that sufficient functions were included to represent all the bound states of the problems for several values of $\theta$. Details of the optimised radial functions are given in Table 6.1. As usual, Legendre functions were used in the angular co-ordinate.

Table 6.1: Details of the radial basis functions used. $r_e$, $\omega_e$ and $D_e$ are in atomic units. $N_R$ is the number of DVR points in each radial co-ordinate.

| Coordinate | Oscillator | $N_R$ | $r_e$ | $\omega_e$ | $D_e$ |
|---|---|---|---|---|---|
| $r_1$ | Morse-like[32] | 36 | 3.16 | 0.11085 | 0.0060 |
| $r_2$ | Spherical[34] | 40 | - | 0.0095 | - |

As the size of the final 3D Hamiltonian, $L$, was not actually dependent on the number of radial grid points used (because $\theta$ is the last coordinate included), we can be generous in the provision of radial points. Convergence is thus assured

provided the final step includes sufficient contracted radial points at each angular grid point.

The final results were computed using a grid of 32 Gauss-Legendre quadrature points for the $\theta$ coordinate. The symmetry in the potential was once again exploited, so only 16 of the points need be explicitly considered. Tests showed that increasing this number degraded the final results as, for fixed $L$, less radial functions per angle could be considered. Calculations which increased the number of angular points using a fixed energy selection criterion for the radial functions showed the calculations to be stable with respect to increasing the size of the angular grid. The uncontracted DVR grids used here are equivalent to a basis set expansion comprising 23,040 functions for each symmetry. Interestingly, more radial grid points than in the earlier calculations were required, but actually less angular points.

Table 6.2 shows the convergence of a selection of levels as a function of dimension, $L$, of the final Hamiltonian matrix. Inspection of the table suggests that the top levels are converged to within 10 $cm^{-1}$ (note that even level 701 is actually above the dissociation energy of the MBB potential[93]). The lower levels are considerably better converged than this. It is possible to get an independent view of the convergence by comparing the energies of the even and odd symmetry calculations. About half the $J = 0$ states of $H_3^+$ should be of degenerate E symmetry. In this case one even and one odd eigenvalue should be degenerate. Experience with the previous $H_3^+$ calculations (and also the $^7Li_3^+$ studies of chapter 2) has shown that the splitting between these levels (the odd level is nearly always of lower energy) gives a good measure of the convergence.

The energies of the lowest 180 states are in good agreement with those of the previous chapter, and also those of Carter and Meyer[59] They represent a systematic improvement on the previous work, where it was estimated that the

Table 6.2: Convergence of a selection of even symmetry $H_3^+$ vibrational band origins as a function of dimension, $L$, of the final Hamiltonian. All values are given in $cm^{-1}$ relative to the $H_3^+$ ground state at 4363.5 $cm^{-1}$ above the minimum of the surface. These results were obtained for the MBB potential function.

| $L$ | 2100 | 2400 | 2700 | 3000 | 3300 |
|---|---|---|---|---|---|
| Level | | | | | |
| 1 | 2521.28 | 2521.28 | 2521.28 | 2521.28 | 2521.28 |
| 51 | 15202.9 | 15202.8 | 15202.7 | 15202.7 | 15202.6 |
| 151 | 22265.8 | 22264.3 | 22263.6 | 22263.3 | 22262.3 |
| 251 | 26170.1 | 26164.8 | 26162.1 | 26160.3 | 26158.3 |
| 351 | 29014.3 | 29008.6 | 29004.6 | 29002.8 | 29001.1 |
| 451 | 31239.8 | 31226.9 | 31218.5 | 31212.5 | 31209.7 |
| 551 | 33104.6 | 33082.7 | 33070.7 | 33063.6 | 33059.1 |
| 651 | 34733.1 | 34688.6 | 34668.0 | 34657.6 | 34652.2 |
| 701 | 35443.4 | 35368.2 | 35341.3 | 35332.0 | 35323.8 |

highest levels were only converged to 10 $cm^{-1}$. Carter and Meyer[59], conversely, claimed convergence for all their levels to 0.2 $cm^{-1}$. Detailed comparison with their results suggest while their states of $A_1$ symmetry may well be accurate to this amount, their states of $A_2$ and E symmetries are often as much as 6 $cm^{-1}$ higher than the results presented here.

To estimate the total number of bound states obtained it is necessary to assign all the E levels, something that becomes increasingly difficult near the dissociation limit where the splitting of the E states becomes greater than the mean spacing between states. Alternatively, at high energy, it is possible to make a statistical assumption about the symmetry of the states calculated. It was assumed that two-thirds of the odd states were E, the remaining being $A_2$. With this assumption the total number of states below a particular energy is given by the number of even states plus one-third the number of odd states. Figure 6.1 shows the number of vibrational bound states against energy, under this assumption, for the MBB surface. This figure illustrates the dramatic increase in the density of states with increasing energy. Table 6.3 compares this approximation with the actual numbers for the lowest 400 MBB states which been have assigned. The lowest 180 were assigned by comparison with Carter and Meyer[59], the remainder by looking for degeneracies in the even and odd calculations. This latter method is likely to overestimate the total number of E states slightly, and hence underestimate the total number of states, because pairs of $A_1$ and $A_2$ states which happen to be close in energy will be assigned as E. Table 6.4 gives the 400 energy levels which were assigned.

Table 6.3 shows that the statistical approximation is a reasonably good one. Using this approximation we predict that the MBB potential supports 881 states. As these calculations behave variationally this number gives a lower bound on the actual number of bound states. However, tests strongly suggest that it is unlikely

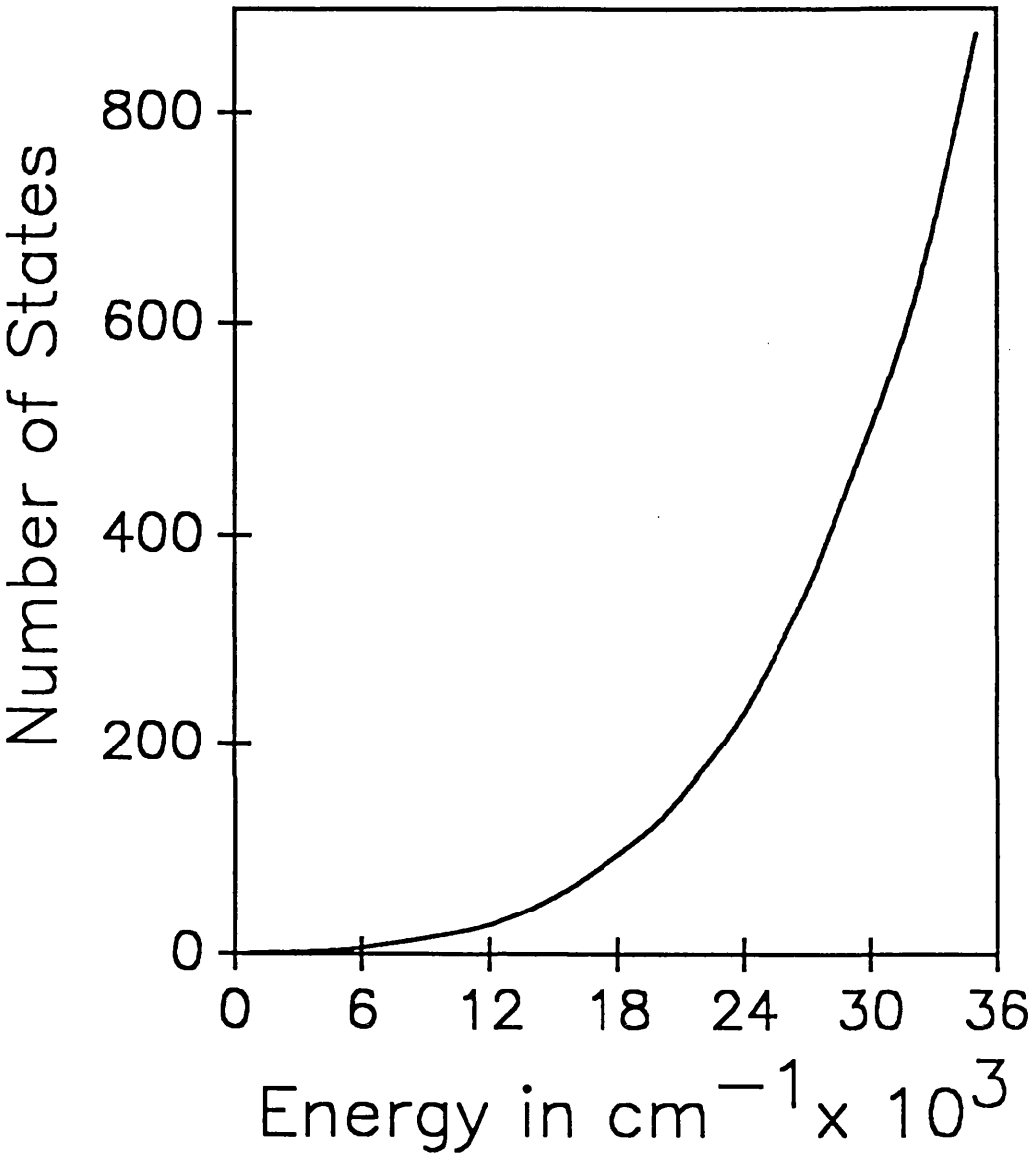


Figure 6.1: Density of states graph for $H_3^+$ on the MBB surface. The number of states up to a particular energy was predicted using the statistical assumption described in the text.

Table 6.3: The number of bound states supported by each of the three surfaces for a range of energies. The energies are given relative to the $H_3^+$ ground state for each surface. $D_0$ is the dissociation energy[93]: 35035.2 $cm^{-1}$ for MBB, 37810.6 $cm^{-1}$ for DIM, and 34424.5 $cm^{-1}$ for the SDL surface.

| Energy ($cm^{-1}$) | MBB (assigned) | MBB | DIM | SDL |
|---|---|---|---|---|
| 10000 | 19 | 21 | 22 | 20 |
| 14000 | 44 | 47 | 52 | 47 |
| 18000 | 95 | 100 | 106 | 100 |
| 22000 | 174 | 183 | 192 | 184 |
| 26000 | 303 | 314 | 317 | 315 |
| 28000 | 397 | 401 | 398 | 404 |
| 30000 | - | 502 | 495 | 510 |
| 32000 | - | 624 | 607 | 637 |
| 34000 | - | 781 | 739 | 792 |
| $D_0$ | - | 881 | 1071 | 828 |

Table 6.4: The first 400 energy levels of $H_3^+$, computed on the MBB surface, for which symmetry assignments have been made. They are given relative to the ground state, which is at 4363.5 $cm^{-1}$ above the minimum of the well.

| Level no. | Symmetry | Frequency in $cm^{-1}$ | Level no. | Symmetry | Frequency in $cm^{-1}$ |
|---|---|---|---|---|---|
| 1 | $A_1$ | 0.0 | 20 | $A_2$ | 10208.4 |
| 2 | E | 2521.3 | 21 | $A_1$ | 10592.1 |
| 3 | $A_1$ | 3178.4 | 22 | E | 10642.6 |
| 4 | $A_1$ | 4777.0 | 23 | E | 10853.3 |
| 5 | E | 4997.4 | 24 | $A_1$ | 10913.1 |
| 6 | E | 5553.7 | 25 | E | 11321.5 |
| 7 | $A_1$ | 6262.0 | 26 | $A_2$ | 11525.4 |
| 8 | E | 7003.4 | 27 | E | 11651.2 |
| 9 | $A_1$ | 7282.5 | 28 | $A_1$ | 11809.2 |
| 10 | $A_2$ | 7492.6 | 29 | E | 12073.2 |
| 11 | $A_1$ | 7769.1 | 30 | $A_1$ | 12145.9 |
| 12 | E | 7868.6 | 31 | E | 12294.2 |
| 13 | E | 8487.0 | 32 | $A_1$ | 12363.5 |
| 14 | $A_1$ | 8996.6 | 33 | E | 12467.5 |
| 15 | E | 9107.6 | 34 | $A_1$ | 12584.4 |
| 16 | $A_1$ | 9251.6 | 35 | E | 12694.0 |
| 17 | E | 9650.6 | 36 | $A_2$ | 12828.2 |
| 18 | $A_1$ | 9964.0 | 37 | $A_1$ | 13284.8 |
| 19 | E | 9996.5 | 38 | E | 13313.4 |

Table 6.4:(continued)

| Level no. | Symmetry | Frequency in $cm^{-1}$ | Level no. | Symmetry | Frequency in $cm^{-1}$ |
|---|---|---|---|---|---|
| 39 | E | 13385.1 | 60 | E | 15324.4 |
| 40 | $A_1$ | 13391.7 | 61 | $A_2$ | 15367.7 |
| 41 | E | 13580.4 | 62 | E | 15771.1 |
| 42 | E | 13680.9 | 63 | $A_1$ | 15867.7 |
| 43 | $A_1$ | 13705.5 | 64 | E | 15881.0 |
| 44 | $A_2$ | 13746.7 | 65 | $A_1$ | 15909.0 |
| 45 | E | 14052.3 | 66 | $A_2$ | 15950.7 |
| 46 | $A_1$ | 14185.6 | 67 | E | 16005.7 |
| 47 | E | 14210.9 | 68 | $A_1$ | 16195.4 |
| 48 | E | 14464.7 | 69 | E | 16243.0 |
| 49 | $A_2$ | 14563.6 | 70 | E | 16441.7 |
| 50 | $A_1$ | 14662.7 | 71 | $A_1$ | 16443.4 |
| 51 | E | 14878.1 | 72 | E | 16544.1 |
| 52 | E | 14885.6 | 73 | $A_2$ | 16577.3 |
| 53 | $A_1$ | 14887.0 | 74 | E | 16666.4 |
| 54 | $A_1$ | 14938.8 | 75 | $A_1$ | 16693.9 |
| 55 | $A_1$ | 15061.2 | 76 | E | 16712.0 |
| 56 | E | 15103.1 | 77 | E | 16857.9 |
| 57 | $A_1$ | 15157.8 | 78 | E | 16908.8 |
| 58 | $A_2$ | 15178.1 | 79 | $A_1$ | 17060.9 |
| 59 | E | 15202.6 | 80 | $A_2$ | 17076.4 |

Table 6.4:(continued)

| Level no. | Symmetry | Frequency in $cm^{-1}$ | Level no. | Symmetry | Frequency in $cm^{-1}$ |
|---|---|---|---|---|---|
| 81 | E | 17216.0 | 101 | E | 18431.5 |
| 82 | $A_1$ | 17272.6 | 102 | $A_1$ | 18454.0 |
| 83 | E | 17385.2 | 103 | E | 18566.4 |
| 84 | $A_1$ | 17428.4 | 104 | $A_1$ | 18582.9 |
| 85 | E | 17439.0 | 105 | E | 18709.3 |
| 86 | $A_1$ | 17585.7 | 106 | E | 18791.9 |
| 87 | E | 17600.7 | 107 | $A_1$ | 18795.2 |
| 88 | $A_2$ | 17670.5 | 108 | $A_2$ | 18864.9 |
| 89 | $A_1$ | 17680.7 | 109 | E | 18912.4 |
| 90 | E | 17690.2 | 110 | E | 19036.2 |
| 91 | $A_1$ | 17744.5 | 111 | E | 19076.9 |
| 92 | $A_2$ | 17802.8 | 112 | $A_1$ | 19096.6 |
| 93 | $A_2$ | 17841.4 | 113 | $A_2$ | 19170.2 |
| 94 | E | 17845.9 | 114 | E | 19202.2 |
| 95 | E | 17955.9 | 115 | $A_1$ | 19254.0 |
| 96 | E | 18207.9 | 116 | $A_2$ | 19254.5 |
| 97 | $A_1$ | 18226.2 | 117 | E | 19267.2 |
| 98 | $A_2$ | 18315.4 | 118 | E | 19298.0 |
| 99 | E | 18344.8 | 119 | E | 19409.7 |
| 100 | $A_1$ | 18358.8 | 120 | $A_1$ | 19412.2 |

Table 6.4:(continued)

| Level no. | Symmetry | Frequency in $cm^{-1}$ | Level no. | Symmetry | Frequency in $cm^{-1}$ |
|---|---|---|---|---|---|
| 121 | E | 19506.2 | 141 | E | 20489.7 |
| 122 | $A_2$ | 19719.5 | 142 | E | 20593.5 |
| 123 | E | 19752.2 | 143 | $A_1$ | 20611.9 |
| 124 | $A_1$ | 19759.0 | 144 | E | 20752.1 |
| 125 | $A_1$ | 19803.4 | 145 | E | 20773.9 |
| 126 | E | 19825.0 | 146 | $A_2$ | 20805.6 |
| 127 | E | 19859.5 | 147 | $A_1$ | 20830.3 |
| 128 | E | 20042.7 | 148 | E | 20850.1 |
| 129 | $A_2$ | 20044.2 | 149 | $A_2$ | 20921.9 |
| 130 | $A_1$ | 20067.6 | 150 | $A_1$ | 20922.3 |
| 131 | E | 20087.2 | 151 | E | 20970.2 |
| 132 | $A_1$ | 20174.4 | 152 | $A_1$ | 21024.4 |
| 133 | E | 20203.4 | 153 | E | 21101.4 |
| 134 | $A_1$ | 20205.3 | 154 | E | 21140.7 |
| 135 | E | 20236.6 | 155 | $A_2$ | 21174.4 |
| 136 | $A_2$ | 20266.9 | 156 | $A_1$ | 21204.7 |
| 137 | $A_1$ | 20334.2 | 157 | $A_1$ | 21216.8 |
| 138 | $A_2$ | 20356.0 | 158 | E | 21262.7 |
| 139 | E | 20422.9 | 159 | E | 21302.6 |
| 140 | $A_1$ | 20487.6 | 160 | $A_2$ | 21320.1 |

Table 6.4:(continued)

| Level no. | Symmetry | Frequency in $cm^{-1}$ | Level no. | Symmetry | Frequency in $cm^{-1}$ |
|---|---|---|---|---|---|
| 161 | E | 21424.6 | 181 | $A_1$ | 22262.3 |
| 162 | $A_1$ | 21464.0 | 182 | E | 22283.8 |
| 163 | E | 21531.0 | 183 | $A_2$ | 22302.2 |
| 164 | $A_2$ | 21570.8 | 184 | E | 22365.2 |
| 165 | E | 21587.1 | 185 | $A_1$ | 22408.5 |
| 166 | $A_1$ | 21626.5 | 186 | $A_2$ | 22410.4 |
| 167 | E | 21659.4 | 187 | $A_1$ | 22472.2 |
| 168 | E | 21662.5 | 188 | E | 22493.1 |
| 169 | $A_1$ | 21724.6 | 189 | E | 22499.8 |
| 170 | $A_1$ | 21756.5 | 190 | $A_1$ | 22504.6 |
| 171 | E | 21876.8 | 191 | $A_2$ | 22546.8 |
| 172 | $A_2$ | 21884.0 | 192 | E | 22572.0 |
| 173 | E | 21895.5 | 193 | $A_1$ | 22612.3 |
| 174 | $A_1$ | 21989.1 | 194 | E | 22639.3 |
| 175 | $A_1$ | 22083.6 | 195 | $A_1$ | 22689.2 |
| 176 | E | 22115.1 | 196 | E | 22713.6 |
| 177 | $A_2$ | 22139.2 | 197 | E | 22777.6 |
| 178 | E | 22156.1 | 198 | $A_1$ | 22832.0 |
| 179 | $A_1$ | 22171.2 | 199 | $A_2$ | 22864.9 |
| 180 | E | 22201.3 | 200 | E | 22899.3 |

Table 6.4:(continued)

| Level no. | Symmetry | Frequency in $cm^{-1}$ | Level no. | Symmetry | Frequency in $cm^{-1}$ |
|---|---|---|---|---|---|
| 201 | $A_2$ | 22946.9 | 221 | $A_1$ | 23607.0 |
| 202 | $A_2$ | 22986.6 | 222 | E | 23638.3 |
| 203 | E | 23007.3 | 223 | $A_2$ | 23651.3 |
| 204 | E | 23026.4 | 224 | E | 23725.1 |
| 205 | $A_1$ | 23035.2 | 225 | E | 23798.5 |
| 206 | E | 23074.6 | 226 | $A_1$ | 23886.4 |
| 207 | $A_1$ | 23139.7 | 227 | E | 23897.1 |
| 208 | E | 23161.5 | 228 | E | 23929.9 |
| 209 | $A_1$ | 23197.8 | 229 | E | 23935.5 |
| 210 | E | 23136.4 | 230 | E | 23953.8 |
| 211 | $A_1$ | 23306.0 | 231 | E | 24004.6 |
| 212 | E | 23347.4 | 232 | $A_2$ | 24033.9 |
| 213 | E | 23380.4 | 233 | $A_1$ | 24047.4 |
| 214 | $A_1$ | 23394.4 | 234 | $A_1$ | 24064.4 |
| 215 | $A_2$ | 23409.6 | 235 | E | 24075.0 |
| 216 | $A_2$ | 23462.9 | 236 | E | 24143.4 |
| 217 | E | 23465.4 | 237 | $A_2$ | 24150.7 |
| 218 | E | 23515.2 | 238 | $A_1$ | 24169.4 |
| 219 | $A_1$ | 23525.7 | 239 | E | 24222.9 |
| 220 | E | 23561.8 | 240 | E | 24307.0 |

Table 6.4:(continued)

| Level no. | Symmetry | Frequency in $cm^{-1}$ | Level no. | Symmetry | Frequency in $cm^{-1}$ |
|---|---|---|---|---|---|
| 241 | $A_1$ | 24325.4 | 261 | $A_2$ | 24892.4 |
| 242 | E | 24351.9 | 262 | E | 24899.8 |
| 243 | $A_1$ | 24359.2 | 263 | E | 24955.8 |
| 244 | $A_1$ | 24377.4 | 264 | $A_2$ | 24969.6 |
| 245 | $A_2$ | 24380.9 | 265 | $A_1$ | 24978.7 |
| 246 | E | 24412.3 | 266 | $A_1$ | 24994.7 |
| 247 | $A_2$ | 24453.6 | 267 | E | 25051.3 |
| 248 | E | 24474.3 | 268 | E | 25082.3 |
| 249 | E | 24527.0 | 269 | $A_2$ | 25115.2 |
| 250 | E | 24566.7 | 270 | $A_2$ | 25128.3 |
| 251 | $A_1$ | 24589.8 | 271 | $A_1$ | 25137.8 |
| 252 | $A_2$ | 24631.7 | 272 | E | 25140.3 |
| 253 | E | 24671.6 | 273 | $A_1$ | 25210.9 |
| 254 | $A_2$ | 24680.2 | 274 | E | 25223.9 |
| 255 | $A_1$ | 24694.4 | 275 | $A_2$ | 25282.1 |
| 256 | E | 24714.3 | 276 | $A_1$ | 25317.7 |
| 257 | E | 24750.6 | 277 | E | 25326.2 |
| 258 | E | 24800.7 | 278 | $A_1$ | 25372.1 |
| 259 | $A_1$ | 24834.2 | 279 | E | 25373.9 |
| 260 | $A_1$ | 24860.4 | 280 | E | 25400.0 |

Table 6.4:(continued)

| Level no. | Symmetry | Frequency in $cm^{-1}$ | Level no. | Symmetry | Frequency in $cm^{-1}$ |
|---|---|---|---|---|---|
| 281 | $A_2$ | 25411.5 | 301 | E | 25959.3 |
| 282 | E | 25456.6 | 302 | $A_2$ | 25991.4 |
| 283 | E | 25508.1 | 303 | $A_1$ | 25997.4 |
| 284 | $A_1$ | 25545.0 | 304 | E | 26031.5 |
| 285 | $A_2$ | 25580.5 | 305 | E | 26083.5 |
| 286 | $A_1$ | 25588.1 | 306 | E | 26093.5 |
| 287 | $A_2$ | 25590.0 | 307 | $A_2$ | 26110.7 |
| 288 | E | 25674.3 | 308 | $A_1$ | 26121.1 |
| 289 | $A_1$ | 25682.2 | 309 | $A_1$ | 26158.2 |
| 290 | $A_1$ | 25690.1 | 310 | $A_1$ | 26195.7 |
| 291 | E | 25703.8 | 311 | E | 26200.7 |
| 292 | $A_1$ | 25731.7 | 312 | E | 26212.2 |
| 293 | $A_2$ | 25755.2 | 313 | $A_1$ | 26243.3 |
| 294 | $A_1$ | 25764.0 | 314 | $A_2$ | 26262.8 |
| 295 | E | 25833.0 | 315 | $A_1$ | 26272.4 |
| 296 | $A_2$ | 25855.7 | 316 | $A_2$ | 26295.0 |
| 297 | E | 25910.3 | 317 | $A_2$ | 26320.2 |
| 298 | E | 25918.0 | 318 | E | 26336.0 |
| 299 | E | 25932.3 | 319 | E | 26379.2 |
| 300 | $A_2$ | 25957.6 | 320 | $A_1$ | 26386.6 |

Table 6.4:(continued)

| Level no. | Symmetry | Frequency in $cm^{-1}$ | Level no. | Symmetry | Frequency in $cm^{-1}$ |
|---|---|---|---|---|---|
| 321 | E | 26441.5 | 341 | E | 26879.7 |
| 322 | $A_1$ | 26446.4 | 342 | $A_1$ | 26898.3 |
| 323 | $A_1$ | 26468.8 | 343 | $A_2$ | 26899.8 |
| 324 | $A_2$ | 26459.7 | 344 | $A_2$ | 26925.8 |
| 325 | $A_2$ | 26472.0 | 345 | $A_1$ | 26934.5 |
| 326 | E | 26505.8 | 346 | E | 26969.0 |
| 327 | $A_1$ | 26520.8 | 347 | E | 26972.2 |
| 328 | $A_1$ | 26548.9 | 348 | $A_2$ | 27003.3 |
| 329 | $A_2$ | 26570.5 | 349 | $A_1$ | 27015.4 |
| 330 | E | 26587.3 | 350 | $A_1$ | 27027.0 |
| 331 | E | 26649.4 | 351 | $A_2$ | 27040.9 |
| 332 | $A_1$ | 26676.9 | 352 | E | 27095.2 |
| 333 | $A_2$ | 26689.6 | 353 | $A_2$ | 27103.0 |
| 334 | $A_1$ | 26701.0 | 354 | E | 27141.6 |
| 335 | $A_2$ | 26723.8 | 355 | $A_1$ | 27158.3 |
| 336 | $A_1$ | 26731.8 | 356 | E | 27167.7 |
| 337 | $A_2$ | 26752.6 | 357 | E | 27195.4 |
| 338 | E | 26809.3 | 358 | $A_1$ | 27205.1 |
| 339 | $A_1$ | 26822.2 | 359 | $A_2$ | 27246.1 |
| 340 | E | 26854.8 | 360 | $A_1$ | 27259.1 |

Table 6.4:(continued)

| Level no. | Symmetry | Frequency in $cm^{-1}$ | Level no. | Symmetry | Frequency in $cm^{-1}$ |
|---|---|---|---|---|---|
| 361 | $A_1$ | 27261.2 | 381 | E | 27700.0 |
| 362 | $A_2$ | 27316.6 | 382 | $A_2$ | 27710.3 |
| 363 | $A_1$ | 27326.6 | 383 | $A_1$ | 27718.4 |
| 364 | $A_1$ | 27331.1 | 384 | E | 27751.7 |
| 365 | $A_2$ | 27348.9 | 385 | $A_2$ | 27759.2 |
| 366 | E | 27353.4 | 386 | E | 27764.2 |
| 367 | $A_2$ | 27389.7 | 387 | E | 27806.0 |
| 368 | E | 27444.1 | 388 | $A_1$ | 27815.6 |
| 369 | $A_1$ | 27453.6 | 389 | $A_1$ | 27825.9 |
| 370 | $A_2$ | 27479.5 | 390 | E | 27858.9 |
| 371 | $A_1$ | 27491.1 | 391 | E | 27867.2 |
| 372 | $A_2$ | 27526.6 | 392 | E | 27875.9 |
| 373 | $A_1$ | 27536.6 | 393 | E | 27878.8 |
| 374 | $A_1$ | 27544.9 | 394 | E | 27911.0 |
| 375 | $A_2$ | 27570.8 | 395 | $A_2$ | 27958.0 |
| 376 | $A_1$ | 27590.1 | 396 | $A_1$ | 27969.2 |
| 377 | E | 27601.0 | 397 | $A_1$ | 27983.4 |
| 378 | $A_1$ | 27640.5 | 398 | $A_2$ | 28006.6 |
| 379 | E | 27663.0 | 399 | $A_1$ | 28014.8 |
| 380 | E | 27667.4 | 400 | $A_2$ | 28029.0 |

that this number is wrong by more than 10. The statistical approximation may add a further error of 10 states, giving a total maximum error of 20 states.

Table 6.3 also presents results for the SDL and DIM potentials. The SDL results are very similar to those obtained using the MBB potential; this potential supports a slightly higher density of states at higher energies but a smaller total number of states because of its lower dissociation energy. At low energies the DIM potential supports more states than the other two, but the density drops near dissociation. The DIM potential overestimates the dissociation energy of $H_3^+$ and this results in the potential supporting over a 1000 bound vibrational states. Although a detailed convergence analysis has not been done for the DIM potential it is probable that the DIM calculations are not quite so well converged as the others. Previous studies[72,136] have shown the DIM potential to be classically more chaotic (strongly coupled) than the MBB potential and hence harder to obtain converged results for.

## 6.3 Discussion

As in the previous chapters on LiCN and $H_3^+$, plots of the wavefunction have proved very useful as a method of obtaining insight into the nature of individual states. However, analysing many hundreds of 3D states with 2D plots is a formidable undertaking. So far we have only looked at the even states and at the DVR point nearest $\theta = 90°$; this corresponds to the previous analysis of $H_3^+$ wavefunctions in chapter 5. The 'horseshoe' states can be identified, extending in a single progression all the way from the bending fundamental ($\nu_2$) to dissociation — and indeed above it; a $19\nu_2$ state was found just above the dissociation limit of the MBB potential. Table 6.5 gives the energies and assignments of all the 'horseshoe' states identified, including the two (0,19) states *just* above

Table 6.5: Assignments to $H_3^+$ 'horseshoe' states for the levels of even symmetry. The numbering of the states is that for the even levels only. Uncertainties in the assignments are denoted by a ?.

| Level no. | Frequency $cm^{-1}$ | Assignment $\nu_1$ | $\nu_2$ | Level no. | Frequency $cm^{-1}$ | Assignment $\nu_1$ | $\nu_2$ |
|---|---|---|---|---|---|---|---|
| 21 | 10853.3 | 0 | 5 | 111 | 20088.8 | 1 | 10 |
| 22 | 10913.1 | 0 | 5 | 114 | 20208.1 | 0 | 11 |
| 28 | 12294.3 | 0 | 6 | 115 | 20239.2 | 0 | 11 |
| 29 | 12363.5 | 0 | 6 | 125 | 20851.6 | 1 | 10 |
| 38 | 13681.1 | 0 | 7 | 139 | 21659.9 | 2 | 8 |
| 39 | 13705.5 | 0 | 7 | 148 | 22116.4 | 0 | 12 |
| 45 | 14879.1 | 0 | 8 | 150 | 22171.2 | 0 | 12 |
| 47 | 14887.1 | 1 | 5 | 151 | 22210.6 | 0 | 12 |
| 50 | 15103.6 | 0 | 8 | 160 | 22612.3 | 1 | 11 |
| 60 | 16244.8 | 1 | 7 | 163 | 22715.3 | 1 | 11 |
| 65 | 16693.9 | 0 | 9 | 172 | 23166.7 | 2 | 10 |
| 66 | 16712.2 | 0 | 9 | 180 | 23517.3 | 2 | 10? |
| 76 | 17601.6 | 1 | 8 | 194 | 24064.5 | 0 | 13 |
| 79 | 17744.5 | 1 | 8 | 196 | 24145.9 | 0 | 13 |
| 86 | 18431.6 | 0 | 10 | 245 | 25932.3 | 0 | 14 |
| 87 | 18454.0 | 0 | 10 | 246 | 25965.4 | 1 | 12 |
| 95 | 19078.3 | 1 | 9 | 263 | 26468.8 | 1 | 12 |
| 96 | 19096.6 | 1 | 9 | 308 | 27815.6 | 0 | 15 |
| 103 | 19507.6 | 1 | 10 | 310 | 27861.0 | 0 | 15 |

Table 6.5:(continued)

| Level no. | Frequency $cm^{-1}$ | Assignment $\nu_1$ | $\nu_2$ | Level no. | Frequency $cm^{-1}$ | Assignment $\nu_1$ | $\nu_2$ |
|---|---|---|---|---|---|---|---|
| 312 | 27880.6 | 0 | 15 | 495 | 32008.9 | 1 | 16 |
| 327 | 28338.6 | 1 | 14 | 498 | 32069.3 | 1 | 16 |
| 328 | 28365.4 | 1 | 14 | 566 | 33311.0 | 0 | 18 |
| 385 | 29746.4 | 0 | 16 | 569 | 33334.9 | 0 | 18 |
| 405 | 30187.6 | 1 | 15 | 593 | 33719.1 | 1 | 17 |
| 420 | 30575.4 | 1 | 15? | 601 | 33838.3 | 1 | 17 |
| 454 | 31251.8 | 0 | 17? | 602 | 33850.0 | 1 | 17? |
| 469 | 31519.1 | 0 | 17 | 681 | 35047.6 | 0 | 19 |
| 470 | 31563.4 | 0 | 17 | 682 | 35058.6 | 0 | 19? |
| 473 | 31612.7 | 0 | 17? | | | | |

dissociation. Note that the quantum of stretching excitation, $\nu_1$, is still present at very high energy. Also of interest is the fact that the 'horseshoes' tend to appear in groups of two or three, usually with one or more of the assigments being somewhat uncertain. These are labelled with a question mark in Table 6.5.

Figures 6.2 and 6.3 illustrate typical contour plots of the wavefunctions of the high-lying states. Note that the numbering of the states is for the *even* symmetry, not the total number of states. Figure 6.2 shows two even states with $18\nu_2$ (numbers 566 and 569) and their immediate neighbours. Figure 6.3 shows even states (numbers 327 and 328) with $14\nu_2$ as well as a quantum of excitation in the transverse stretching mode ($\nu_1$). Again, neighbouring states are included for comparison. The high lying states that are assigned to horseshoe modes have a large gathering of amplitude in the vicinity of the horseshoe periodic orbit or in other words are scarred by it. However, none of the assignments made in the high energy region are particularly clear cut. This is in contrast to the intermediate energy horseshoe states analysed previously which showed very clear nodal structures (see Figures 5.1, 5.2 and 5.3).

## 6.4 Conclusions

In summary we have developed a 3D DVR method in scattering coordinates with which we obtain converged vibrational wavefunctions for $H_3^+$ up to dissociation. This is a major advance in our ability to treat this challenging and dynamically rich system. It has yielded theoretical data and information about the system in the very high energy region for the first time. The motivation comes mainly from the puzzling spectrum recorded by Carrington and co-workers[1,2].

A search for other regular (and stable) features in the wavefunctions needs

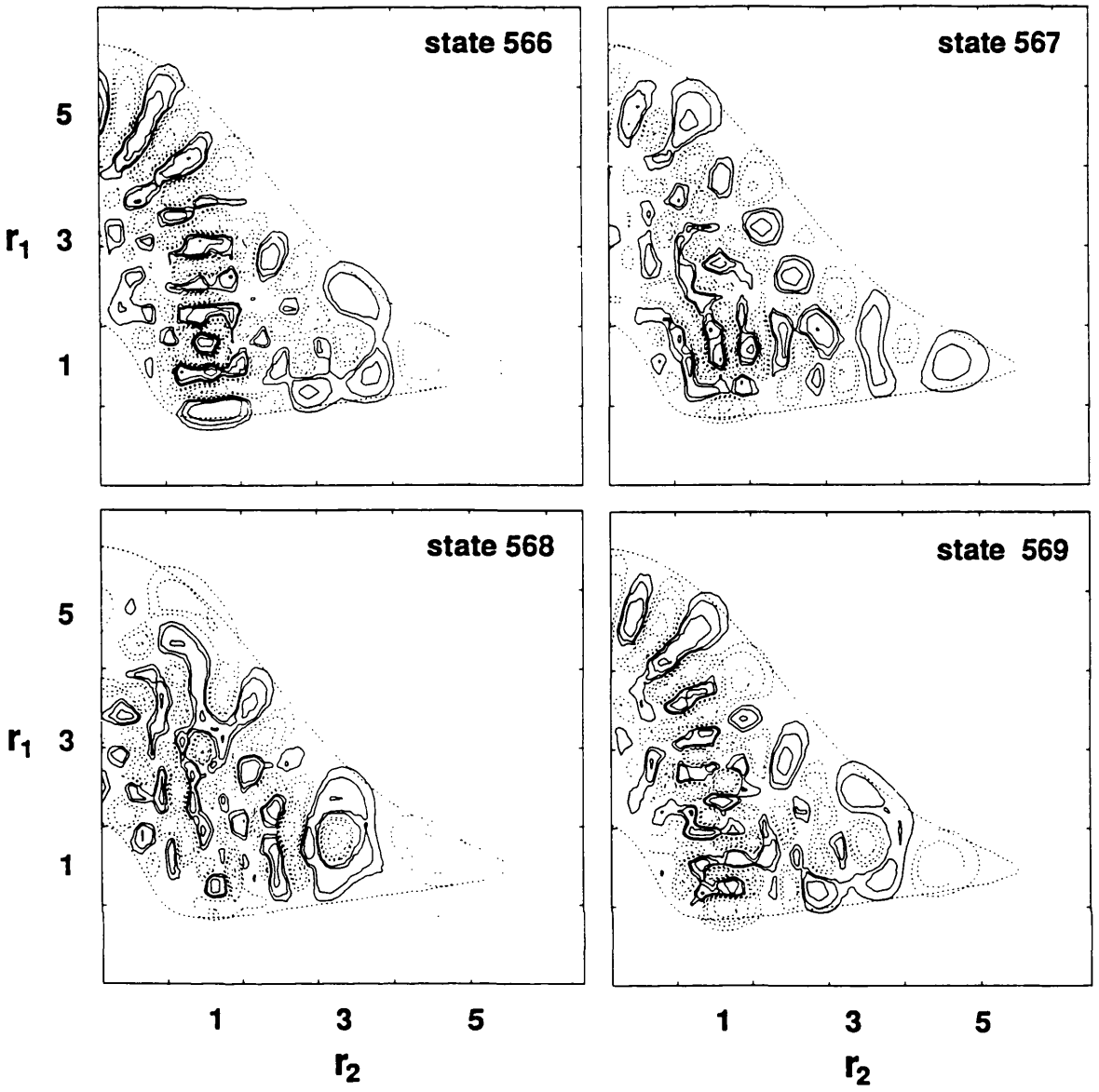


Figure 6.2: Cuts through the wavefunction of 4 even J = 0 states calculated using the MBB potential with $\theta = 90^o$. Contours are for 64%, 32%, 16% and 8% of the maximum amplitude with solid (dashed) curves enclosing regions of positive (negative) amplitude. The outer contour gives the classical turning point. The band origins of the states are 33311, 33317, 33326 and 33335 $cm^{-1}$. The radial co-ordinates are given in atomic units ($a_0$).

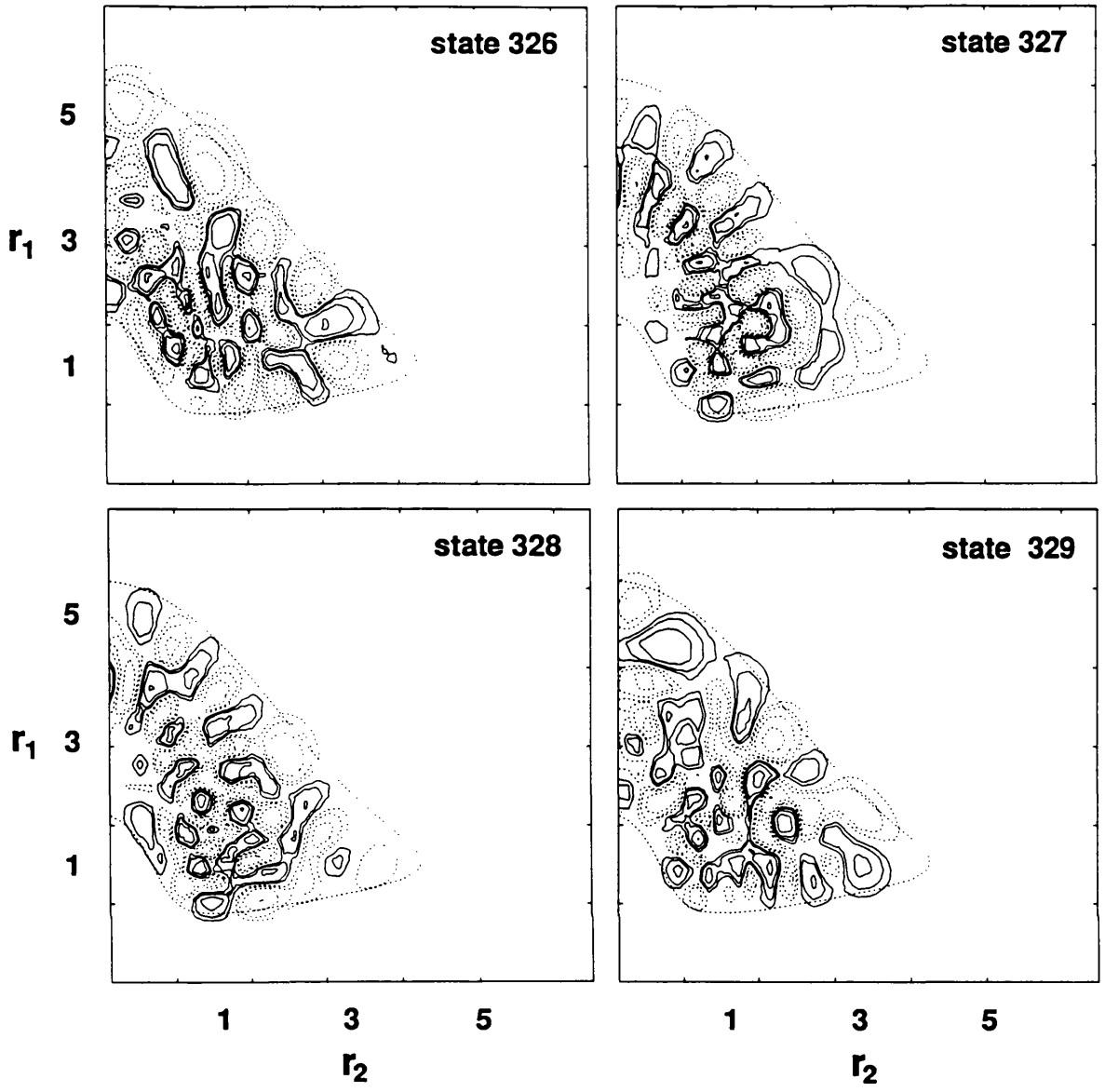


Figure 6.3: Cuts through the wavefunction of 4 even J = 0 states calculated using the MBB potential with $\theta = 90^o$. Contours as in figure 6.1. The band origins of the states are 28014, 28055, 28091 and 28138 $cm^{-1}$. The radial co-ordinates are given in atomic units ($a_0$).

to made; it is still not certain that the 'horseshoe' motion is (solely) responsible for the coarse-grained regularity in the Carrington-Kennedy spectrum. This will best be done by plotting different cuts through the wavefunctions and also by transforming the wavefunctions to coordinates which better display other classical periodic orbits.

Clearly, it remains for the calculations to be extended to quasi-bound levels, rotational calculations to be made, and thereafter spectra computed. It is still uncertain, however, exactly what values of total angular momentum $J$ are of interest. The theory for rotational excitation in a multidimensional DVR has been developed by the author, but not yet applied. Investigations into resonances and quasi-bound states can be made using the method of Choi and Light[142].

Finally, a matter of prime importance is the potential energy surface. An accurate, global surface which dissociates correctly is needed urgently. Although the surfaces used in these studies probably predict the correct dynamics, it is unlikely that, at very high energy, close agreement with the experimental spectra will be obtained.

Should these needs be met, it is likely that a proper quantal treatment of the predissociating states of $H_3^+$ observed by Carrington and co-workers[1,2] can soon be achieved. As has been demonstrated in this thesis, the Discrete Variable Representation will prove invaluable to studies of this type.

# Bibliography


[1] A. Carrington J. Buttenshaw and R.A. Kennedy, *Mol. Phys.*, 45, 753 (1982).

[2] A. Carrington and R.A. Kennedy, *J. Chem. Phys.*, 81, 91 (1984).

[3] M. Born and R. J. Oppenheimer, *Ann. Phys.*, 84, 457 (1927).

[4] G. Woolley, *New Scientist*, 84, 457 (1988).

[5] N.C. Handy, Y. Yamaguchi and H.F. Schaefer III, *J. Chem. Phys.*, 84, 4481 (1986).

[6] W. Meyer, P. Botschwina and P.G. Burton, *J. Chem. Phys.*, 84, 891 (1986).

[7] P. Drossart, J.-P. Maillard, J. Caldwell, S.J. Kim, J.K.G. Watson, W.A. Majewski, J. Tennyson, S. Miller, S. Atreya, J. Clarke, J.H. Waite Jr. and R. Wagener, *Nature*, 340, 539 (1989).

[8] C. Eckart, *Phys. Rev.*, 47, 552 (1935).

[9] J.K.G. Watson, *Mol. Phys.*, 15, 479 (1968).

[10] G.D. Carney, L.L. Sprandel and C.W. Kern, *Advan. Chem. Phys.*, 37, 305 (1978).

[11] B. J. Krohn, W. C. Ermler and C. W. Kern, *J. Chem. Phys.*, 60, 22 (1974).

[12] J. H. Van Vleck, *Phys. Rev.*, 33, 467 (1929).

[13] P.R. Bunker, *Ann. Rev. Phys. Chem.*, 34, 59 (1983).

[14] A. R. Hoy and P.R. Bunker, *J. Mol. Spectr.*, 52, 439 (1974).

[15] A. R. Hoy and P.R. Bunker, *J. Mol. Spectr.*, 74, 1 (1979).

[16] P. Jensen, P.R. Bunker and A. R. Hoy, *J. Chem. Phys.*, 77, 5370 (1982).

[17] P.R. Bunker and P. Jensen, *J. Chem. Phys.*, 79, 1224 (1983).

[18] Lord Rayleigh, *Theory of Sound*, volume 1, sec. 88 (Macmillan, London 1937, reprinted Dover, New York) and W. Ritz, *J. Reine Angew Math.*, 135, 1 (1908).

[19] *Modern Theoretical Chemistry: Electronic Structure Theory*, Vols. 3 (Methods) and 4 (Applications), H. F. Schaefer III, Ed., Plenum, New York, 1977.

[20] J. K. L. MacDonald, *Phys. Rev.*, 43, 830 (1933).

[21] I. Suzuki, *Bull. Chem. Soc. Jap.*, 44, 3277 (1971).

[22] I. Suzuki, *Bull. Chem. Soc. Jap.*, 48, 3565 (1975).

[23] I. Suzuki, *Bull. Chem. Soc. Jap.*, 48, 1685 (1975).

[24] R.J. Whitehead and N.C. Handy, *J. Mol. Spectrosc.*, 55, 356 (1975).

[25] G.D. Carney and R.N.Porter, *J. Chem. Phys.*, 60, 4251 (1974).

[26] G.D. Carney and R.N.Porter, *J. Chem. Phys.*, 65, 3547 (1976).

[27] G.D. Carney and R.N.Porter, *Chem. Phys. Letts.*, 50, 327 (1977).

[28] G.D. Carney and R.N.Porter, *Phys. Rev. Letts.*, 45, 537 (1980).

[29] T. Oka, *Phys. Rev. Letts.*, 45, 531 (1980).

[30] J.-T. Shy, J.W. Farley, W.E. Lamb Jnr. and W.H. Wing, *Phys. Rev. Letts.*, 45, 535 (1980).

[31] R.J. Le Roy and J.S. Carley, *Advan. Chem. Phys.*, 42, 353 (1980).

[32] J. Tennyson and B.T. Sutcliffe, *Mol. Phys.*, 46, 97 (1982).

[33] J. Tennyson and A. van der Avoird, *J. Chem. Phys.*, 76, 5710 (1982).

[34] J. Tennyson and B.T. Sutcliffe, *J. Chem. Phys.*, 77, 4061 (1982).

[35] R. Bartholomae, D. Martin and B.T. Sutcliffe, *J. Mol. Spectrosc.*, 87, 367 (1981).

[36] S. Carter and N.C. Handy, *J. Mol. Spectrosc.*, 95, 9 (1982).

[37] J. Tennyson and B.T. Sutcliffe, *J. Mol. Spectrosc.*, 101, 71 (1983).

[38] S. Carter, N.C. Handy and B.T. Sutcliffe, *Mol. Phys.*, 49, 745 (1983).

[39] S. Carter and N.C. Handy, *Mol. Phys.*, 52, 1367 (1984).

[40] B.T. Sutcliffe and J. Tennyson, *J. Chem. Soc., Faraday Trans. 2*, 83, 1663 (1987).

[41] J.S. Lee and D. Secrest, *J. Chem. Phys.*, 92, 1821 (1989).

[42] E.C.K. Lai, Master's Thesis, Department of Chemistry, Indiana University (1975).

[43] G. Brocks, A. van der Avoird, B.T. Sutcliffe and J. Tennyson, *Mol. Phys.*, 50, 1025 (1983).

[44] P. Jensen, *J. Mol. Spectrosc.*, 128, 478 (1988).

[45] R.M. Whitnell and J.C. Light, *J. Chem. Phys.*, 90, 1774 (1989).

[46] B.T. Sutcliffe, in: *Current Aspects of Quantum Chemistry* (R. Carbo, ed.), Studies in Theoretical Chemisry, Vol. 21, pp.99, Elsivier (1982).

[47] B.T. Sutcliffe and J. Tennyson, *Int. J. Quantum Chem.*, (in press).

[48] J. Tennyson and B.T. Sutcliffe, *Mol. Phys.*, 58, 1067 (1986).

[49] S. Miller and J. Tennyson, *Chem. Phys. Letts.*, 145, 117 (1988).

[50] C.-L. Chen, B. Maessen and M. Wolfsberg, *J. Chem. Phys.*, 83, 1795 (1985).

[51] J. Tennyson and S. Miller, *Comp. Phys. Comm.*, 55, 149 (1989).

[52] J. M. Hutson, BOUND computer program, distributed by Collaborative Computational Project 6 (CCP6).

[53] Z. Bačić and J.C. Light, *J. Chem. Phys.*, 85, 4594 (1986).

[54] J.C. Light, I.P. Hamilton and J.V. Lill, *J. Chem. Phys.*, 92, 1400 (1985).

[55] D.O. Harris, G.O. Engerholm and W. Gwinn, *J. Chem. Phys.*, 43, 1515 (1965).

[56] A.S. Dickinson and P.R. Certain, *J. Chem. Phys.*, 49, 4209 (1968).

[57] S. Carter and N.C. Handy, *Mol. Phys.*, 57, 175 (1986).

[58] S. Carter, N.C. Handy and I.M. Mills, *Phil. Trans. Roy. Soc.*, 332, 121 1990.

[59] S. Carter and W. Meyer, *J. Chem. Phys.*, 1990 (in press).

[60] C. Clay Marston and G. G. Balint-Kurti, *J. Chem. Phys.*, 91, 3571 (1989).

[61] W. Yang and A.C. Peet, *Chem. Phys. Letts.*, 153, 98 (1988).

[62] W. Yang and A.C. Peet, *J. Chem. Phys.*, 92, 522 (1990).

[63] A.C. Peet and W. Yang, *J. Chem. Phys.*, 90, 1746 (1989).

[64] B.R. Johnson and W.P. Reinhardt, *J. Chem. Phys.*, 85, 4538 (1986).

[65] A.M. Arthurs and A. Dalgarno, *Proc. Roy. Soc. Ser. A*, 256, 540 (1960).

[66] E.U. Condon and G.H. Shortley, *The theory of atomic spectra*, Cambridge University Press, Cambridge (1935).

[67] R.J. Le Roy and J. Van Kranendonk, *J. Chem. Phys.*, 61, 4750 (1974).

[68] J. Tennyson, *Chem. Phys. Letts.* 86, 181 (1982).

[69] G. Brocks and J. Tennyson, *J. Mol. Spectrosc.* 99, 263 (1983).

[70] I.S. Gradshteyn and I.H. Ryzhik, *Tables of Integrals, Series and Products*, Academic, New York (1980).

[71] J. Tennyson, *Computer Phys. Comms.*, 32, 109 (1984).

[72] J. Tennyson, O.Brass and E. Pollak, *J. Chem. Phys.*, 92, 3005 (1990).

[73] J.M. Hutson, *J. Chem. Soc., Faraday Trans. 2*, 82, 1163 (1986).

[74] J.M. Hutson and R.J. Le Roy, *J. Chem. Phys.*, 83, 1197 (1985).

[75] J.M. Bowman, J.S. Bitman and L.B. Harding, *J. Chem. Phys.*, 85, 911 (1986).

[76] J. Tennyson, *Computer Phys. Reports*, 4, 1 (1986).

[77] A.H. Stroud and D. Secrest, *Gaussian Quadrature Formulas*, Prentice-Hall, London (1966).

[78] P.R. Bunker, *Molecular Symmetry and Spectroscopy*, Academic Press, New York (1979).

[79] G.S. Ezra, Symmetry Properties of Molecules, *Lecture Notes in Chemistry*, Vol. 28, Springer-Verlag, Berlin (1982).

[80] J. Tennyson and B.T. Sutcliffe, *Mol. Phys.*, 51, 887 (1984).

[81] J.M. Brown, J.T. Hougen, K.-P. Huber, J.W.C. Johns, I. Kopp, H. Lefrebvre-Brion, A.J. Merer, D.A. Ramsay, J. Rostos and R.N. Zare, *J. Mol. Spectrosc.*, 55, 500 (1975).

[82] S.L. Holmgren, M. Waldman and W. Klemperer, *J. Chem. Phys.*, 67, 4414 (1977).

[83] J. Tennyson, S. Miller and B.T. Sutcliffe, *J. Chem. Soc., Faraday Trans. 2*, 84, 1295 (1988).

[84] B.T. Sutcliffe, S. Miller and J. Tennyson, *Computer Phys. Comms.*, 51, 73 (1988).

[85] B.T. Sutcliffe, J. Tennyson and S. Miller, *Theor. Chim. Acta*, 72, 265 (1987).

[86] J. Tennyson, S. Miller and B.T. Sutcliffe, in: Supercomputer Algorithms for Reactivity, Dynamics and Kinetics of Small Molecules, (A. Laganà ed.), NATO ASI series C, Vol. 277, pp. 261, Kluwer, Dordrecht (1989).

[87] W.C. Stwalley and M.E. Koch, *Opt. Eng*, 19, 71 (1980).

[88] S.J. Dunne, D.J. Searles and E.I. von Nagy-Felsobuki, *Spectrochim. Acta*, 43A, 699 (1987).

[89] D.J. Searles, S.J. Dunne, and E.I. von Nagy-Felsobuki, *Spectrochim. Acta*, 44A, 505 (1988).

[90] D.J. Searles, S.J. Dunne, and E.I. von Nagy-Felsobuki, *Spectrochim. Acta*, 44A, 985 (1988).

[91] J. Tennyson and B.T. Sutcliffe, *J. Chem. Soc. Faraday Trans. 2*, 82, 1151 (1986).

[92] S. Miller and J. Tennyson, *J. Mol. Spectrosc.*, 128, 183 (1987).

[93] S. Miller and J. Tennyson, *J. Mol. Spectrosc.*, 128, 530 (1988).

[94] S. Miller and J. Tennyson, *Chem. Phys. Letts.*, 145, 117 (1988).

[95] S. Miller and J. Tennyson, *Ap. J.*, 335, 486 (1988).

[96] J. Tennyson, *Computer Phys. Comms.*, 42, 257 (1986).

[97] J. Tennyson and S. Miller, *Computer Phys. Comms.*, 55, 149 1989.

[98] G. Brocks, J. Tennyson and A. van der Avoird, *J. Chem. Phys.*, 80, 3223 (1984).

[99] S. Miller, J. Tennyson and B.T. Sutcliffe, *Mol. Phys.*, 66, 429 (1989).

[100] S. Miller and J. Tennyson, *J. Mol. Spectr.*, 126, 183 (1987).

[101] J.K.G. Watson, S.C. Foster, A.R.W. McKellar, P. Bernath, T. Amano, F.S. Pan, M.W. Crofton, R.S. Altman and T. Oka, *Canad. J. Phys.*, 62, 1886 (1984).

[102] S.C. Foster, A.R.W. McKellar, I.R. Peterkin, J.K.G. Watson, F.S. Pan, M.W. Crofton, R.S. Altman and T. Oka, *J. Chem. Phys.*, 84, 91 (1985).

[103] J.K.G. Watson, *J. Mol. Spectrosc.*, 103, 350 (1984).

[104] J.-T. Shy, J.W. Farley and W.H. Wing, *Phys. Rev. A* 24, 1146 (1981).

[105] J.L. Martins, R. Car and J. Buttet, *J. Chem. Phys.*, 78, 5646 (1983).

[106] D.J. Searles and E.I. von Nagy-Felsobuki, *Aust. J. Chem*, 42, 737 (1989).

[107] G.D. Carney, S.R. Langhopp and L.A. Curtiss, *J. Chem. Phys.*, 66, 3724 (1977).

[108] Z. Bačić and J.C. Light, *J. Chem. Phys.*, 86, 3065 (1987).

[109] J.C. Light and Z. Bačić, *J. Chem. Phys.*, 87, 4008 (1987).

[110] D.M. Leitner, R.S. Berry and R.M. Whitnell, *J. Chem. Phys.*, 91, 3470 (1989).

[111] Z. Bačić, D. Watt and J.C. Light, *J. Chem. Phys.*, 89, 947 (1988).

[112] J.R. Henderson, S. Miller and J. Tennyson, *J. Chem. Soc., Faraday Trans.*, 86, 1963 (1990).

[113] R.M. Whitnell and J.C. Light, *J. Chem. Phys.* 89, 3674 (1988).

[114] J.C. Light, R.M. Whitnell, T.J. Pack and S.E. Choi, in *"Supercomputer Algorithms for Reactivity, Dynamics and Kinetics of Small Molecules"*, A. Lagana (Ed.), NATO ASI series C, 277, 187 (Kluwer, Dordrecht, 1989).

[115] Z. Bačić and J.C. Light, *Ann. Rev. Phys. Chem.*, 40, 469 (1989).

[116] V.A. Isotomin, N.F. Stepanov and B.I. Zhilinski, *J. Mol. Spectrosc.*, 67, 265 (1977).

[117] S.C. Farantos and J. Tennyson, *J. Chem. Phys.*, 82, 800 (1985).

[118] J. Tennyson and S.C. Farantos, *Chem. Phys.*, 93, 237 (1985).

[119] J. Tennyson, G. Brocks and S.C. Farantos, *Chem. Phys.*, 104, 399 (1986).

[120] R.M. Benito, F. Borondo, J-H. Kim, B.G. Sumpter and G.S. Ezra, *Chem. Phys. Letts.*, 161, 60 (1989).

[121] R. Essers, J. Tennyson and P.E.S. Wormer, *Chem. Phys. Letts.*, 89, 223 (1982).

[122] J.J. van Vaals, W.L. Meerts and A. Dymanus, *Chem. Phys.*, 77, 4061 (1984).

[123] M.V. Berry and M. Tabor, *Proc. Roy. Soc. London Ser. A*, 356, 375 (1977).

[124] P. Pechukas, *Phys. Rev. Letters*, 51, 943 (1983).

[125] T.A. Brody, *Lett. Nuovo Cimento*, 7, 482 (1973).

[126] E. Haller, H. Koppel and L.S. Cederbaum, *Phys. Rev. Letters*, 52, 1665 (1984).

[127] For example: O. Bohigas, M-J. Giannoni and C. Schmidt, in: Quantum Chaos and Statistical Nuclear Physics, Lecture Notes in Physics, (Springer-Verlag) Vol. 263, p. 18 (1986).

[128] For example: I. Benjamin, V. Buch, R.B. Gerber and R.D. Levine, *Chem. Phys. Letters*, 107, 515 (1984); H-D. Meyer, E. Haller, H. Koppel and L.S. Cederbaum, *J. Phys. A: Math. Gen.*, 17, L831 (1984).

[129] F. Borondo, private communication.

[130] M.S. Child, *J. Phys. Chem.*, 90, 3595 (1986).

[131] R. Pfeiffer and M.S. Child, *Mol. Phys.*, 60, 1367 (1987).

[132] M. Berblinger, E. Pollak and Ch. Schlier, *J. Chem. Phys.*, 88, 5643 (1988).